Accelerated Phosphorus Magnetic Resonance Spectroscopic Imaging (^{31}P-MRSI) for the Evaluation of Energy Metabolism

Accelerated Phosphorus Magnetic Resonance Spectroscopic Imaging (^{31}P-MRSI) for the Evaluation of Energy Metabolism

By ALEJANDRO Santos Díaz, B. Eng, M.Sc.

A Thesis Submitted to the School of Graduate Studies in the Partial Fulfillment of the Requirements for the Degree Doctor of Philosophy

Doctor of Philosophy (2018)

School of Biomedical Engineering

McMaster University

Hamilton, Ontario, Canada

TITLE: Accelerated Phosphorus Magnetic Resonance Spectroscopic Imaging (^{31}P-MRSI) for the Evaluation of Energy Metabolism

AUTHOR: ALEJANDRO Santos Díaz, B.eng,M. Sc.

SUPERVISOR: Dr. Michael D. Noseworthy

NUMBER OF PAGES: xvii,144

Abstract

Phosphorus magnetic resonance spectroscopy and spectroscopic imaging (^{31}P-MRS/MRSI) non-invasively provide very important information regarding energy metabolism as they can detect high energy metabolites and membrane phospholipids in vivo. They have repeatedly proven their utility in the study of healthy and disease conditions, as many disorders are related to imbalances in bioenergetic processes. However, they are not often used in a clinic setting as there are technical challenges that lead to very long acquisition times. To address this issue, the present work focused on the implementation of two fast Phosphorus Magnetic Resonance Spectroscopic Imaging (^{31}P-MRSI) pulse sequences. The first one, "fidEPSI" uses a flyback echo planar readout trajectory calculated in real time to achieve an acceleration factor up to x10. The second, "fidepsiCS" further accelerates the acquisition by combining the flyback EPSI readout with a compressed sensing (CS) sampling scheme. For this latter approach two different data reconstruction processes were compared. Both sequences were tested in phantoms as well as in skeletal muscle and brain tissues of healthy volunteers. The results showed feasibility of the flyback Echo planar spectroscopic imaging (EPSI) to acquire good quality data in a fraction of the time when compared to traditional phase encoded MRSI. Furthermore, the compressed sensing approach was used in an exercise-recovery paradigm to evaluate skeletal muscle high energy phosphate dynamics, achieving a temporal resolution of 9 seconds. Additionally, the comparison of CS reconstruction algorithms suggested that a low-rank approach is more suitable for ^{31}P-MRSI data, compared to traditional thresholding, due to the fact that it exploits the sparsity of the NMR signal as the least number of

spectral peaks rather than the fewest amount of non-zero values. Overall, this thesis presents new accelerated methods for the acquisition of ^{31}P-MRSI, and its use in the evaluation of energy metabolism.

Acknowledgements

First and foremost, I would like to thank my supervisor and friend, Dr. Michael D. Noseworthy for all his guidance, support and encouragement to get this work to succeed. I have been excessively lucky for having such a kind, warm and wise person to guide me through my PhD journey.

I would also like to thank the members of my committee for their support and invaluable feedback during these years. Drs. Carol DeMatteo, John Connolly and Nicholas Bock, thank you very much.

A big thank you goes to the Senior Scientific Research Officer at the Imaging Research Center, Norm Konyer. He taught me the witchcraft behind building MRI RF coils as well as many details to account for when using the scanner. Also, I want to deeply thank three wonderful women whom taught me so much about how to use the MRI scanner; Carol Awde, Julie Lecomte and Cheryl Contant, thank you very much.

An special thank you goes also to Dr. Rolf Schulte from GE Healthcare and Dr. Peder Larson from UCSF, they helped me a lot with the EPIC task of programming pulse sequences.

To continue, I would also like to thank all my friends and colleagues at the IRC and the McMaster School of Biomedical Engineering, for all the fantastic experiences along these four years. Specially, a big thanks to my friend, Dr. Alireza Akbari for showing me the ropes with the MRI scanner and the troubleshooting of MNS.

Also, Thank you to all my friends outside the academic life, they have made this

journey much more enjoyable.

Finally, I would like to acknowledge the Consejo Nacional de Ciencia y Tecnología (CONACYT) and the Secretaría de Educación Pública from México, for providing a scholarship to fund part of this project (CVU: 304930).

“ *Look up at the stars and not down at your feet. Try to make sense of what you see, and wonder about what makes the universe exist. Be curious.”*

Stephen Hawking

“*Try not to become a man of success, but rather try to become a man of value.”*

Albert Einstein

To my parents, María Eugenia y Eduardo, for always giving me the strength and support to achieve my goals...

To my brother, Dr. Eduardo Santos Díaz, for opening the door that led us to follow this path...

To the memory of my grandfather, "Don" Antonio Santos Navarro...

Contents

List of Figures

List of Tables

List of acronyms and abbreviations

ADHD attention deficit/hyperactive disorder

ADP adenosine di-phosphate

AF acceleration factor

ATP adenosine tri-phosphate

BD bipolar disease

CK Creatine-kinase

C_{met} concentration of the metabolite

Cr Creatine

C_{ref} reference compound

CS compressed sensing

CSDE chemical shift displacement error

CSI chemical shift imaging

DRESS depth-resolved surface coil MRS

EPSI Echo planar spectroscopic imaging

FID free induction decay

FWHM full width half maximum

GM Gray matter

GPC glycerolphpsphpcholine

GPE glycerolphosphoethanolamine

GRAPPA generalized autocalibrating partial paralell acquisition

ISIS image selected in vivo spectroscopy

MDD major depression disorder

MRI magnetic resonance imaging

MRS magnetic resonance spectroscopy

mTBI mild Traumatic Brain Injury

MVC maximum voluntary contraction

NAD nicotinamide adenine dinucleotide

NMR nuclear magnetic resonance

NOE nuclear Overhauser effect

^{31}P**-MRSI** Phosphorus Magnetic Resonance Spectroscopic Imaging

^{31}P**-MRS** Phosphorus magnetic resonance spectroscopy

PC phosphochiline

PCr Phosphocreatine

PDE phosphodiester

PE phosphoethanolamine

pH(i) intracellular pH

Pi inorganic phosphate

PME phosphomonoester

PRESS point resolved spectroscopy

^{1}H**-MRS** proton MRS

PSF point spread function

RARE rapid acquisition with relaxation enhancement

RF radio-frequency

RMSE root mean squared error

SAR specific absorption rate

semi-LASER slice selective excitation combined with localization by adiabatic selective refocusing

SNR signal to noise ratio

STEAM stimulated echo acquisition mode

SVS single voxel spectroscopy

τPCr time constant of PCr recovery rate

UDPG uridine diphosphate glucose

WM White matter

Chapter 1

Introduction

Living organisms require a considerable amount of energy to carry out their life-dependent proecsses. At a cellular level, adenosine tri-phosphate (ATP) is considered the "currency" of energy metabolism as its production and expenditure are at the center of most metabolic interactions. As a consequence, research in the field has been able to recognize that an imbalance in ATP production and demand is the cause (or consequence) of many human diseases (DeBerardinis and Thompson 2012). Therefore, methods capable to detect such imbalance are highly valuable. Due to its non-ionizing nature, in vivo nuclear magnetic resonance (NMR) spectroscopy, also known as magnetic resonance spectroscopy (MRS) awakes the interest of scientists in the study of living organisms. Scientists started to see the potential of NMR as a diagnostic tool in the early 1970's with Damadian's report on differentiated properties (relaxation times) between tumors and normal tissue using proton experiments (Damadian 1971). Around the same time, the first ^{31}P NMR experiments in living tissues were performed; Moon and Richards 1973 used blood cells to show how intracellular pH can be determined using the

chemical shift differences in ^{31}P-NMR whereas Hoult et al. 1974 reported the first ^{31}P NMR experiment in excised rat leg. In parallel, major advancements in the field were achieved as Mandsfield and Lauterbur independently described an application to create images that show the spatial distribution of spins using NMR signals (Mansfield and Grannell 1973; Lauterbur et al. 1973), giving birth to what we know today as magnetic resonance imaging (MRI). Since then, MRS and MRI have evolved from simple methods comprising a few radio-frequency (RF) pulses to very complex sequences involving spatial localization, signals suppression, time varying field gradients and multi-parametric acquisition schemes.

Although less popular than proton (^{1}H), Phosphorus magnetic resonance spectroscopy (^{31}P-MRS) has also played an important role in the development of MR technology due to its unique capability of assessing high energy metabolism compounds such as Phosphocreatine (PCr), ATP and inorganic phosphate (Pi) as well as membrane integrity markers such as phosphomonoesters (PMEs) and phosphodiesters (PDEs). The dampened popularity is due to the challenges associated with the acquisition of ^{31}P signals. First, the lower sensitivity of this nucleus as a result of the lower gyromagnetic ratio as well as the low concentration of metabolites in tissues. Additionally, the relatively short T_2 relaxation times of some ^{31}P compounds limit the spatial localization techniques available to pulse-acquire or non-echo type sequences (e.g free induction decay, FID). All together, these limitations make ^{31}P-MRS experiments usually long and infrequently used in clinical settings. Thus, the development of techniques to accelerate the acquisition speed while preserving enough signal to noise ratio (SNR) for spectral quantification have been one of the main drivers of research in the field.

This work presents contributions in the development of accelerated Phosphorus Magnetic Resonance Spectroscopic Imaging (^{31}P-MRSI) pulse sequences for the evaluation of energy metabolism. Chapter 2 presents a thorough review of the use of ^{31}P-MRS methods for the evaluation of energy metabolism in skeletal muscle and brain tissue, making strong emphasis on the methodological aspects. Chapter 3 states the objectives of the project and gives a brief description of the methodology. After that, chapter 4 presents the first research article of this project were a fast ^{31}P-MRSI sequence using flyback readout gradient trajectories was developed. Following that, chapter 5 describes a further acceleration of the technique by the inclusion of compressed sensing (CS) and its use in the evaluation of muscle dynamics. In chapter 6, an evaluation of two different reconstruction methods for the data acquired using compressed sensing is presented. Finally, Chapter 7 concludes this work with a summary of the main contributions and providing some future directions.

References

Damadian, R. (1971) Tumor detection by nuclear magnetic resonance *Science* 171.(3976), 1151–1153.

DeBerardinis, R. J. and Thompson, C. B. (2012) Cellular metabolism and disease: what do metabolic outliers teach us? *Cell* 148.(6), 1132–1144.

Hoult, D. I., Busby, S., Gadian, D. G., Radda, G. K., Richards, R. E., and Seeley, P. J. (1974) Observation of tissue metabolites using 31P nuclear magnetic resonance *Nature* 252.(5481), 285.

Lauterbur, P. C. et al. (1973) Image formation by induced local interactions: examples employing nuclear magnetic resonance.

Mansfield, P. and Grannell, P. K. (1973) NMR'diffraction'in solids? *Journal of Physics C: solid state physics* 6.(22), L422.

Moon, R. B. and Richards, J. H. (1973) Determination of intracellular pH by 31P magnetic resonance *Journal of Biological Chemistry* 248.(20), 7276–7278.

Chapter 2

The nature of phosphorus magnetic resonance spectroscopy

Phosphorus magnetic resonance spectroscopy (^{31}P-MRS) and Phosphorus Magnetic Resonance Spectroscopic Imaging (^{31}P-MRSI) offer a very unique window to non-invasively look at tissue metabolism in vivo. These approaches are capable of tracking high energy metabolites and membrane phospholipids, all of which are involved in cellular energetic processes (De Graaf 2013). Thus phosphorus spectroscopic methods have been attractive across the scientific community in order to study energy metabolism in healthy and pathophysiological conditions. Furthermore, its noninvasive nature makes it an excellent candidate to perform repeated measurements and track disease progression or treatment response. In addition to the information contained in the static spectra, these methods also allow the evaluation of oxidative energy production by the mitochondria through an exercise challenge and subsequent recovery in skeletal muscle (Kemp et al. 2015). Although these methods have been around since the beginnings of MRI in the 1970's, the

current technological developments have been spearheaded by the ultra high magnetic field community. This includes improved radio-frequency (RF) coil designs, new data sampling methods and better reconstruction approaches all of which provide significant improvements to the technology making them more attractive to clinicians and researchers.

This chapter provides an overview of the current status of ^{31}P-MRS / ^{31}P-MRSI with focus on the technological developments and the main contributions in the study of skeletal muscle and brain metabolism.

2.1 Information of interest in the phosphorus spectrum

The phosphorus nucleus is visible to nuclear magnetic resonance (NMR) due to its natural spin of $^1/_2$. This isotope has a 100% natural abundance and albeit its relatively low sensitivity of 6.7% when compared to proton (^1H), it has encountered relevance when used for in vivo applications due to its presence in important high energy and phospholipid metabolites (De Graaf 2013; Lee et al. 2012).

The chemical shift range where in vivo phosphorus compounds resonate spans around 30 parts per million (ppm) in contrast to the narrow 5ppm window for ^1H MR spectra, additionally the amount of relevant metabolites is considerably less. Within the ^{31}P-MRS spectrum, the fundamental high-energy metabolite Phosphocreatine (PCr) is the dominant signal (in brain and skeletal muscle), thus it is often used as a reference and assigned the value of 0ppm. PCr serves as an

immediately available energy reserve ready to restore the expenditure of adenosine tri-phosphate (ATP) in energy demanding processes. ATP contains three phosphate groups; α, β and γ that give rise to three independent signals in the spectrum at -7.56 ppm, -16.15 ppm and -2.53 ppm respectively.

The interaction of the phosphorus nuclei with other nearby spins rises into a homonuclear J-coupling effect, causing a line splitting ATP signals into doublets for γ-ATP and α-ATP, and a triplet for β-ATP.

Moving to the positive side of the spectrum, a relatively small singlet signal at approximately 4.85 ppm corresponds to inorganic phosphate (Pi), a degradation product of energy metabolism. Next to Pi, the cell membrane precursors phosphomonoesters (PMEs) phosphochiline (PC) and phosphoethanolamine (PE) are observable at around 6.2 ppm and 6.7ppm, often times measured as a single PME signal at magnetic field strength $B_0 \leq 3T$. Similarly, the phosphodiester (PDE) degradation products of phospholipid metabolism, glycerolphpsphpcholine (GPC) and glycerolphosphoethanolamine (GPE) are observed at 2.95 ppm and 3.50 ppm respectively. Depending on the signal to noise signal to noise ratio (SNR), other important phosphorus containing metabolites such as nicotinamide adenine dinucleotide (NAD) in its oxidized and reduced form (NAD+ and NADH, respectively) and uridine diphosphate glucose (UDPG) are also visible, specially at ultra high field (i.e. 7T).

Aside from these metabolic signals, other important information can be deduced from the analysis of the ^{31}P spectrum. First, the chemical environment where phosphorus-containing metabolites reside may change with different physiological or pathological conditions. Of main relevance, the chemical shift of Pi is dependent

TABLE 2.1: Main ^{31}P metabolites found in brain tissue and skeletal muscle and their corresponding concentrations. Values for brain and muscle were obtained from (Ren et al. 2015) and (Kemp et al. 2007)

Metabolite	δ(ppm)	Concentration (mM)	
		Brain	Muscle
PE	6.76	2.27 ± 0.16	-
PC	6.24	0.30 ± 0.12	-
Pi	4.82	0.85 ± 0.11	4.6 ± 0.20
GPE	3.50	0.80 ± 0.18	-
GPC	2.95	1.32 ± 0.18	-
PCr	0	4.37 ± 0.39	34 ± 1.0
NAD	-8.21	0.28 ± 0.13	4
UDPG	-9.72	0.08 ± 0.04	4
γ-ATP	-2.52	[3.0]	
α-ATP	-7.56	3.09 ± 0.23	8.1 ± 0.2
β-ATP	-16.15	2.82 ± 0.25	

on the intracellular pH (Moon and Richards 1973), while the resonance of PCr remains constant, the resonance of Pi shifts with pH. Thus it is possible to calculate the pH using the difference in chemical shifts from PCr and Pi (δ) through the so-called modified Henderson-Hasselbach equation as follow:

$$pH(i) = pK_A + log\left[\frac{(\delta - \delta_{HA})}{(\delta_A - \delta)}\right] \tag{2.1}$$

Here, $pK_A = 6.75$ is the dissociation constant of Pi, $\delta_{HA} = 3.27$ and $\delta_A = 5.63$ are the chemical shifts of the protonated and non-protonated forms of Pi, respectively. As the main signal of Pi comes from the cytoplasm (sarcoplasm in muscle tissue), it is the the intracellular pH (pH(i)) that is measured. Second, the concentration of adenosine di-phosphate (ADP) under physiological conditions is too low to be detected using ^{31}P-MRS, however it can be determined from the

concentrations of Creatine (Cr), ATP and PCr due to the chemical equilibrium in the Creatine-kinase (CK) reaction (Kemp et al. 1993), thus:

$$C_{ADP} = \frac{[Cr] \times [ATP]}{[PCr] \times [H^+] \times [K_{CK}]} \tag{2.2}$$

Where $K_{CK} = 1.66x10^9$ is the equilibrium constant of the CK reaction, assuming that PCr accounts for 85% of total Cr (Kemp et al. 2007; Ren et al. 2015). Finally, the cellular concentration of free Mg_2^+, a physiologically important divalent cation, influences the chemical shift of phosphorus compounds as the Mg complexes of ADP and ATP act as substrates for ATPases and kinases. Thus, the concentration of free Mg_2^+ can be deducted from the chemical shifts of βand αATP or PCr and β-ATP (Gupta et al. 1984; Iotti et al. 1996). Fig. 2.1 shows examples of ^{31}P-MRS spectra acquired at 3T whereas Table 2.1 summarizes the metabolites, chemical shifts and their in vivo concentrations in skeletal muscle and brain tissue (Kemp et al. 2007; Ren et al. 2015).

2.2 Signal processing and quantification

Prior to metabolite quantification, free induction decay (FID) curves acquired from a ^{31}P-MRS experiment are usually preprocessed. This step usually includes zero and first order phase corrections, zero filling to increase spectral resolution and spectral apodization, the latter applied mainly for visualization, especially when SNR is poor.

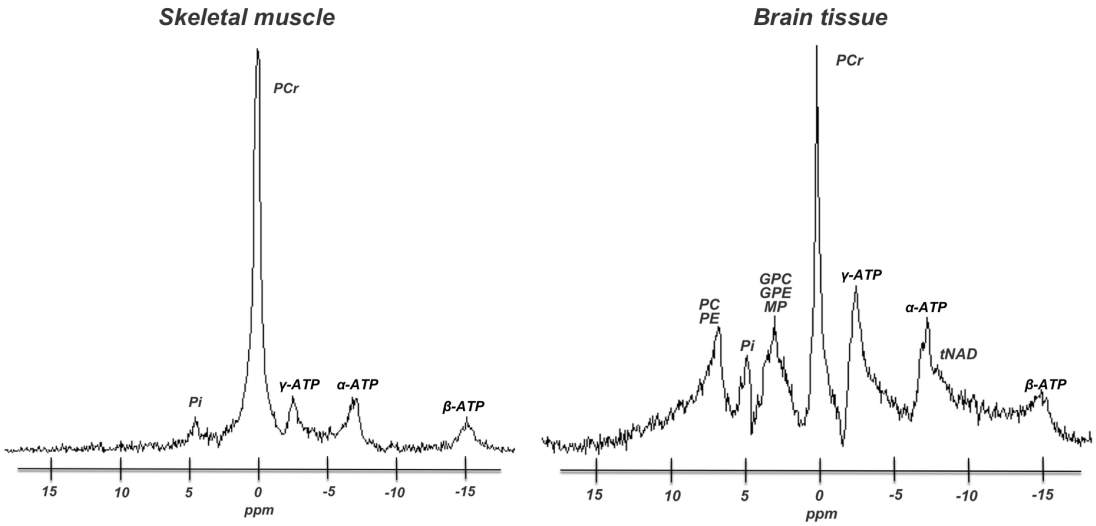

FIGURE 2.1: ^{31}P-MRS spectra of skeletal muscle (left) and brain tissue (right).

SNR is perhaps the most important characteristic in obtaining reliable metabolite quantification. If adequate, a common procedure for performing spectral fitting is to use 'Advanced Method for Accurate, Robust and Efficient Spectral Fitting (AMARES)' (Vanhamme et al. 1997), a time domain algorithm that incorporates prior knowledge and offers flexibility of the fitting parameters. The AMARES routine is available in the jMRUI software package (Stefan et al. 2009) or as part of the MATLAB based OXSA toolbox (Purvis et al. 2017). Also, the popular MRS fitting package LCModel has been successfully used in the quantification of ^{31}P spectra (Deelchand et al. 2015).

Accurate quantification of ^{31}P metabolites in vivo is a challenging task as factors such as field inhomogeneity, relaxation times and coil sensitivities may influence the measurements. Thus, metabolite ratios are often used when reporting results from MRS experiments, especially in clinical literature. However, ratios are incapable of providing information about metabolic changes in pathological conditions,

as they may be ambiguous. In order to properly assess them, metabolite concentrations need to be reported. Such quantification requires a calibration or reference compound (C_{ref}) of known concentration and generally, one of two methods is used to obtain the absolute values: in the first one, an external solution with a known concentration is placed outside of the object of study but within the coil sensitivity region. This requires the chemical standard to resonate outside of the spectral metabolite regions to avoid overlap and subsequent difficulty in differentiation. Furthermore, that approach is made more complicated by variation in B_1+ field and B_0 homogeneity, with respect to the sampled tissue volume. In the second approach, a metabolite naturally found in the tissue with established concentration is selected as the reference. From a quantitative review of experiments conducted in skeletal muscle (Kemp et al. 2007), the concentration of ATP ($[ATP] \approx 8.2 mmol/L$ cell water) is appropriate as an internal reference for quantification of healthy muscle metabolites. In the case of brain tissue, a reference value of $3 mmol/L$ for γ-ATP is often used as internal reference (Ren et al. 2015; Du et al. 2007).

Thus, the concentration of the metabolite (C_{met}) of interest is determined as follow:

$$C_{met} = [C_{ref}] \cdot \frac{S_{met}}{S_{ref}} \cdot C_{MR} \tag{2.3}$$

Where S_{ref} and S_{met} are the signals detected from the reference and the metabolite respectively, and C_{MR} is a correction factor accounting for differences in relaxation time, position relative to the coil, magnetic susceptibility or in general any other difference between the reference and the metabolite of interest.

2.3 MR system requirements

A straightforward way to understand the main requirements for ^{31}P-MRS is by comparing it with ^{1}H as all clinical and research MR systems focus on it. Some disadvantages can be deducted from that comparison such as the lower sensitivity, lower concentration in tissue, longer T_1 and shorter T_2 relaxation times of ^{31}P compounds. On the other hand, some advantages are also present. First, the significantly larger spectral dispersion of phosphorus metabolites leads to a better separation of signals. This is especially important when measuring PE, PC and GPC as they all are choline-containing metabolites that cannot be separated by proton MRS (^{1}H-MRS) spectroscopy. Also, there are no fat or water dominating signals in phosphorus spectra, meaning no frequency selective suppression techniques are required to null these dominating signals. A further difference lies in the relaxation mechanisms that govern each nucleus, whereas for ^{1}H the T_1 relaxation is dominated by the magnetic dipole-dipole interaction, the relaxation of ^{31}P metabolites is strongly influenced by the chemical shift anisotropy mechanism, which gets stronger as the magnetic field increases (Qiao et al. 2006; Bogner et al. 2009).

The lower gyromagnetic ratio and consequently lower Larmor frequency of phosphorus compounds is the main difference resulting in differing technical aspects, when comparing to proton, as all components in clinical scanners are tuned/optimized to the later. Thus, in order to use those same hardware systems, additional hardware such as a broadband transmitter/receiver and RF-coils are required. Most organ specific ^{31}P-MRS studies are performed using single loop surface coils to

take advantage of their high sensitivity, however their strong variability in B_1+ flip angle due to the inhomogeneous excitation profile can compromise the results for spectroscopic imaging applications. As a result, complex phase arrays and whole volume coverage coils with high sensitivity and homogeneous B_1+ excitation have been developed (Bank et al. 2015; Avdievich 2011; Goluch et al. 2015; Löring et al. 2016; Brown et al. 2016).

A technological development that has played a key role in improving the spectral quality of ^{31}P-MRS experiments is the use of ultra-high field MR systems ($i.e. B_0 \geq 7T$) (Bogner et al. 2009; Lei et al. 2003; Bogner et al. 2011). The main features include an SNR boost of roughly double as well as better spectral resolution and the possibility to gain more SNR per unit of time due to the shortening of T_1 relaxation times as a consequence of the above mentioned chemical shift anisotropy mechanism (Bogner et al. 2009). This gain in SNR can be traded for a higher resolution or faster acquisition times. Unfortunately, the availability of such systems is still very limited.

Further improvement of signal in phosphorus MRS experiments is possible through the following mechanisms. First, analogous to the homonuclear coupling, there is another coupling interaction between the ^{31}P and ^{1}H nuclei that causes line broadening of the in vivo spectra, especially at the PME and PDE resonances. Applying RF irradiation at the proton frequency during the ^{31}P signal acquisition reduces this heteronuclear coupling. This process effectively decouples the interaction and results in narrower spectral lines, making possible the separation of signals such as PC and PE as well as GPC and GPE at low field strength ($i.e. B_0 \leq 3T$)

(Luyten et al. 1989). Second, the utilization of the nuclear Overhauser effect (NOE) can also enhance the signal of interest. By applying proton RF irradiation during the ^{31}P interpulse delay, the sensitivity for the detection of the later has been reported to improve up to 80% in skeletal muscle at low field (Brown et al. 1995) and 44% in brain at ultra high field (Lei et al. 2003). Here, it is important to mention that a drawback of the above-mentioned techniques is the significant increment in the specific absorption rate (SAR) due to the ^{1}H-RF irradiation. Additionally, other polarization transfer methods have been explored to enhance the sensitivity of some ^{31}P-MRS signals (Gonen et al. 1997; Klomp et al. 2008; Van der Kemp et al. 2013; Van der Kemp et al. 2014).

2.4 Spatial localization of the ^{31}P-MRS signal

Due to the low intrinsic SNR of ^{31}P-MRS, it is common to use high sensitivity surface coils, especially when studying body parts of easy access such as skeletal muscle (i.e. lower leg muscles). Nevertheless, limiting the localization to the sensitive volume of the coil does not allow one to distinguish between signals coming from different compartments (i.e. different muscle groups) or deeper structures, thus at least a simple localization strategy is needed. Furthermore, two additional constraints have to be considered in this regard; first, the relatively short T_2 relaxation times of phosphorus metabolites (Bogner et al. 2009) (i.e. $T_{2-\gamma ATP} \approx 45ms$ at 3T) make "pulse-acquire" type of sequences preferable. Second, the wide spectral bandwidth is prone to significant localization bias due to chemical shift displacement

error (CSDE), thus a careful design of RF-pulses and the use of CSDE-insensitive methods is desired (Bogner et al. 2011; Chmelik et al. 2013).

2.4.1 Single voxel localization

There are various techniques for the acquisition of an MRS signal from a cuboid volume known as single voxel spectroscopy (SVS). Among the most popular, the single shot point resolved spectroscopy (PRESS) and stimulated echo acquisition mode (STEAM) are widely used in ^{1}H experiments, however their use is very limited in ^{31}P-MRS experiments due to the following reasons; the first has relatively long TE values which are not suitable for short T_2 relaxation (i.e. ATP) whereas the second has a reduction in SNR of almost a half compared to the first (Moonen et al. 1989).

The only SVS pulse-acquire based sequence that achieves sufficient SNR is the so-called image selected in vivo spectroscopy (ISIS). It is a multi shot technique that combines eight acquisitions with different configurations of spatially selective inversion pulses to accurately localize a 3D volume (Ordidge et al. 1986). Furthermore, an extended version of this sequence has been shown with accurate results from isotropic voxels of 2.3-3 cm at clinical and ultra-high field strengths in less than 5 minutes (Bogner et al. 2011). However, the ISIS sequence has the limitation of being susceptible to motion errors and cannot be used in studies that require a high temporal resolution (i.e. dynamic muscle studies). For this purpose, a STEAM sequence has been shown to be sufficient for single muscle localization

at 3T, although its temporal resolution is lower compared to pulse-acquire methods as it requires averaging to retain useful SNR (Meyerspeer et al. 2005). When moving to 7T systems, a scheme using slice selective excitation combined with localization by adiabatic selective refocusing (semi-LASER) can provide accurate localization (Meyerspeer et al. 2011).

In some cases, full 3D localization of the volume is not strictly needed, especially when using surface coils, as they are spatially restricted in their sensitivity. Thus, a method in which the pulse sequence provides localization in one dimension and the coil sensitivity restricts the volume in the other two is known as "slice selectivity". An example of this acquisition is the so-called 1D-ISIS, which has been used in single muscle dynamic experiments with low CSDE (Walter et al. 1997). More recently, another method of this kind, the depth-resolved surface coil MRS (DRESS) using a slice selective excitation was proved useful for dynamic experiments (Valkovic et al. 2014). Overall, slice selective methods are effective for the investigation of homogeneous tissue and systemic diseases. However, they are far from optimal in the study of deeper structures (i.e. deeper muscles).

2.4.2 Multi-voxel localization

All the techniques described above are limited to target a single volume per experiment, therefore they are not very practical when investigating multiple targets (i.e. different muscle groups), as they have to be repeated (Fiedler et al. 2015). Therefore, methods able to track multiple volumes simultaneously are more suitable for such experiments.

Recently presented, an interleaved scheme using the semi-LASER acquisition. This was capable of tracking the activity from two different muscle groups during the same dynamic experiment (Niess et al. 2017). Nevertheless, the spatial resolution is still very coarse and small injuries or myopathies can be overlooked if not present in the selected volume.

^{31}P-MRSI is a technique that combines the information content of MRS with the spatial localization of magnetic resonance imaging (MRI). This method also known as chemical shift imaging (CSI) acquires a FID signal from a specific volume location (i.e. voxel) localized through the application of a phase encoding gradient in each dimension, thus it is totally insensitive to CSDE. This method has been applied to the study of brain and muscle (Murphy-Boesch et al. 1993; Kan et al. 2010; Hetherington et al. 2001). However, it can be very time consuming especially when large matrix sizes are needed as it uses one excitation per localized voxel (i.e. a 8x8 matrix using six signal averages, 24x24cm2 and TR= 5s, would take 32 minutes). Using the SNR advantage of ultra-high field and overcoming the CSDE through an adiabatic slice selection, a 2D-CSI acquisition is feasible within clinically acceptable time (i.e. 6-8 min) (Chmelik et al. 2013).

Multiple acceleration methods first proposed for ^{1}H-MRSI have been translated to phosphorus spectroscopic acquisitions in order to reduce the acquisition time as much as possible, while retaining sufficient SNR for spectral analysis. EPSI is an acceleration method where the application of a rapidly oscillating gradient waveform, that allows encoding of simultaneous spatial and spectral information, can reduce the acquisition time by a factor equal to the number of encoding steps in one of the dimensions (i.e. an 8x8 matrix would have an acceleration factor of 8). This

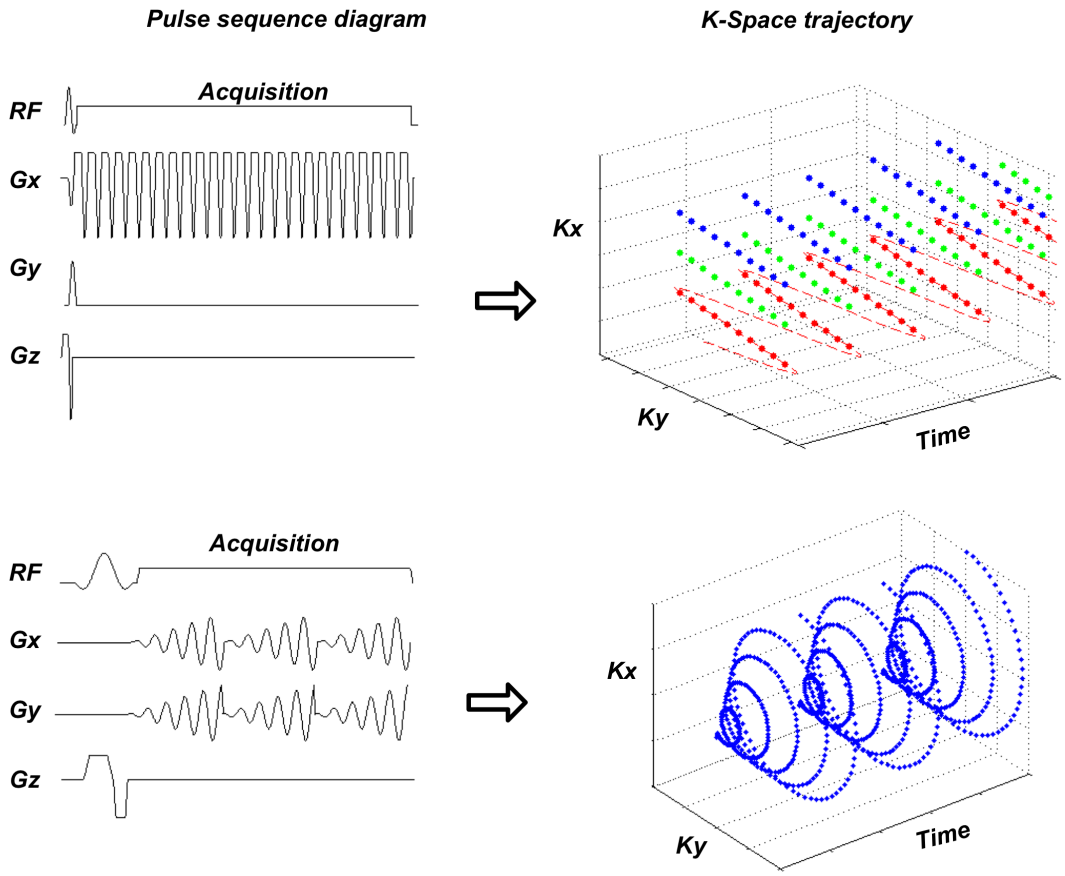

FIGURE 2.2: Accelerated ^{31}P-MRSI methods. **(Top Row)** Flyback EPSI with its corresponding K-space trajectory: Only three phase encoding steps and five temporal points are shown. **(Bottom row)** Uniform density spiral trajectory. This figures are for visual representation only.

technique was first demonstrated for ^{31}P-MRSI studies of muscle (Wilhelm and Bachert 2001) and brain (Ulrich et al. 2007) using sinusoidal gradient waveforms, which have the limitation of requiring extra hardware to trigger the acquisition and are thus sensitive to timing errors. Recently, a flexible robust EPSI sequence using flyback readout gradient trajectories was introduced for clinical field strengths (Santos-Díaz et al. 2018) (see chapter 4) and a bipolar variation was presented

at ultra-high field (Korzowski and Bachert 2018). Another acceleration method with non-Cartesian sampling trajectory was also successfully presented recently for dynamic studies of calf muscle at 7T (Valkovic et al. 2016). Examples of the pulse sequence diagrams and *K-space* trajectories are shown in Figure 2.2. Here, it is important to mention that neither EPSI nor spiral trajectories match the SNR efficiency of traditional chemical shift imaging (Pohmann et al. 1997).

Other acceleration approaches that have been translated from ^{1}H to ^{31}P-MRSI include the use of a generalized autocalibrating partial paralell acquisition (GRAPPA) scheme (Raghavan et al. 2009) in a feasibility study with phantoms, and sparse sampling methods such as compressed sensing (CS)compressed sensing (Hatay et al. 2017) and a low-rank tensor model (Ma et al. 2017).

2.4.3 Spectrally selective ^{31}P-MRI

A more straightforward translation from proton MRI to phosphorus applications is the spectrally selective ^{31}P-MR imaging. These methods allow creating maps of specific phosphorus metabolites by applying narrow spectrally selective RF-pulses at the desired frequency, followed with commonly used MRI frequency and phase encoding techniques for spatial localization, thus achieving high spatial resolution in relatively short acquisition times. The majority of these experiments target PCr and Pi due to their importance in energy metabolism, and due to their relatively long T_2 relaxation times (Bogner et al. 2009). Encoding methods such as turbo

spin-echo (Parasoglou et al. 2013c) or rapid acquisition with relaxation enhancement (RARE) (Greenman and Smithline 2011) have also been investigated. The RARE method has shown capability to create maps of more than one metabolite simultaneously with an interleaved acquisition (Greenman et al. 2011). Other developments in the field with similar capabilities include the use of a gradient-echo sequence (Schmid et al. 2016), non-Cartesian FLORET scheme (Khegai et al. 2018) and a compressed sensing acquisition (Parasoglou et al. 2012). Figure 2.3 shows PCr maps acquired using a 3D turbo spin echo sequence, comparing 3T and 7T.

2.5 Assessment of skeletal muscle metabolism

The acquisition of a phosphorus MR spectrum from the lower leg muscles is probably the most common experiment due to the relatively easy access, and high ^{31}P concentrations. Additionally, their physiological importance and high metabolic activity made them a popular target to be studied with a non-invasive technique such as ^{31}P-MRS. The analysis of resting spectra gathers information about muscle fiber composition that is relevant in the assessment of fitness/training status, especially when ultra-high field systems are used as they offer the capability of measuring cell membrane phospholipids PDE independently.

Higher levels of PDEs have been correlated with a sedentary life style particularly accentuated by obesity (Valkovič et al. 2016). Also, higher levels of PDE have been reported in professional cyclists (Hug et al. 2005; Hug et al. 2006) and long distance runners (Bernús et al. 1993), reinforcing the utility of PDE levels in skeletal

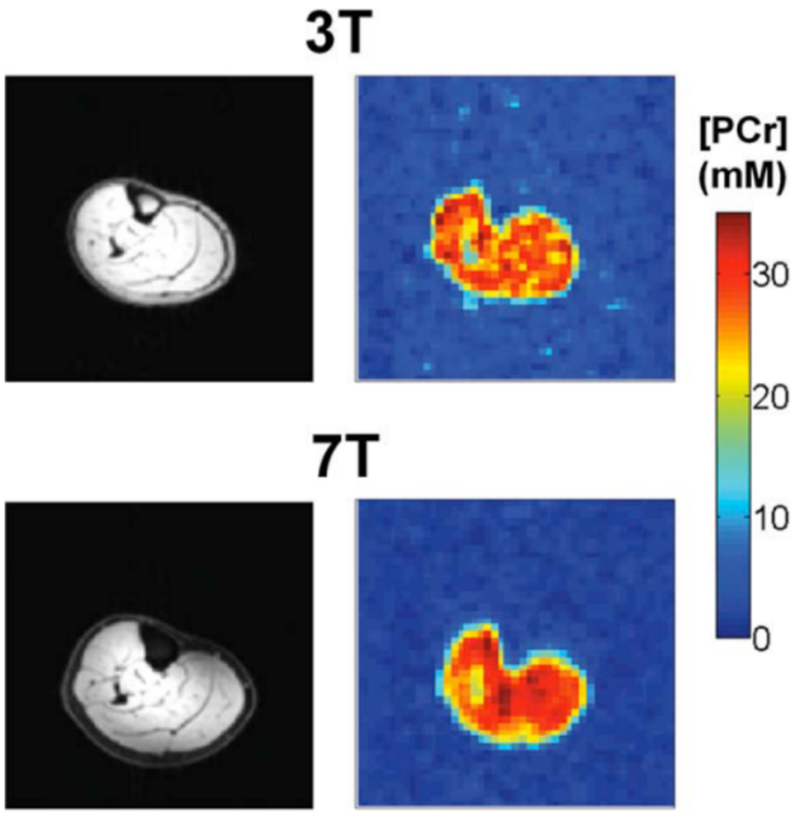

FIGURE 2.3: PCr concentration maps and respective anatomical ^1H images from the human calf muscles of the same volunteer acquired at 3T **(Top Row)** and 7T **(Bottom row)**. Reprint with permission from (Parasoglou et al. 2013a)

muscle as a marker of training status. To note, proper selection of participants and matched controls is fundamental in these experiments, as the PDE concentration levels increase with age (Valkovič et al. 2016; Satrústegui et al. 1988).

Other findings in resting muscle spectra have correlated altered levels of PDE with congenital lipodystrophy (Sleigh et al. 2012), fibromyalgia (Park et al. 1998) and muscular dystrophies (Wokke et al. 2014), as well as increased Pi and reduced PCr levels in patients with mitochondrial myopathy (Taylor et al. 1994).

In addition to the information deducted from the resting spectra, ^{31}P-MRS also offers a way to look at muscle metabolism in a dynamic fashion through the study of muscle response to an exercise challenge and its posterior recovery. Thus, these dynamic experiments allow the assessment of mitochondrial function, intracellular pH homeostasis and ATP synthesis regulation (Figure 2.4) (Kemp et al. 2007; Kemp and Radda 1994).

Oxidative metabolism of muscle is of particular interest in dynamic ^{31}P-MRS studies as it offers important information on the effects of aging (Tonson et al. 2010) and helps defining the training status (Valkovič et al. 2016). Also, these types of experiments can identify mitochondrial disturbances in muscular and systemic diseases such as Duchenne muscular dystrophy (Newman et al. 1982), mitochondrial myopathy (Taivassalo et al. 2001), diabetes mellitus (Crowther et al. 2003; Scheuermann-Freestone et al. 2003) and peripheral arterial disease (Greiner et al. 2006; Isbell et al. 2006).

A thorough review of the physiology and evaluation of muscle mitochondrial oxidative capacity is out of the scope of this review, the readers interested in a deeper insight of the subject are referred to (Kemp et al. 2007; Valkovič et al. 2017).

In skeletal muscle, PCr acts as a reserve of energy that is immediately available to compensate the expenditure of ATP due to oxidative phosphorylation. This happens through the temporally buffering reaction in Eq. 2.4, which catalyzed by CK enzyme, ensures that the ATP concentration levels remain stable.

$$PCr + ADP + H^{+} \longleftrightarrow ATP + Cr \tag{2.4}$$

The consequent depletion of PCr levels is matched by an increase in the free Cr such that the amount of total creatine ($T_{Cr} = Cr + PCr$) remains constant. Also, the levels of Pi rises in the same time course and then goes back to normal during the recovery period. As a consequence, the PCr hydrolization process is also involved in pH regulation. These effects can be observed in the plot of a dynamic experiment in calf muscle and corresponding time courses for PCr, Pi and pH shown in Figure 2. The drop in PCr also leads to an increase in the free ADP, which can be calculated through the CK equilibrium expression as stated in Eq.2.2.

The resynthesis of PCr in the recovery period is considered an aerobic process, thus it is indicative of the suprabasal synthesis rate (Kemp et al. 2007). The time constant of PCr recovery (τ_{PCr}) can be fitted as a mono-exponential function as:

$$[PCr](t) = [PCr]_{end} + \Delta[PCr] \cdot \left(1 - exp\left(\frac{-t}{\tau_{PCr}}\right)\right) \tag{2.5}$$

Where PCr_{end} is the concentration of PCr at the end of the exercise challenge, and ΔPCr is the difference between the PCr concentrations at rest and PCr_{end}. The oxidative phosphorylation flux (V_{iPCr}) is related to the initial PCr re-synthesis rate (Jeneson et al. 2009), which can be calculated as:

$$V_{iPCr} = \frac{\Delta PCr}{\tau_{PCr}} \tag{2.6}$$

Finally, it is also possible to quantify the maximal rate of oxidative ATP resynthesis (Q_{max}) from a PCr recovery experiment. To do so, one of three models is

often used, however here we only describe the "ADP-based" model. It states that the concentration of ADP at the end of exercise (ADP_{end}), calculated through Eq.2.2, is related to the mitochondrial capacity ($Q_{max-ADP}$) through a sigmoid relationship with a Hill coefficient ($n_H = 2$), which also includes a basal ATP turnover ($Q_b \approx 1.5 - 2.4 mM/min$) (Kemp et al. 2007; Valkovič et al. 2017):

$$Q_{max-ADP} = (V_{iPCr} + Q_b) \cdot \left[1 + \left(\frac{k_m}{[ADP]_{end}}\right)^{n_H}\right] \tag{2.7}$$

Here, k_m is the value of [ADP] at the half-maximal oxidation rate, which ranges between 22μM and 44μM in skeletal muscle (Kemp and Radda 1994; Jeneson et al. 2009; Jeneson et al. 1996).

Aside of the multinuclear capability of the MR system, the success of these types of experiments require additional components. First, one of the above discussed pulse sequences with a temporal resolution on the order of a few seconds (i.e. <10s), as the processes being investigated are relatively fast. PCr recovery happens in a few minutes for healthy individuals. Also, the exercise has to be carefully synchronized with the MR-data acquisition and performed using an MR compatible device inside the system's bore. The design of such a device depends on the task to be performed. Usually, plantar flexion with a load is the paradigm of choice in order to stimulate the calf muscles and create the PCr depletion. This task can be performed in a variety of ways, ranging from the simple use of elastic bands (Parasoglou et al. 2012; Parasoglou et al. 2013b) to more complex commercially available MR compatible ergometers that offer measurements of force (Isbell et al. 2007; Pesta et al. 2013; Schocke et al. 2005). However, a common approach

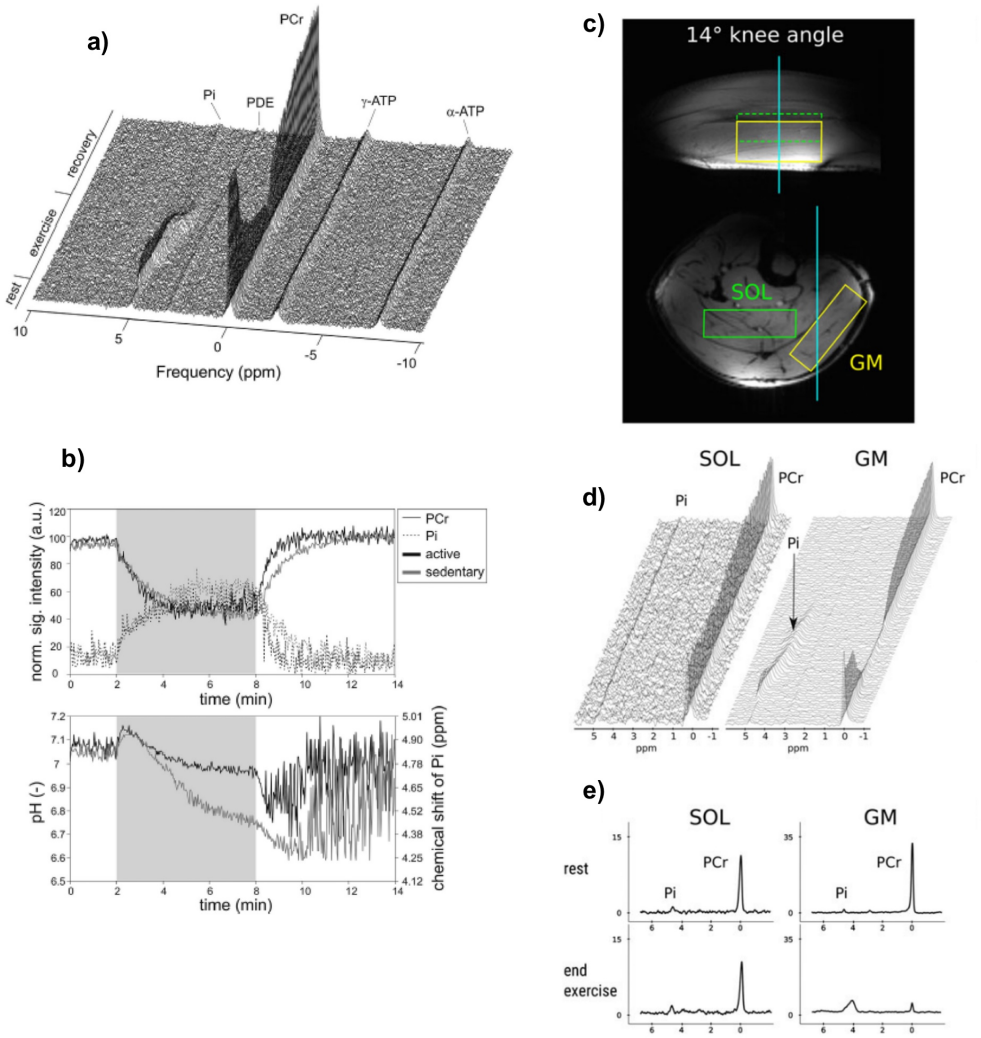

FIGURE 2.4: ^{31}P-MRS dynamic experiment of exercise challenge. Dynamically acquired spectra are depicted in **a)**. Note that while PCr depletes and Pi rises, ATP levels remain constant. **b)** shows the time-courses of the normalized PCr and Pi signal intensities and the evolution of the calculated pH based on the chemical shift of Pi. Dara compares regularly active (black lines) and sedentary (grey lines) volunteers. The grey area indicates the 6-min long exercise period (reprint from Valkovič et al. 2017). **c-e)** show the ^{1}H images with voxel placement in gastrocnemius (GM, yellow) and soleus (SOL, green) muscles, the time series of dynamic spectra and examples of spectra at rest and the end of exercise, respectively(reprint from Niess et al. 2018).

is to use in-house-built ergometers that fit the needs of the particular study (Meyerspeer et al. 2005; Layec et al. 2008; Jeneson et al. 2010; Meyerspeer et al. 2012; Tschiesche et al. 2014). Overall, it is important to consider the task, positioning and ergometer design to perform a successful dynamic experiment, especially if the study at hand involves multiple sites (Šedivý et al. 2015).

2.6 Assessment of brain metabolism

The powerful capability of ^{31}P-MRS to non-invasively measure fundamental compounds in energy metabolism has been exploited to better characterize and understand the energetic processes happening in the brain, whether healthy or in diseased condition.

The first step towards understanding energy metabolism processes in the brain is by characterizing the properties of phosphorus metabolites in a healthy condition. First, it is necessary to account for tissue differences in the metabolite concentrations and correct for it in order to produce more reliable results. Gray matter (GM) has been found to have higher ratios of PCr/ATP and PCr to total ^{31}P signal compared to White matter (WM) whereas no differences were found in pH and PCr/Pi (Hetherington et al. 2001; Mason et al. 1998). Aging also plays an important role when understanding the measurements, as there is an increase in PCr and decrease in pH and PME with age, probably reflecting reduced synthesis and degradation of cell membranes (Forester et al. 2010; Rae et al. 2003). To note, no differences were found in any of the metabolites when comparing men and women (Forester et al. 2010).

The brain is highly dependent on energy production, more so when compared to other organs. Thus it is logical to infer that various neurological disorders are related to energetic abnormalities. ^{31}P-MRS has been used in the investigation of many of these disorders; it has been use to study energetic impairments in neurodegenerative disorders such as Alzheimer's disease (Rijpma et al. 2018; Forlenza et al. 2005) and Parkinson's disease (Hu et al. 2000; Rango et al. 2006), multiple sclerosis (Husted et al. 1994), migraine (Schulz et al. 2007; Schulz et al. 2009), epilepsy (Laxer et al. 1992; Chu et al. 1998; Andrade et al. 2011; Andrade et al. 2014) and cerebral ischemia (Levine et al. 1992; Azzopardi et al. 1989; Martin et al. 1996; Yang et al. 2008). Also it has provided a tool to better determine the metabolic profile of brain tumors (Figure 2.5), where the main findings suggest a trend to alkalinization of meningiomas, glial tumors, lymphomas and astrocytomas. Furthermore, there are also differences in metabolite ratios noted in these masses (Maintz et al. 2002; Ha et al. 2013).

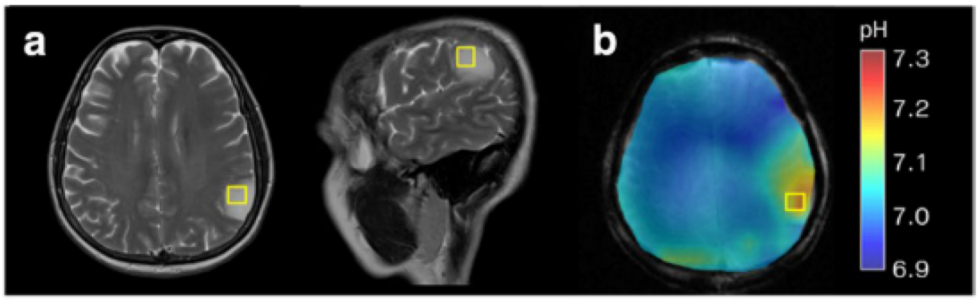

FIGURE 2.5: ^{31}P FID MRSI at 9.4T allows visualization of pH changes in a brain tumor (reprint with permission from Mirkes et al. 2016)

In spite of the widespread applications in neurological pathologies, ^{31}P-MRS has played a bigger role in the study of psychiatric illness. In a recent review of phosphorus spectroscopy studies in schizophrenia, Yuksel et al. 2015 summarized

the main findings. According to his review, literature showed multiple discrepancies and weak patterns. One of the reported abnormalities was reduced PME and increased PDE in the frontal lobe, however medication may play a crucial role. Another pattern was decreased PDE in subcortical structures, consistent across chronic patient studies. Regarding energy metabolites, the author and colleagues were not able to find any consistent pattern. Nonetheless, the non-conclusive findings using ^{31}P-MRS, research in this field remains promising. In that same review, suggestions were made regarding future directions; (1) Perform studies in higher field strengths; (2) To correct for tissue composition and (3) Investigate dynamic enzyme reactions in addition to metabolite concentrations.

With regards to bipolar disease (BD), major findings support mitochondrial dysfunction depicted by decreased intracellular pH and metabolic differences in PCr and PME, when compared to controls (Lee et al. 2012). In more recent studies, Dudley et al. have proposed age and tissue dependencies in patients with BD (Dudley et al. 2015; Dudley et al. 2016).

Another mood disorder that has been studied using ^{31}P-MRS is major depression disorder (MDD), where a recent report showed tissue specific bioenergetic abnormalities, in particular, variations of PCr and Pi in opposite directions when comparing gray and white matter of depressed adults to healthy controls (Harper et al. 2017).

A much less studied condition is attention deficit/hyperactive disorder (ADHD), however the few reports on it suggest alterations in the PME levels across different brain regions such as prefrontal cortex and basal ganglia (Stanley et al. 2006; Stanley et al. 2008).

Finally, the study of brain energy metabolism using ^{31}P-MRS will be strongly benefited by the use of ultra-high field MR systems. A recent review in the field points to the contributions and advantages of using such systems (Henning 2018). To highlight from the limited amount of studies conducted so far, amongst the main contributions we have: findings suggesting that 77% of the energy consumption in the brain happens in GM (Zhu et al. 2012), the in vivo detection of NAD+/NADH redox state (Zhu et al. 2015) and the capability to create high-resolution maps of brain intracellular pH at 9.4T (Mirkes et al. 2016).

References

Andrade, C. S., Otaduy, M. C., Valente, K. D., Maia, D. F., Park, E. J., Valerio, R. M., Tsunemi, M. H., and Leite, C. C. (2011) Phosphorus magnetic resonance spectroscopy in malformations of cortical development *Epilepsia* 52.(12), 2276–2284.

Andrade, C. S., Otaduy, M. C. G., Valente, K. D. R., Park, E. J., Kanas, A. F., Silva Filho, M. R. M. da, Tsunemi, M. H., and Leite, C. C. (2014) Widespread pH abnormalities in patients with malformations of cortical development and epilepsy: A phosphorus-31 brain MR spectroscopy study *Brain and Development* 36.(10), 899–906.

Avdievich, N. I. (2011) Transceiver-phased arrays for human brain studies at 7 T *Applied magnetic resonance* 41.(2-4), 483–506.

Azzopardi, D., Wyatt, J., Cady, E., Delpy, D., Baudin, J., Stewart, A., Hope, P., Hamilton, P., and Reynolds, E. (1989) Prognosis of newborn infants with

hypoxic-ischemic brain injury assessed by phosphorus magnetic resonance spectroscopy *Pediatric Research* 25.(5), 445.

Bank, B. L. van de, Orzada, S., Smits, F., Lagemaat, M. W., Rodgers, C. T., Bitz, A. K., and Scheenen, T. W. (2015) Optimized 31P MRS in the human brain at 7 T with a dedicated RF coil setup *NMR in Biomedicine* 28.(11), 1570–1578.

Bernús, G., Suso González, J. de, Alonso, J., Martin, P. A., Prat, J. A., and Arús, C. (1993) 31P-MRS of quadriceps reveals quantitative differences between sprinters and long-distance runners. *Medicine and science in sports and exercise* 25.(4), 479–484.

Bogner, W., Chmelik, M., Andronesi, O., Sorensen, A., Trattnig, S., and Gruber, S. (2011) In vivo 31P spectroscopy by fully adiabatic extended image selected in vivo spectroscopy: a comparison between 3 T and 7 T *Magnetic resonance in medicine* 66.(4), 923–930.

Bogner, W., Chmelik, M., Schmid, A., Moser, E., Trattnig, S., and Gruber, S. (2009) Assessment of 31P relaxation times in the human calf muscle: a comparison between 3 T and 7 T in vivo *Magnetic Resonance in Medicine: An Official Journal of the International Society for Magnetic Resonance in Medicine* 62.(3), 574–582.

Brown, R., Lakshmanan, K., Madelin, G., and Parasoglou, P. (2016) A nested phosphorus and proton coil array for brain magnetic resonance imaging and spectroscopy *Neuroimage* 124, 602–611.

Brown, T. R., Stoyanova, R., Greenberg, T., Srinivasan, R., and Murphy-Boesch, J. (1995) NOE enhancements and T1 relaxation times of phosphorylated metabolites in human calf muscle at 1.5 Tesla *Magnetic resonance in medicine* 33.(3), 417–421.

Chmelik, M., Just Kukurová, I., Gruber, S., Krssák, M., Valkovic, L., Trattnig, S., and Bogner, W. (2013) Fully adiabatic 31P 2D-CSI with reduced chemical shift displacement error at 7 T—GOIA-1D-ISIS/2D-CSI *Magnetic resonance in medicine* 69.(5), 1233–1244.

Chu, W.-J., Hetherington, H., Kuzniecky, R., Simor, T., Mason, G., and Elgavish, G. A. (1998) Lateralization of human temporal lobe epilepsy by 31P NMR spectroscopic imaging at 4.1 T *Neurology* 51.(2), 472–479.

Crowther, G. J., Milstein, J. M., Jubrias, S. A., Kushmerick, M. J., Gronka, R. K., and Conley, K. E. (2003) Altered energetic properties in skeletal muscle of men with well-controlled insulin-dependent (type 1) diabetes *American Journal of Physiology-Endocrinology and Metabolism* 284.(4), E655–E662.

De Graaf, R. A. (2013) *In vivo NMR spectroscopy: principles and techniques* John Wiley & Sons.

Deelchand, D. K., Nguyen, T.-M., Zhu, X.-H., Mochel, F., and Henry, P.-G. (2015) Quantification of in vivo 31P NMR brain spectra using LCModel *NMR in Biomedicine* 28.(6), 633–641.

Du, F., Zhu, X.-H., Qiao, H., Zhang, X., and Chen, W. (2007) Efficient in vivo 31P magnetization transfer approach for noninvasively determining multiple kinetic parameters and metabolic fluxes of ATP metabolism in the human brain *Magnetic Resonance in Medicine: An Official Journal of the International Society for Magnetic Resonance in Medicine* 57.(1), 103–114.

Dudley, J. A., Lee, J.-H., Durling, M., Strakowski, S. M., and Eliassen, J. C. (2015) Age-dependent decreases of high energy phosphates in cerebral gray matter of patients with bipolar I disorder: a preliminary phosphorus-31 magnetic resonance spectroscopic imaging study *Journal of affective disorders* 175, 251–255.

Dudley, J., DelBello, M. P., Weber, W. A., Adler, C. M., Strakowski, S. M., and Lee, J.-H. (2016) Tissue-dependent cerebral energy metabolism in adolescents with bipolar disorder *Journal of affective disorders* 191, 248–255.

Fiedler, G. B., Meyerspeer, M., Schmid, A. I., Goluch, S., Schewzow, K., Laistler, E., Mirzahosseini, A., Niess, F., Unger, E., Wolzt, M., et al. (2015) Localized semi-LASER dynamic 31 P magnetic resonance spectroscopy of the soleus during and following exercise at 7 T *Magnetic Resonance Materials in Physics, Biology and Medicine* 28.(5), 493–501.

Forester, B. P., Berlow, Y. A., Harper, D. G., Jensen, J. E., Lange, N., Froimowitz, M. P., Ravichandran, C., Iosifescu, D. V., Lukas, S. E., Renshaw, P. F., et al. (2010) Age-related changes in brain energetics and phospholipid metabolism *NMR in Biomedicine* 23.(3), 242–250.

Forlenza, O. V., Wacker, P., Nunes, P. V., Yacubian, J., Castro, C. C., Otaduy, M. C., and Gattaz, W. F. (2005) Reduced phospholipid breakdown in Alzheimer's brains: a 31 P spectroscopy study *Psychopharmacology* 180.(2), 359–365.

Goluch, S., Kuehne, A., Meyerspeer, M., Kriegl, R., Schmid, A. I., Fiedler, G. B., Herrmann, T., Mallow, J., Hong, S.-M., Cho, Z.-H., et al. (2015) A form-fitted three channel 31P, two channel 1H transceiver coil array for calf muscle studies at 7 T *Magnetic resonance in medicine* 73.(6), 2376–2389.

Gonen, O., Mohebbi, A., Stoyanova, R., and Brown, T. R. (1997) In vivo phosphorus polarization transfer and decoupling from protons in three-dimensional localized nuclear magnetic resonance spectroscopy of human brain *Magnetic resonance in medicine* 37.(2), 301–306.

Greenman, R. L. and Smithline, H. A. (2011) The feasibility of measuring phosphocreatine recovery kinetics in muscle using a single-shot 31P RARE MRI sequence *Academic radiology* 18.(7), 917–923.

Greenman, R. L., Wang, X., and Smithline, H. A. (2011) Simultaneous acquisition of phosphocreatine and inorganic phosphate images for Pi: PCr ratio mapping using a RARE sequence with chemically selective interleaving *Magnetic resonance imaging* 29.(8), 1138–1144.

Greiner, A., Esterhammer, R., Messner, H., Biebl, M., Mühlthaler, H., Fraedrich, G., Jaschke, W. R., and Schocke, M. F. (2006) High-energy phosphate metabolism during incremental calf exercise in patients with unilaterally symptomatic peripheral arterial disease measured by phosphor 31 magnetic resonance spectroscopy *Journal of vascular surgery* 43.(5), 978–986.

Gupta, R. K., Gupta, P., and Moore, R. D. (1984) NMR studies of intracellular metal ions in intact cells and tissues *Annual review of biophysics and bioengineering* 13.(1), 221–246.

Ha, D.-H., Choi, S., Oh, J. Y., Yoon, S. K., Kang, M. J., and Kim, K.-U. (2013) Application of 31P MR spectroscopy to the brain tumors *Korean journal of radiology* 14.(3), 477–486.

Harper, D. G., Jensen, J. E., Ravichandran, C., Perlis, R. H., Fava, M., Renshaw, P. F., and Iosifescu, D. V. (2017) Tissue type-specific bioenergetic abnormalities in adults with major depression *Neuropsychopharmacology* 42.(4), 876.

Hatay, G. H., Yildirim, M., and Ozturk-Isik, E. (2017) Considerations in applying compressed sensing to in vivo phosphorus MR spectroscopic imaging of human brain at 3T *Medical & biological engineering & computing* 55.(8), 1303–1315.

Henning, A. (2018) Proton and multinuclear magnetic resonance spectroscopy in the human brain at ultra-high field strength: A review *NeuroImage* 168, 181–198.

Hetherington, H., Spencer, D., Vaughan, J., and Pan, J. (2001) Quantitative 31P spectroscopic imaging of human brain at 4 Tesla: assessment of gray and white matter differences of phosphocreatine and ATP *Magnetic Resonance in Medicine: An Official Journal of the International Society for Magnetic Resonance in Medicine* 45.(1), 46–52.

Hu, M., Taylor-Robinson, S. D., Chaudhuri, K. R., Bell, J. D., Labbe, C., Cunningham, V., Koepp, M., Hammers, A., Morris, R., Turjanski, N., et al. (2000) Cortical dysfunction in non-demented Parkinson's disease patients: A combined 31P-MRS and 18FDG-PET study *Brain* 123.(2), 340–352.

Hug, F., Bendahan, D., Le, Y. F., Cozzone, P. J., and GrÉlot, L. (2005) Metabolic recovery in professional road cyclists: a 31P-MRS study. *Medicine and science in sports and exercise* 37.(5), 846–852.

Hug, F., Marqueste, T., Le Fur, Y., Cozzone, P. J., Grélot, L., and Bendahan, D. (2006) Selective training-induced thigh muscles hypertrophy in professional road cyclists *European journal of applied physiology* 97.(5), 591–597.

Husted, C., Matson, G., Adams, D., Goodin, D., and Weiner, M. (1994) In vivo detection of myelin phospholipids in multiple sclerosis with phosphorus magnetic resonance spectroscopic imaging *Annals of Neurology: Official Journal of the American Neurological Association and the Child Neurology Society* 36.(2), 239–241.

Iotti, S., Frassineti, C., Alderighi, L., Sabatini, A., Vacca, A., and Barbiroli, B. (1996) In vivo assessment of free magnesium concentration in human brain

by 31P MRS. A new calibration curve based on a mathematical algorithm *NMR in Biomedicine: An International Journal Devoted to the Development and Application of Magnetic Resonance In Vivo* 9.(1), 24–32.

Isbell, D. C., Berr, S. S., Toledano, A. Y., Epstein, F. H., Meyer, C. H., Rogers, W. J., Harthun, N. L., Hagspiel, K. D., Weltman, A., and Kramer, C. M. (2006) Delayed calf muscle phosphocreatine recovery after exercise identifies peripheral arterial disease *Journal of the American College of Cardiology* 47.(11), 2289–2295.

Isbell, D. C., Epstein, F. H., Zhong, X., DiMaria, J. M., Berr, S. S., Meyer, C. H., Rogers, W. J., Harthun, N. L., Hagspiel, K. D., Weltman, A., et al. (2007) Calf muscle perfusion at peak exercise in peripheral arterial disease: Measurement by first-pass contrast-enhanced magnetic resonance imaging *Journal of Magnetic Resonance Imaging: An Official Journal of the International Society for Magnetic Resonance in Medicine* 25.(5), 1013–1020.

Jeneson, J. A., Schmitz, J. P., Broek, N. M. van den, Riel, N. A. van, Hilbers, P. A., Nicolay, K., and Prompers, J. J. (2009) Magnitude and control of mitochondrial sensitivity to ADP *American Journal of Physiology-Endocrinology and Metabolism* 297.(3), E774–E784.

Jeneson, J. A., Schmitz, J. P., Hilbers, P. A., and Nicolay, K. (2010) An MR-compatible bicycle ergometer for in-magnet whole-body human exercise testing *Magnetic Resonance in Medicine: An Official Journal of the International Society for Magnetic Resonance in Medicine* 63.(1), 257–261.

Jeneson, J. A., Wiseman, R. W., Westerhoff, H. V., and Kushmerick, M. J. (1996) The signal transduction function for oxidative phosphorylation is at least second order in ADP *Journal of Biological Chemistry* 271.(45), 27995–27998.

Kan, H., Klomp, D., Wong, C., Boer, V., Webb, A., Luijten, P., and Jeneson, J. (2010) In vivo 31P MRS detection of an alkaline inorganic phosphate pool with short T1 in human resting skeletal muscle *NMR in biomedicine* 23.(8), 995–1000.

Kemp, G., Ahmad, R., Nicolay, K., and Prompers, J. (2015) Quantification of skeletal muscle mitochondrial function by 31 P magnetic resonance spectroscopy techniques: a quantitative review *Acta physiologica* 213.(1), 107–144.

Kemp, G. and Radda, G. (1994) Quantitative interpretation of bioenergetic data from 31P and 1H magnetic resonance spectroscopic studies of skeletal muscle: an analytical review. *Magnetic resonance quarterly* 10.(1), 43–63.

Kemp, G., Taylor, D., Thompson, C., Hands, L., Rajagopalan, B., Styles, P., and Radda, G. (1993) Quantitative analysis by 31P magnetic resonance spectroscopy of abnormal mitochondrial oxidation in skeletal muscle during recovery from exercise *NMR in biomedicine* 6.(5), 302–310.

Kemp, G. J., Meyerspeer, M., and Moser, E. (2007) Absolute quantification of phosphorus metabolite concentrations in human muscle in vivo by 31P MRS: a quantitative review *NMR in Biomedicine: An International Journal Devoted to the Development and Application of Magnetic Resonance In vivo* 20.(6), 555–565.

Khegai, O., Madelin, G., Brown, R., and Parasoglou, P. (2018) Dynamic phosphocreatine imaging with unlocalized pH assessment of the human lower leg muscle following exercise at 3T *Magnetic resonance in medicine* 79.(2), 974–980.

Klomp, D., Wijnen, J., Scheenen, T., and Heerschap, A. (2008) Efficient 1H to 31P polarization transfer on a clinical 3T MR system *Magnetic Resonance in*

Medicine: An Official Journal of the International Society for Magnetic Resonance in Medicine 60.(6), 1298–1305.

Korzowski, A. and Bachert, P. (2018) High-resolution 31 P echo-planar spectroscopic imaging in vivo at 7 T *Magnetic resonance in medicine* 79.(3), 1251–1259.

Laxer, K. D., Hubesch, B., Sappey-Marinier, D., and Weiner, M. W. (1992) Increased pH and Seizure Foci Inorganic Phosphate in Temporal Demonstrated by [31P] MRS *Epilepsia* 33.(4), 618–623.

Layec, G., Bringard, A., Vilmen, C., Micallef, J.-P., Le Fur, Y., Perrey, S., Cozzone, P. J., and Bendahan, D. (2008) Accurate work-rate measurements during in vivo MRS studies of exercising human quadriceps *Magnetic Resonance Materials in Physics, Biology and Medicine* 21.(3), 227–235.

Lee, J.-H., Komoroski, R. A., Chu, W.-J., and Dudley, J. A. (2012) Methods and Applications of Phosphorus NMR Spectroscopy In Vivo *Annual Reports on NMR Spectroscopy* 75, 115.

Lei, H., Zhu, X.-H., Zhang, X.-L., Ugurbil, K., and Chen, W. (2003) In vivo 31P magnetic resonance spectroscopy of human brain at 7 T: an initial experience *Magnetic Resonance in Medicine: An Official Journal of the International Society for Magnetic Resonance in Medicine* 49.(2), 199–205.

Levine, S., Helpern, J., Welch, K., Vande Linde, A., Sawaya, K., Brown, E., Ramadan, N., Deveshwar, R., and Ordidge, R. (1992) Human focal cerebral ischemia: evaluation of brain pH and energy metabolism with P-31 NMR spectroscopy. *Radiology* 185.(2), 537–544.

Löring, J., Kemp, W. van der, Almujayyaz, S., Oorschot, J. van, Luijten, P., and Klomp, D. (2016) Whole-body radiofrequency coil for 31P MRSI at 7 T *NMR in biomedicine* 29.(6), 709–720.

Luyten, P. R., Bruntink, G., Sloff, F. M., Vermeulen, J. W., Van Der Heijden, J. I., Den Hollander, J. A., and Heerschap, A. (1989) Broadband proton decoupling in human 31P NMR spectroscopy *NMR in Biomedicine* 1.(4), 177–183.

Ma, C., Clifford, B., Liu, Y., Gu, Y., Lam, F., Yu, X., and Liang, Z.-P. (2017) High-resolution dynamic 31P-MRSI using a low-rank tensor model *Magnetic resonance in medicine* 78.(2), 419–428.

Maintz, D., Heindel, W., Kugel, H., Jaeger, R., and Lackner, K. J. (2002) Phosphorus-31 MR spectroscopy of normal adult human brain and brain tumours *NMR in Biomedicine: An International Journal Devoted to the Development and Application of Magnetic Resonance In Vivo* 15.(1), 18–27.

Martin, E., Buchli, R., Ritter, S., Schmid, R., Largo, R. H., Boltshauser, E., Fanconi, S., Duc, G., and Rumpel, H. (1996) Diagnostic and prognostic value of cerebral 31 P magnetic resonance spectroscopy in neonates with perinatal asphyxia *Pediatric research* 40.(5), 749.

Mason, G. F., Chu, W.-J., Vaughan, J. T., Ponder, S. L., Twieg, D. B., Adams, D., and Hetherington, H. P. (1998) Evaluation of 31P metabolite differences in human cerebral gray and white matter *Magnetic resonance in medicine* 39.(3), 346–353.

Meyerspeer, M., Krššák, M., Kemp, G., Roden, M., and Moser, E. (2005) Dynamic interleaved 1 H/31 P STEAM MRS at 3 Tesla using a pneumatic force-controlled plantar flexion exercise rig *Magnetic Resonance Materials in Physics, Biology and Medicine* 18.(5), 257–262.

Meyerspeer, M., Robinson, S., Nabuurs, C. I., Scheenen, T., Schoisengeier, A., Unger, E., Kemp, G. J., and Moser, E. (2012) Comparing localized and nonlocalized dynamic 31P magnetic resonance spectroscopy in exercising muscle at 7T *Magnetic resonance in medicine* 68.(6), 1713–1723.

Meyerspeer, M., Scheenen, T., Schmid, A. I., Mandl, T., Unger, E., and Moser, E. (2011) Semi-LASER localized dynamic 31P magnetic resonance spectroscopy in exercising muscle at ultra-high magnetic field *Magnetic resonance in medicine* 65.(5), 1207–1215.

Mirkes, C., Shajan, G., Chadzynski, G., Buckenmaier, K., Bender, B., and Scheffler, K. (2016) 31P CSI of the human brain in healthy subjects and tumor patients at 9.4 T with a three-layered multi-nuclear coil: initial results *Magnetic Resonance Materials in Physics, Biology and Medicine* 29.(3), 579–589.

Moon, R. B. and Richards, J. H. (1973) Determination of intracellular pH by 31P magnetic resonance *Journal of Biological Chemistry* 248.(20), 7276–7278.

Moonen, C. T., Kienlin, M. V., Van Zijl, P. C., Cohen, J., Gillen, J., Daly, P., and Wolf, G. (1989) Comparison of single-shot localization methods (STEAM and PRESS) for in vivo proton NMR spectroscopy *NMR in Biomedicine* 2.(5-6), 201–208.

Murphy-Boesch, J., Stoyanova, R., Srinivasan, R., Willard, T., Vigneron, D., Nelson, S., Taylor, J. S., and Brown, T. R. (1993) Proton-decoupled 31P chemical shift imaging of the human brain in normal volunteers *NMR in biomedicine* 6.(3), 173–180.

Newman, R. J., Bore, P. J., Chan, L., Gadian, D. G., Styles, P., Taylor, D., and Radda, G. K. (1982) Nuclear magnetic resonance studies of forearm muscle in Duchenne dystrophy. *Br Med J (Clin Res Ed)* 284.(6322), 1072–1074.

Niess, F., Fiedler, G. B., Schmid, A. I., Goluch, S., Kriegl, R., Wolzt, M., Moser, E., and Meyerspeer, M. (2017) Interleaved multivoxel 31P MR spectroscopy *Magnetic resonance in medicine* 77.(3), 921–927.

Niess, F., Fiedler, G. B., Schmid, A. I., Laistler, E., Frass-Kriegl, R., Wolzt, M., Moser, E., and Meyerspeer, M. (2018) Dynamic multivoxel-localized 31P MRS during plantar flexion exercise with variable knee angle *NMR in Biomedicine* 31.(6), e3905.

Ordidge, R. J., Connelly, A., and Lohman, J. A. (1986) Image-selected in vivo spectroscopy (ISIS). A new technique for spatially selective NMR spectroscopy *Journal of Magnetic Resonance (1969)* 66.(2), 283–294.

Parasoglou, P., Feng, L., Xia, D., Otazo, R., and Regatte, R. R. (2012) Rapid 3D-imaging of phosphocreatine recovery kinetics in the human lower leg muscles with compressed sensing *Magnetic resonance in medicine* 68.(6), 1738–1746.

Parasoglou, P., Xia, D., Chang, G., and Regatte, R. R. (2013a) 3D-mapping of phosphocreatine concentration in the human calf muscle at 7 T: Comparison to 3 T *Magnetic Resonance in Medicine* 70.(6), 1619–1625.

Parasoglou, P., Xia, D., Chang, G., and Regatte, R. R. (2013b) Dynamic three-dimensional imaging of phosphocreatine recovery kinetics in the human lower leg muscles at 3T and 7T: a preliminary study *NMR in Biomedicine* 26.(3), 348–356.

Parasoglou, P., Xia, D., and Regatte, R. R. (2013c) Spectrally selective 3D TSE imaging of phosphocreatine in the human calf muscle at 3 T *Magnetic resonance in medicine* 69.(3), 812–817.

Park, J. H., Phothimat, P., Oates, C. T., Hernanz-Schulman, M., and Olsen, N. J. (1998) Use of P-31 magnetic resonance spectroscopy to detect metabolic abnormalities in muscles of patients with fibromyalgia *Arthritis & Rheumatism: Official Journal of the American College of Rheumatology* 41.(3), 406–413.

Pesta, D., Paschke, V., Hoppel, F., Kobel, C., Kremser, C., Esterhammer, R., Burtscher, M., Kemp, G. J., and Schocke, M. (2013) Different metabolic responses during incremental exercise assessed by localized 31P MRS in sprint and endurance athletes and untrained individuals *Int J Sports Med* (34), 669–675.

Pohmann, R., Von Kienlin, M., and Haase, A. (1997) Theoretical evaluation and comparison of fast chemical shift imaging methods *Journal of Magnetic Resonance* 129.(2), 145–160.

Purvis, L. A., Clarke, W. T., Biasiolli, L., Valkovič, L., Robson, M. D., and Rodgers, C. T. (2017) OXSA: An open-source magnetic resonance spectroscopy analysis toolbox in MATLAB *PloS one* 12.(9), e0185356.

Qiao, H., Zhang, X., Zhu, X.-H., Du, F., and Chen, W. (2006) In vivo 31P MRS of human brain at high/ultrahigh fields: a quantitative comparison of NMR detection sensitivity and spectral resolution between 4 T and 7 T *Magnetic resonance imaging* 24.(10), 1281–1286.

Rae, C., Scott, R. B., Lee, M., Simpson, J. M., Hines, N., Paul, C., Anderson, M., Karmiloff-Smith, A., Styles, P., and Radda, G. K. (2003) Brain bioenergetics and cognitive ability *Developmental neuroscience* 25.(5), 324–331.

Raghavan, R. S., Panda, A., Valette, J., James, J., Heberlein, K., Boettcher, U., Henry, P., Bansal, N., and Dydak, U. (2009) 31P spectroscopic imaging with

GRAPPA in: *Proceedings of the 17th Annual Meeting of ISMRM, Honolulu, Hawaii, USA*, 4317.

Rango, M., Bonifati, C., and Bresolin, N. (2006) Parkinson's disease and brain mitochondrial dysfunction: a functional phosphorus magnetic resonance spectroscopy study *Journal of Cerebral Blood Flow & Metabolism* 26.(2), 283–290.

Ren, J., Sherry, A. D., and Malloy, C. R. (2015) 31P-MRS of healthy human brain: ATP synthesis, metabolite concentrations, pH, and T1 relaxation times *NMR in Biomedicine* 28.(11), 1455–1462.

Rijpma, A., Graaf, M. van der, Meulenbroek, O., Rikkert, M. G. O., and Heerschap, A. (2018) Altered brain high-energy phosphate metabolism in mild Alzheimer's disease: A 3-dimensional 31P MR spectroscopic imaging study *NeuroImage: Clinical* 18, 254.

Santos-Díaz, A., Obruchkov, S. I., Schulte, R. F., and Noseworthy, M. D. (2018) Phosphorus magnetic resonance spectroscopic imaging using flyback echo planar readout trajectories *Magnetic Resonance Materials in Physics, Biology and Medicine*, 1–12.

Satrústegui, J., Berkowitz, H., Boden, B., Donlon, E., Mclaughlin, A., Maris, J., Warnell, R., and Chance, B. (1988) An in vivo phosphorus nuclear magnetic resonance study of the variations with age in the phosphodiers' content of human muscle *Mechanisms of ageing and development* 42.(2), 105–114.

Scheuermann-Freestone, M., Madsen, P. L., Manners, D., Blamire, A. M., Buckingham, R. E., Styles, P., Radda, G. K., Neubauer, S., and Clarke, K. (2003) Abnormal cardiac and skeletal muscle energy metabolism in patients with type 2 diabetes *Circulation* 107.(24), 3040–3046.

Schmid, A. I., Meyerspeer, M., Robinson, S. D., Goluch, S., Wolzt, M., Fiedler, G. B., Bogner, W., Laistler, E., Krššák, M., Moser, E., et al. (2016) Dynamic PCr and pH imaging of human calf muscles during exercise and recovery using 31P gradient-Echo MRI at 7 Tesla *Magnetic resonance in medicine* 75.(6), 2324–2331.

Schocke, M. F. H., Esterhammer, R., Arnold, W., Kammerlander, C., Burtscher, M., Fraedrich, G., Jaschke, W. R., and Greiner, A. (2005) High-energy phosphate metabolism during two bouts of progressive calf exercise in humans measured by phosphorus-31 magnetic resonance spectroscopy *European Journal of Applied Physiology* 93.(4), 469–479.

Schulz, U., Blamire, A., Corkill, R., Davies, P., Styles, P., and Rothwell, P. (2007) Association between cortical metabolite levels and clinical manifestations of migrainous aura: an MR-spectroscopy study *Brain* 130.(12), 3102–3110.

Schulz, U. G., Blamire, A. M., Davies, P., Styles, P., and Rothwell, P. M. (2009) Normal cortical energy metabolism in migrainous stroke: A 31P-MR spectroscopy study *Stroke* 40.(12), 3740–3744.

Šedivý, P., Christina Kipfelsberger, M., Dezortová, M., Krššák, M., Drobný, M., Chmelík, M., Rydlo, J., Trattnig, S., Hájek, M., and Valkovič, L. (2015) Dynamic 31P MR spectroscopy of plantar flexion: influence of ergometer design, magnetic field strength (3 and 7 T), and RF-coil design *Medical physics* 42.(4), 1678–1689.

Sleigh, A., Stears, A., Thackray, K., Watson, L., Gambineri, A., Nag, S., Campi, V. I., Schoenmakers, N., Brage, S., Carpenter, T. A., et al. (2012) Mitochondrial oxidative phosphorylation is impaired in patients with congenital lipodystrophy *The Journal of Clinical Endocrinology & Metabolism* 97.(3), E438–E442.

Stanley, J. A., Kipp, H., Greisenegger, E., MacMaster, F. P., Panchalingam, K., Keshavan, M. S., Bukstein, O. G., and Pettegrew, J. W. (2008) Evidence of developmental alterations in cortical and subcortical regions of children with attention-deficit/hyperactivity disorder: a multivoxel in vivo phosphorus 31 spectroscopy study *Archives of general psychiatry* 65.(12), 1419–1428.

Stanley, J. A., Kipp, H., Greisenegger, E., MacMaster, F. P., Panchalingam, K., Pettegrew, J. W., Keshavan, M. S., and Bukstein, O. G. (2006) Regionally specific alterations in membrane phospholipids in children with ADHD: An in vivo 31P spectroscopy study *Psychiatry Research: Neuroimaging* 148.(2-3), 217–221.

Stefan, D., Di Cesare, F., Andrasescu, A., Popa, E., Lazariev, A., Vescovo, E., Strbak, O., Williams, S., Starcuk, Z., Cabanas, M., et al. (2009) Quantitation of magnetic resonance spectroscopy signals: the jMRUI software package *Measurement Science and Technology* 20.(10), 104035.

Taivassalo, T., Shoubridge, E. A., Chen, J., Kennaway, N. G., DiMauro, S., Arnold, D. L., and Haller, R. G. (2001) Aerobic conditioning in patients with mitochondrial myopathies: physiological, biochemical, and genetic effects *Annals of neurology* 50.(2), 133–141.

Taylor, D., Kemp, G., and Radda, G. (1994) Bioenergetics of skeletal muscle in mitochondrial myopathy *Journal of the neurological sciences* 127.(2), 198–206.

Tonson, A., Ratel, S., Le Fur, Y., Vilmen, C., Cozzone, P. J., and Bendahan, D. (2010) Muscle energetics changes throughout maturation: a quantitative 31P-MRS analysis *Journal of Applied Physiology* 109.(6), 1769–1778.

Tschiesche, K., Rothamel, M., Rzanny, R., Gussew, A., Hiepe, P., and Reichenbach, J. R. (2014) MR-compatible pedal ergometer for reproducible exercising of the human calf muscle *Medical engineering & physics* 36.(7), 933–937.

Ulrich, M., Wokrina, T., Ende, G., Lang, M., and Bachert, P. (2007) 31P-{1H} echo-planar spectroscopic imaging of the human brain in vivo *Magnetic Resonance in Medicine: An Official Journal of the International Society for Magnetic Resonance in Medicine* 57.(4), 784–790.

Valkovič, L., Chmelík, M., and Krššák, M. (2017) In-vivo 31P-MRS of skeletal muscle and liver: a way for non-invasive assessment of their metabolism *Analytical biochemistry* 529, 193–215.

Valkovic, L., Chmelík, M., Meyerspeer, M., Gagoski, B., Rodgers, C. T., Krssák, M., Andronesi, O. C., Trattnig, S., and Bogner, W. (2016) Dynamic 31P–MRSI using spiral spectroscopic imaging can map mitochondrial capacity in muscles of the human calf during plantar flexion exercise at 7 T *NMR in Biomedicine* 29.(12), 1825–1834.

Valkovic, L., Chmelik, M., Just Kukurova, I., Jakubova, M., Kipfelsberger, M. C., Krumpolec, P., Tušek Jelenc, M., Bogner, W., Meyerspeer, M., Ukropec, J., et al. (2014) Depth-resolved surface coil MRS (DRESS)-localized dynamic 31P-MRS of the exercising human gastrocnemius muscle at 7 T *NMR in Biomedicine* 27.(11), 1346–1352.

Valkovič, L., Chmelík, M., Ukropcová, B., Heckmann, T., Bogner, W., Frollo, I., Tschan, H., Krebs, M., Bachl, N., Ukropec, J., et al. (2016) Skeletal muscle alkaline Pi pool is decreased in overweight-to-obese sedentary subjects and relates to mitochondrial capacity and phosphodiester content *Scientific reports* 6, 20087.

Van der Kemp, W., Boer, V., Luijten, P., and Klomp, D. (2014) Increased sensitivity of 31P MRSI using direct detection integrated with multi-echo polarization transfer (DIMEPT) *NMR in Biomedicine* 27.(10), 1248–1255.

Van der Kemp, W., Boer, V., Luijten, P., Stehouwer, B., Veldhuis, W., and Klomp, D. (2013) Adiabatic multi-echo 31P spectroscopic imaging (AMESING) at 7 T for the measurement of transverse relaxation times and regaining of sensitivity in tissues with short T2* values *NMR in biomedicine* 26.(10), 1299–1307.

Vanhamme, L., Boogaart, A. van den, and Van Huffel, S. (1997) Improved method for accurate and efficient quantification of MRS data with use of prior knowledge *Journal of magnetic resonance* 129.(1), 35–43.

Walter, G., Vandenborne, K., McCULLY, K. K., and Leigh, J. S. (1997) Noninvasive measurement of phosphocreatine recovery kinetics in single human muscles *American Journal of Physiology-Cell Physiology* 272.(2), C525–C534.

Wilhelm, T. and Bachert, P. (2001) *In vivo31P echo-planar spectroscopic imaging of human calf muscle*.

Wokke, B., Hooijmans, M., Bergen, J. van den, Webb, A., Verschuuren, J., and Kan, H. (2014) Muscle MRS detects elevated PDE/ATP ratios prior to fatty infiltration in Becker muscular dystrophy *NMR in Biomedicine* 27.(11), 1371–1377.

Yang, H., Tang, X., Tan, L., Zeng, L., and Hu, Z. (2008) Use of 31P magnetic resonance spectroscopy to study the effect of cortical magnesium and energy metabolism after subarachnoid hemorrhage *Cerebrovascular Diseases* 26.(3), 223–230.

Yuksel, C., Tegin, C., O'Connor, L., Du, F., Ahat, E., Cohen, B. M., and Ongur, D. (2015) Phosphorus magnetic resonance spectroscopy studies in schizophrenia *Journal of psychiatric research* 68, 157–166.

Zhu, X.-H., Lu, M., Lee, B.-Y., Ugurbil, K., and Chen, W. (2015) In vivo NAD assay reveals the intracellular NAD contents and redox state in healthy human brain and their age dependences *Proceedings of the National Academy of Sciences*, 201417921.

Zhu, X.-H., Qiao, H., Du, F., Xiong, Q., Liu, X., Zhang, X., Ugurbil, K., and Chen, W. (2012) Quantitative imaging of energy expenditure in human brain *Neuroimage* 60.(4), 2107–2117.

Chapter 3

Objectives and Methodology

3.1 Objectives

The assessment of energy metabolism through Phosphorus magnetic resonance spectroscopy (^{31}P-MRS) techniques plays a fundamental role in understanding bioenegetic processes in healthy and pathophysiological conditions. Thus, it is imperative to continue with the development of tools to achieve faster and better results. Under these premises, the work herein presented had the following objectives.

- To develop a Magnetic Resonance Imaging (MRI) pulse sequence using Echo planar spectroscopic imaging (EPSI) with flyback readout trajectories.
- To Characterize and test the sequence in phantoms and the calf muscles and brains of a group of healthy volunteers.

- To further accelerate the acquisition by modifying the EPSI sequence through the incorporation of compressed sensing (CS).

- To test and characterize the highly accelerated pulse sequence in phantoms and dynamic ^{31}P muscle experiments.

- To compare the performance of different CS reconstruction algorithms using data acquired from phantom experiments and brain tissue of healthy volunteers.

3.2 Methodology

This section gives a general description of the methodology followed in the development of this thesis work. Further details are explained in the chapter corresponding to each study.

3.2.1 MR system and Pulse sequences

All experiments were performed using a 60cm bore 3T GE MR750 (GE Healthcare, Milwaukee, WI) scanner (50mT/m amplitude and 200T/m/s slew rate gradient system). Pulse sequences were written in the EPIC programing language version DV25 (GE Healthcare, Milwaukee, WI).

For the first study, the EPSI pulse sequence with a flyback readout gradient trajectory was used to acquire data traversing k-space logical X direction in an asymmetric echo planar fashion with a constant gradient amplitude segment. This was

then reversing as fast as possible by maximizing the gradient slew rate to cover the same area. A pair of gradient trapezoids achieved this trajectory. The readout was performed only in one direction (during the constant segment) such that the phase evolution of spins happened always in the same direction, minimizing artifacts associated with phase reversal, gradient delays and eddy currents typically seen in echo planar techniques (see details in chapter 4). The acceleration factor achieved by this sequence was equal to the number of phase encoding steps in the Ky dimension when compared with chemical shift imaging (CSI) (i.e. an 8x8 matrix is acquired eight times faster).

In the second study, the flyback EPSI sequence was further accelerated through the inclusion of pseudo randomly distributed gradient blips in the ky direction during the flyback readout such that multiple ky-kt lines were sampled within the same phase encoding step. This increased the acceleration by a factor of x2.7, enough to perform dynamic studies of skeletal muscle (see chapter 5).

Finally, in the third study data was acquired using the same pulse sequences with CS acceleration factors ranging from x2 to x4. In this case, the objective was to assess the performance of two different reconstruction algorithms. The first one was the "traditional" compressed sensing reconstruction first proposed by Lustig (Lustig et al. 2007), which seeks for the sparse solution as the signal in the frequency domain with the least amount of non-zero values. And second, the low rank Hankel matrix completion approach presented by Qu (Qu et al. 2015) which exploits the sparsity of the NMR signal seeking for the solution with the least amount of spectral peaks (see chapter 6).

All data processing and reconstruction was performed using MATLAB R2014a

and R2015b (The Mathworks, Natick, MA, USA).

3.2.2 Participants and data acquisition

All the pulse sequences developed in this work were first tested using custom built spherical phantoms (volume = 1L) containing different concentrations of sodium phosphate and phosphocreatine disodium salt in order to mimic in vivo concentrations.

For the first study, data was collected from the calf muscles and brain of 5 healthy volunteers (2 female, 3 male, 25.6 ± 3.4 years old). In the second, dynamic experiments were performed in a total of 11 healthy volunteers (three female, eight male, 30.1 ± 6.48 years of age) whereas in the third, data was collected from the brain of 5 healthy volunteers (24.2 ± 6.5 years of age). Informed consent was obtained from all individual participants included in the three studies, and all procedures were done in accordance to ethical standards of our institutional research ethics committee as defined by the 1964 Helsinki declaration for human ethical standards.

Calf muscle experiments were performed using a home designed/built ^{31}P-tuned (51.705 MHz), 7.62cm diameter surface coil ($B1_{max} = 7.48\mu T$) matched specifically for calf muscles, while brain experiments were done with a home designed/built 12.7cm surface coil ($B1_{max} = 20.68\mu T$) similarly tuned but matched for brain. In the second study, dynamic experiments were performed using a home made wooden ergometer designed for plantarflexion within the magnet bore.

References

Lustig, M., Donoho, D., and Pauly, J. M. (2007) Sparse MRI: The application of compressed sensing for rapid MR imaging *Magnetic Resonance in Medicine: An Official Journal of the International Society for Magnetic Resonance in Medicine* 58.(6), 1182–1195.

Qu, X., Mayzel, M., Cai, J.-F., Chen, Z., and Orekhov, V. (2015) Accelerated NMR Spectroscopy with Low-Rank Reconstruction *Angewandte Chemie* 127.(3), 866–868.

Chapter 4

Phosphorus Magnetic Resonance Spectroscopic Imaging using Flyback Echo Planar Readout Trajectories

4.1 Context of the study

Phosphorus Magnetic Resonance Spectroscopic Imaging (^{31}P-MRSI) is capable of creating metabolic maps in vivo and assessing phosphate-containing metabolites such as Phosphocreatine (PCr), inorganic phosphate (Pi), adenosine tri-phosphate (ATP), phosphomonoester (PME) and phosphodiester (PDE). Its main limitation is the long acquisition time needed due to the limited sensitivity of this nucleus. Furthermore, the T_2 relaxation time of some ^{31}P metabolites (i.e. $T_2 \approx 60ms$ for γ-ATP at 3T) and the wide spectral dispersion of 30 ppm (>2000 Hz at 3T) limit

the possible spatial localization techniques as pulse-acquire or non-echo sequences are preferred.

In order to accelerate the acquisition, we developed a ^{31}P Echo planar spectroscopic imaging (EPSI) sequence using flyback readout gradients that achieved acceleration factors up to 10x compared to traditional phase encoded chemical shift imaging (CSI). This sequence was first tested in phantom experiments ant then in the calf muscles and brain of 5 healthy volunteers. Results showed the proposed sequence to be reliable in acquiring in vivo ^{31}P-MRSI in a relatively short acquisition time, using a clinical 3T MR system.

4.2 Declaration statement

Alejandro Santos Díaz, as first author, optimized the pulse sequence parameters, recruited the participants, acquired the data, performed the data processing and reconstruction as well as the statistical analysis. Additionally, drafted the article including tables and figures.

Dr. Michael D Noseworthy, as corresponding author, is the primary investigator of our group. He conceptualized the project as part of his as part of his well established trajectory in the development of technology and applications of multinuclear magnetic resonance imaging (MRI). He also performed a critical revision to the manuscript and performed the appropriate corrections in order to be published. Additionally, he provided constant guidance and advice during the development of the whole project.

Dr. Sergei I Obruchkov, as a former PhD student from our research group, started

the project on the development of fast ^{31}P-MRSI and wrote an early version of the pulse sequence. Additionally, provided helpful insight in the manuscript submitted for publication.

Dr. Rolf Schulte as a research scientist working for General Electric Healthcare, Munich, Germany, wrote the code of the pulse sequence and provided helpful insight in the optimization of the study protocol.

This research article was published in the journal Magnetic Resonance Materials in Physics, Medicine and Biology on January 30^{th}, 2018.

Citation: Santos-Díaz, A., Obruchkov, S. I., Schulte, R. F., and Noseworthy, M. D. (2018). Phosphorus magnetic resonance spectroscopic imaging using flyback echo planar readout trajectories. Magnetic Resonance Materials in Physics, Biology and Medicine, 1-12.

4.3 (Research Article) Phosphorus Magnetic Resonance Spectroscopic Imaging using Flyback Echo Planar Readout Trajectories

Alejandro Santos-Diaz[1,2], Sergei I Obruchkov[3], Rolf F Schulte[4] and Michael D. Noseworthy[1,2,5]

1. School of Biomedical Engineering, McMaster University, Hamilton Ontario, Canada.
2. Imaging Research Center, St. Joseph's Healthcare, Hamilton, Ontario, Canada.
3. Robinson Research Institute, Victoria University of Wellington, New Zealand
4. GE Healthcare, Munich, Germany
5. Electrical and Computing Engineering, McMaster University, Hamilton Ontario, Canada.

Corresponding author: †Dr. Michael D. Noseworthy, Ph.D.
Director, McMaster School of Biomedical Engineering,
Professor, Department of Electrical and Computer Engineering,
McMaster University.
Engineering Technology Building, ETB-406
1280 Main St. West, Hamilton, Ontario. Canada L8S 4K1
Phone: +1 (905) 525-9140 ext.23727
http://www.ece.mcmaster.ca/ mikenose/web/HOME.html

Text word Count: 3190
Abstract word count: 182
Number of figures/tables: 4/5
Number of references: 25

Key words: ^{31}P MR Spectroscopy; Echo Planar Imaging; MRSI; EPSI.

4.3.1 Abstract

Objective: To present and evaluate a fast phosphorus magnetic resonance spectroscopic imaging (MRSI) sequence using Echo Planar Spectroscopic Imaging with flyback readout gradient trajectories.

Materials and Methods: Waveforms were designed and implemented using a 3 Tesla MRI system. 31P spectra were acquired with $2x2cm^2$ and $3x3cm^2$ resolution, over 20cm and 21cm field of view and spectral bandwidths up to 1923Hz. The sequence was first tested using a 20cm diameter phosphate phantom and subsequent in vivo tests were performed on healthy human calf muscles and brains from 5 volunteers.

Results: Flyback EPSI achieved 10x and 7x reduction in acquisition time with $68.0 \pm 1.2\%$ and $69.8 \pm 2.2\%$ SNR per unit of time efficiency (theoretical SNR efficiency was 74.5% and 76.4%) for the in vivo experiments, compared to conventional phase encoding MRSI for the 2x2cm2 and 3x3cm2 resolution waveforms respectively. Statistical analysis showed no difference in the quantification of most metabolites. Time saving and SNR comparisons were consistent in phantom, leg and brain experiments.

Conclusion: EPSI using flyback readout trajectories was found to be a reliable alternative to acquire ^{31}P-MRSI data in a shorter acquisition time.

4.3.2 Introduction

Phosphorus magnetic resonance spectroscopic imaging ^{31}P-MRSI is capable of creating metabolic maps in vivo and assessing phosphate-containing metabolites

such as phosphocreatine (PCr), inorganic phosphate (Pi), adenosine triphosphate (ATP), phosphomonoesters (PME) and phosphodiesters (PDE) (Lee et al. 2012). Its main limitation is the long acquisition time needed due to the limited sensitivity of this nucleus. Furthermore, the T_2 relaxation time of some ^{31}P metabolites (i.e. $T2 \approx 60ms$ for γ-ATP at 3T (Bogner et al. 2009)) and the wide spectral dispersion of 30 ppm (>2000 Hz at 3T) limit the possible spatial localization techniques as pulse-acquire or non-echo sequences are prefered.

The latest efforts to reduce scan time while preserving as much signal to noise ratio (SNR) as possible have focused on using a GRAPPA acquisition scheme (Raghavan et al. 2009) and compressed sensing approaches for both traditional MRSI spatial localization (Hatay et al. 2017) and PCr imaging (Parasoglou et al. 2012). However these methods are still in their early stages of development for ^{31}P experiments or require specific hardware capabilities. Single shot fast spectroscopic imaging methods have also been proposed to solve the time issue (Posse et al. 2013). From a previous comparison of this type of techniques(Zierhut et al. 2009), Echo Planar Spectroscopic Imaging (EPSI) with a flyback readout trajectory proved to be highly robust due to its insensitivity to timing errors and simplicity in data reconstruction, for proton experiments. Previously a report on the implementation of ^{31}P-EPSI using a flyback readout showed reliability when tested with a phantom (Obruchkov 2011; Obruchkov and Noseworthy 2009) and in vivo (Santos-Díaz et al. 2016a; Santos-Díaz et al. 2016b). The purpose of this study was to test this approach in human brain and leg muscles using optimized gradient waveforms, and to compare it to a standard MRSI method.

4.3.3 Theory

The EPSI sequence with flyback readout gradient trajectory acquires data traversing the k-space logical X direction in an asymmetric echo planar fashion with a constant gradient amplitude segment and then reversing as fast as possible by maximizing the gradient slew rate to cover the same area. A pair of gradient trapezoids achieves this trajectory (Figure 4.1). The readout is performed only in one direction (during the constant segment) such that the phase evolution of spins happens always in the same direction, minimizing artifacts associated with phase reversal, gradient delays and eddy currents typically seen in echo planar techniques (Posse et al. 1995).

When designing the pair of gradient trapezoids for this sequence, both spectral and spatial bandwidth must be considered. The spectral bandwidth (BW_{spec}) can be defined as the reciprocal of individual gradient waveform duration,

$$BW_{spec} = \frac{1}{T_f + T_r} \tag{4.1}$$

where T_{gepsi} and T_{gflyb} correspond to the duration of the trapezoid pair. Then, the spatial bandwidth ($BW_{spatial}$) requirements are defined by the Nyquist limit across the desired field of view (FOV).

$$BW_{spatial} = \frac{1}{2} \cdot \frac{\gamma}{2\pi} G_x L_x \tag{4.2}$$

Where $G_x(mT/m)$ is the gradient amplitude and L_x (m) is the required FOV such that it defines the optimal sampling rate ($\delta t = 1/BW_{spatial}$). Thus, to calculate the pair of trapezoids for a given set of input parameters (i.e. spatial resolution,

FOV, BW_{spec}) that achieve the maximum SNR possible, the sampling rate has to be maximized.

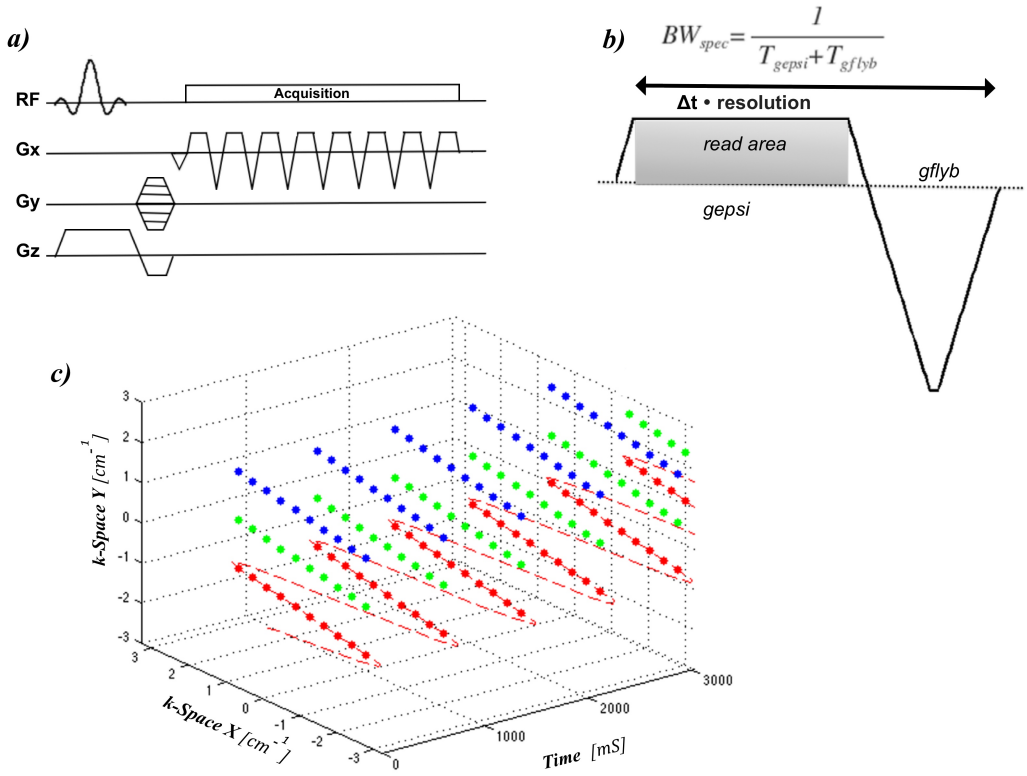

FIGURE 4.1: Pulse sequence diagram and *k-space* sampling. **a)** Flyback Echo Planar Spectroscopic Imaging sequence diagram, data is sampled only during the constant portion of the waveform. **b)** Gradient waveform geometry and parameters. A pair of gradient trapezoids with the same area creates the flyback trajectory based on the prescription of FOV, Spectral bandwidth and spatial resolution; BW_{spec}: spectral bandwidth, T_{gepsi}: duration of gepsi trapezoid, T_{gflyb}: duration of gflyb trapezoid, δt: sampling rate. **c)** Example of how the sequence fills *k-space* for a one slice 2D acquisition. Only three Ky steps and six time points are shown. Circles represent the sampled points in a different color for each Ky phase encode step, dotted line represents the *k-space* trajectory including the flyback portion. Although data is acquired suring the flyback portion, only those points sampled during the flat portion of the gepsi trapezoid are considered in the reconstruction.

The design of the trapezoid pair is constrained by the MR gradient system hardware, which defines the maximum gradient strength and the minimum rise time for a full amplitude ramp. Additionally there is only a discrete number of sampling rates given by its maximum value divided by an integer decimation number and all gradient times have to be a multiple of the gradient sampling rate (4 μs).

The sampling window given by the spatial resolution multiplied by the sampling rate has to be the constant portion of the gepsi trapezoid (T_{cons_gepsi}). The data is acquired during the full gradient train resulting in one data line with data also acquired during the ramp times and rewind trapezoid, thus the added lengths $T = T_{gepsi} + T_{gflyb}$ have to be a multiple of δt. To achieve this without SNR loss, BW_{spec} is adapted (if necessary) by slightly increasing T. In case T is not sufficient even for the highest receiver bandwidth, an interleaved version is calculated. Finally, the EPSI trapezoid pair is repeated as many times as the number of spectral points of the prescription.

Efficiency of the EPSI readout is determined by its duty cycle where the SNR efficiency (E_{SNR}) can be described by equation 4.3 (Cunningham et al. 2005) where the ideal case (i.e. $E_{SNR} = 100\%$) is when $T_{gflyb} = 0$, which represents a simple phase encoding step.

$$E_{SNR} = \sqrt{\frac{T_{cons\_gepsi}}{T_{gepsi} + T_{gflyb}}} \tag{4.3}$$

Finally, In order to be compliant with MR safety regulations, the peripheral nerve stimulation (PNS) threshold has to be considered, thus the trapezoids and ramp times are calculated using a previously described dB/dt optimized algorithm

(Noeske and Schulte 2016) taking into account that the EPSI train happens only in one logic gradient axis and there are no other gradients on at that time in the other two.

4.3.4 Materials and methods

MR system and pulse sequence

All experiments were performed using a 60cm bore 3T GE MR750 (GE Healthcare, Milwaukee, WI) scanner (50mT/m amplitude and 200T/m/s slew rate gradient system). Design and optimization of gradient waveforms was performed by modifying a product sequence "fidCSI" written in EPIC programming language version DV25 (GE Healthcare, Milwaukee, WI). This modified sequence *"fidepsi"* calculates the optimal gradient waveform "on the fly" according to the spectral bandwidth, spatial resolution, number of spectral points and PNS limit, as described in the previous section. Trajectories were optimized to achieve $2 \times 2cm^2$ and $3 \times 3cm^2$ in plane spatial resolution over a 20 cm and 21cm field of view (FOV) to be suitable with in vivo settings such as muscle and brain, this results in datasets of 10x10 and 7x7 voxels of $2 \times 2cm^2$ and $3 \times 3cm^2$ respectively. As this sequence does not acquire data during the "rewinder" part of the gradient, interleaved acquisitions (Cunningham et al. 2005) (consecutive excitations applying a time delay between the first and second readout waveforms) are used to ensure full spectral coverage according to the prescription requirements (i.e. wide spectral coverage over multiple voxels). Figure 4.2 shows an example of the interleaving scheme used for a $2 \times 2cm^2$ resolution and 1879Hz spectral bandwidth. A total

of 512 spectral points were acquired for each trajectory in all experiments (i.e. $2 \times 2cm^2$ and $3 \times 3cm^2$ resolution). In summary, four different EPSI variations were tested and named as follow (Table 4.1): EPSImL: flyback EPSI for muscle experiments and low BW_{spec}, $2 \times 2cm^2$ resolution. EPSImH: flyback EPSI for muscle experiments and high BW_{spec}, $2 \times 2cm^2$ resolution, two interleaved waveforms with a time delay of 532 (µs). EPSIbL: flyback EPSI for brain experiments and low BW_{spec}, $3 \times 3cm^2$ resolution. EPSIbH: flyback EPSI for brain experiments and high BW_{spec}, $3 \times 3cm^2$ resolution, two interleaved waveforms with a time delay of 520 (µs).

Due to the different acquisition compared to standard rectilinear phase encoding,

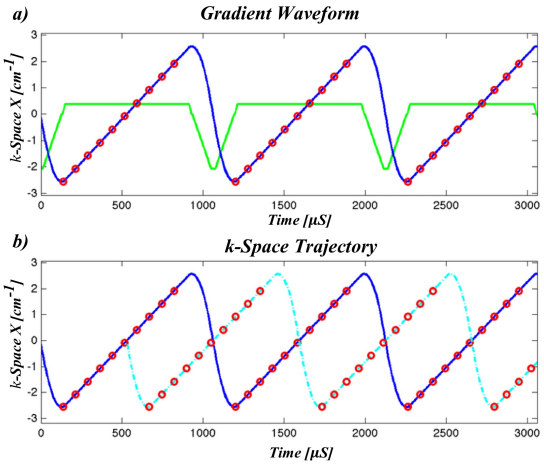

FIGURE 4.2: Flyback EPSI sequence sampling scheme for 2 cm resolution waveform. **a)** Gradient waveform. Readout of the data occurs only on the flat portion of the wave. **b)** *k-Space* trajectory. By applying a time delay in the gradient readout, interleaved acquisitions are formed and then combined to ensure full spectral coverage.

the reconstruction process was implemented separately, using Matlab R2014a (The Mathworks, Natick, MA, USA). First, the data was reshaped into a Cartesian grid according to the prescription parameters (i.e. in plane resolution and number of

spectral points), then the interleaved signals were combined after correcting the phase using singular value decomposition. Finally, the data was zero-filled to 1024 points and fast Fourier transformed to obtain the MRSI dataset.

TABLE 4.1: Parameters for each waveform tested. **fidCSIm**: phase encoded chemical shift imaging for muscle experiments, $2 \times 2cm^2$ resolution. **EPSImL**: flyback EPSI for muscle experiments and low BW_{spec}, $2 \times 2cm^2$ resolution. **EPSImH**: flyback EPSI for muscle experiments and high BW_{spec}, $2 \times 2cm^2$ resolution, two interleaved waveforms with a time delay of 532 (µs). **fidCSIb**: phase encoded chemical shift imaging for brain experiments, $3 \times 3cm^2$ resolution. **EPSIbL**: flyback EPSI for brain experiments and low BW_{spec}, $3 \times 3cm^2$ resolution. **EPSIbH**: flyback EPSI for brain experiments and high BW_{spec}, $3 \times 3cm^2$ resolution, two interleaved waveforms with a time delay of 520 (µs). **Phase steps**: Number of phase encoding steps, where the number of steps doubles for high spectral bandwidth due to the number of interleaves. Intlvs: number of interleaved waveforms.

Sequence	Resolution(cm^2)	$BW_{spec}(Hz)$	FOV(cm)	Matriz size	E_{SNR}%	Intlvs	Phase steps	TR(ms)
fidCSIm		2000			100	NA	100	
EPSImL	2×2	1322	20	10×10	74.54	1	10	1500
EPSImH		1879			84.51	2	20	
fidCSIb		2000			49	NA	100	
EPSIbL	3×3	1488	21	7×7	76.38	1	7	3000
EPSIbH		1923			83.67	2	14	

Participants and data acquisition

The flyback-EPSI sequence was characterized using a custom-built spherical phantom (volume = 1L, pH=7.4) with concentrations of 10mM of both sodium phosphate monobasic (NaH_2PO_4) and dibasic (Na_2HPO_4), to approximate in vivo conditions. Subsequently, the sequence was tested on human calf muscles and brain of 5 healthy volunteers (2 female, 3 male, 25.6 ± 3.4 years old). Informed consent was obtained from all individual participants included in the study, and

all procedures were done in accordance to ethical standards of our institutional research ethics committee as defined by the 1964 Helsinki declaration for human ethical standards.

Calf muscle experiments were performed using a home designed/built 31P-tuned (51.705 MHz), 7.62cm diameter surface coil ($B_{1max} = 7.48(\mu T)$) matched specifically for calf muscles, while brain experiments were done with a home designed/built 12.7cm surface coil ($B_{1max} = 20.68(\mu T)$) similarly tuned but matched for brain. Radiofrequency excitation was calibrated manually in order to achieve a 90 deg flip angle using a half SINC 1.8 (ms) excitation pulse when performing a pulse acquire experiment and was consistent through the experiments. The region of interest was shimmed on a set of T_2-weighted proton images acquired using the system's body coil as anatomical reference. The $2 \times 2cm^2$ and $3 \times 3cm^2$ resolution gradient waveforms were used in the muscle and brain experiments respectively due to the differences in concentrations and metabolites found in each type of tissue, however slice thickness was set to 3cm in all cases resulting in voxel sizes of $2 \times 2 \times 3cm^2$ and $3 \times 3 \times 3cm^2$ for muscle and brain respectively. For the muscle experiments, volunteers were lying on the bed in a supine position and the coil was placed below the right gastrocnemius whereas for the brain studies, subjects were lying in a right lateral recumbent position and the coil was placed on the parietal lobe. Figure 4.3 shows an example of the excited slice and imaging matrix for both muscle and brain settings. Additionally, two different spectral bandwidths were tested due to the impact of this parameter on the waveform design and consequently scan time and SNR. In order to compare acceleration factor and SNR, a regular phase encoded chemical shift imaging (fidCSI) dataset with equivalent parameters was also acquired within the same session. Acquisition parameters for each waveform

and its corresponding description are summarized in Table 4.1.

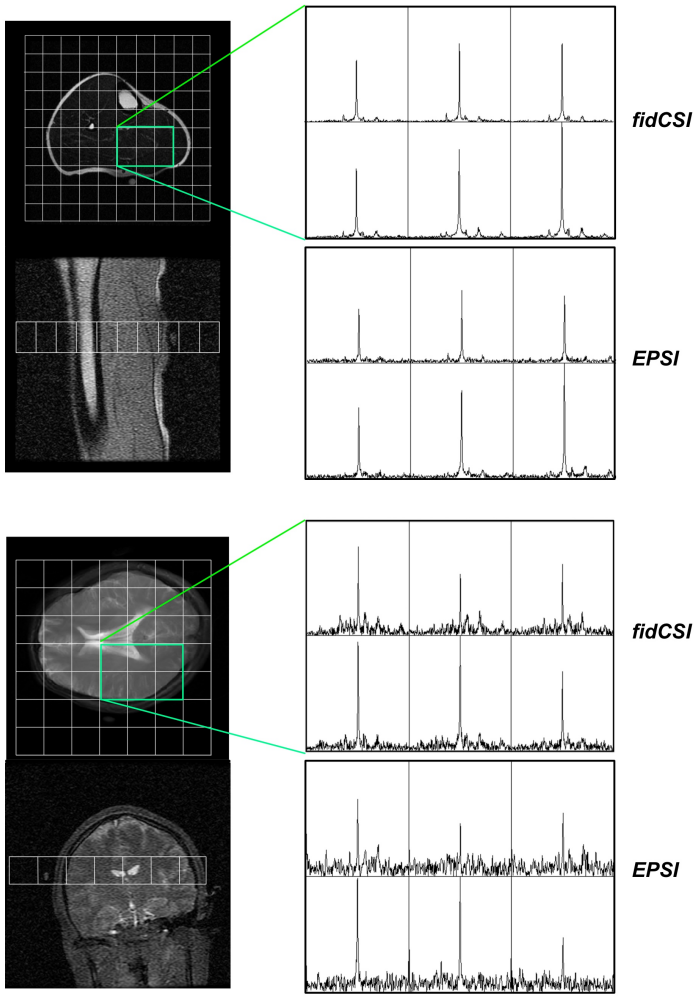

FIGURE 4.3: Examples of excited slice and imaging matrix for calf muscles (top left) and brain (bottom left) settings. Six elements from the MRSI dataset plotted to compare fidCSIm with EPSImH (top right) and fidCSIb with EPSIbH (bottom right). The acquisition was performed in the axial plane and a fiducial marker was placed in the center of the coil as spatial reference (bright object outside the periphery of anatomy). Acquisition times were 10:00, 2:00, 19:36, 5:36 minutes for fidCSIm, EPSImH, fidCSIb and EPSIbH respectively.

Data analysis

SNR for each voxel was calculated as the maximum signal of the sodium phosphate peak (for phantom experiments) and PCr peak (for in vivo experiments) divided by the standard deviation of the noise from a segment in the complex spectrum void of phosphate signal (i.e. 10ppm $<$ noise $<$ 13ppm). Subsequently an average value was computed from the same voxel positions where the phosphate peak was clearly distinguishable for each comparison (i.e. fidCSI vs EPSI). The flyback-EPSI sequence was tested using one average in phantom experiments whereas 4 and 8 averages were used for muscle and brain acquisitions respectively. For the fidCSI sequence as the comparison reference, 1, 4 and 8 averages were used accordingly. A 5Hz and 7Hz Gaussian apodization window was used for the muscle and brain experiments respectively and SNR per unit of time (SNR_t) was calculated as follows (Chen et al. 2007):

$$SNRt = \frac{SNR_{EPSI}}{SNR_{fidcsi}} \cdot \sqrt{\frac{Acq \quad time_{fidcsi}}{Acq \quad time_{EPSI}}} \tag{4.4}$$

Finally, to further assess spectral quality, representative samples from the same spatial position of the fidCSI and wide spectral bandwidth EPSI (EPSImH and EPSIbH) sequences were selected for each subject. These data were normalized and then fitted using the OXSA toolbox (Purvis et al. 2017). From these results we performed statistical analysis of the metabolite's amplitude and full width half maximum (FWHM) using R software (http://www.R-project.org). A Paired T-test was used to compare the metabolites that passed the normality test (Shapiro test, $p > 0.05$) and equality of variances (Bartlett test, $p > 0.05$) whereas a Wilcoxon

TABLE 4.2: Performance of the sequences tested in the phantom experiments. Acq. Time: Acquisition time. AF: Acceleration factor. SNR values were calculated as the average of the SNR for each voxel where the phosphate peak was distinguishable in consistent ROI's for each comparison.

Sequence	Resolution(cm_2)	Matriz size	BW_{spec}	Acq. Time	SNR	E_{SNR}(%)	SNRt(%)	AF
fidCSIm			2000	2:30	68.50	100	100	1x
EPSImL	2×2	10×10	1322	0:15	14.92	74.5	70.2	10x
EPSImH			1879	0:30	24.02	84.5	79.9	5x
fidCSIm			2000	2:27	78.51	100	100	1x
EPSIbL	3×3	7×7	1488	0:21	20.17	76.4	70.7	7x
EPSIbH			1923	0:42	31.88	83.7	79.0	3.5x

test was used for those that failed to prove normal distribution.

TABLE 4.3: E_{SNR} and SNRt were calculated using equations 4.3 and 4.4 respectively. For the later, displayed values are mean ± SD for the 5 volunteers. *Values for fidCSI-1avg were calculated based on the theoretical relationship of SNR being proportional to the squared root of the number of averages.

Tissue	Sequence	Acq. Time	SNR	E_{SNR}(%)	SNRt(%)	AF
Calf Muscles	fidCSIm-4avgs	10:00	54.41 ± 4.36	100	100	1x
	EPSImL-4avgs	1:00	11.64 ± 1.08	74.5	68.0 ± 1.2	10x
	EPSImH-4avgs	2:00	18.91 ± 1.85	84.5	78.1 ± 2.1	5x
	fidCSIm-1avgs	2:30	27.20 ± 2.18	100	100	-
Brain	fidCSIb-4avgs	19:36	22.1 ± 3.61	100	100	1x
	EPSIbL-4avgs	2:48	5.80 ± 3.61	76.4	69.8 ± 2.2	7x
	EPSIbH-4avgs	5:36	8.97 ± 1.56	83.7	76.3 ± 2.2	3.5x
	fidCSIb-1avgs	2:27	7.81 ± 1.28	100	100	-

4.3.5 Results

Both phantom and in vivo experiments correlated well between fidCSI and flyback-EPSI when comparing the amplitudes of the metabolites. Table 4.2 shows SNR, acquisition times and measured SNRt for the sequences compared in the phantom

experiments. Flyback-EPSI showed a 10x and 7x acceleration factor (AF) compared to fidCSI for the low spectral bandwidth waveforms (EPSImL and EPSIbL) whereas for the wider spectral bandwidth approaches (EPSImH and EPSIbH) this factor halves due to the interleaved acquisition. Measured SNRt shows a decrease of roughly four to six percent when compared to the theoretical E_{SNR} (equation 4) value in all phantom experiments. Figure 4.3 shows examples of the excited slice and imaging matrix where a 6 element MRSI data was extracted from the imaging matrix and plotted for calf muscles and brain, respectively.

In vivo mean measured SNRt for calf muscles was $68.0 \pm 1.2\%$ (EPSImL) and $78.1 \pm 2.1\%$ (EPSImH) while for brain experiments it was $69.8 \pm 2.2\%$ (EPSIbL) and $76.3 \pm 2.2\%$ (EPSIbH) (Table 4.3). Figure 4.4 depicts example spectra obtained in vivo with fidCSI and flyback-EPSI. For resting muscle, PCr and Pi were observed. The ATP resonances were also visible, albeit smaller in size relative to PCr. In the brain, clear depiction of PME and PDE metabolites was not possible with the parameters used, however PCr and all ATP resonances were distinguishable.

Amplitude and FWHM values for the fitted metabolites are shown in Table 4.4. For muscle experiments, neither PCr nor α-ATP showed differences in peak amplitude ($p = 0.62 \quad and \quad 0.10$, respectively) nor FWHM (0.20 and 0.85, respectively). However, the γ-ATP acquired using EPSI showed a significantly greater amplitude but not FWHM ($p = 0.02 \quad and \quad 0.1$, respectively), compared to fidCSI. The fitting of the β-ATP multiplet did not converge for EPSI, and Pi could not be fitted in three of the participants, neither for fidCSI nor EPSI, using the parameters herein presented. For brain data, the algorithm fitted PCr, Pi, β-ATP and neither amplitude nor FWHM were different, when comparing fidCSI to EPSI (Table 4.4),

however as in the muscle experiments, γ-ATP showed difference in amplitude but not in FWHM ($p = 0.03$ and $p = 0.37$, respectively). The results from PME, PDE and α-ATP were not included because the algorithm did not converge for these metabolites in at least three of the participants for either fidCSI or EPSI.

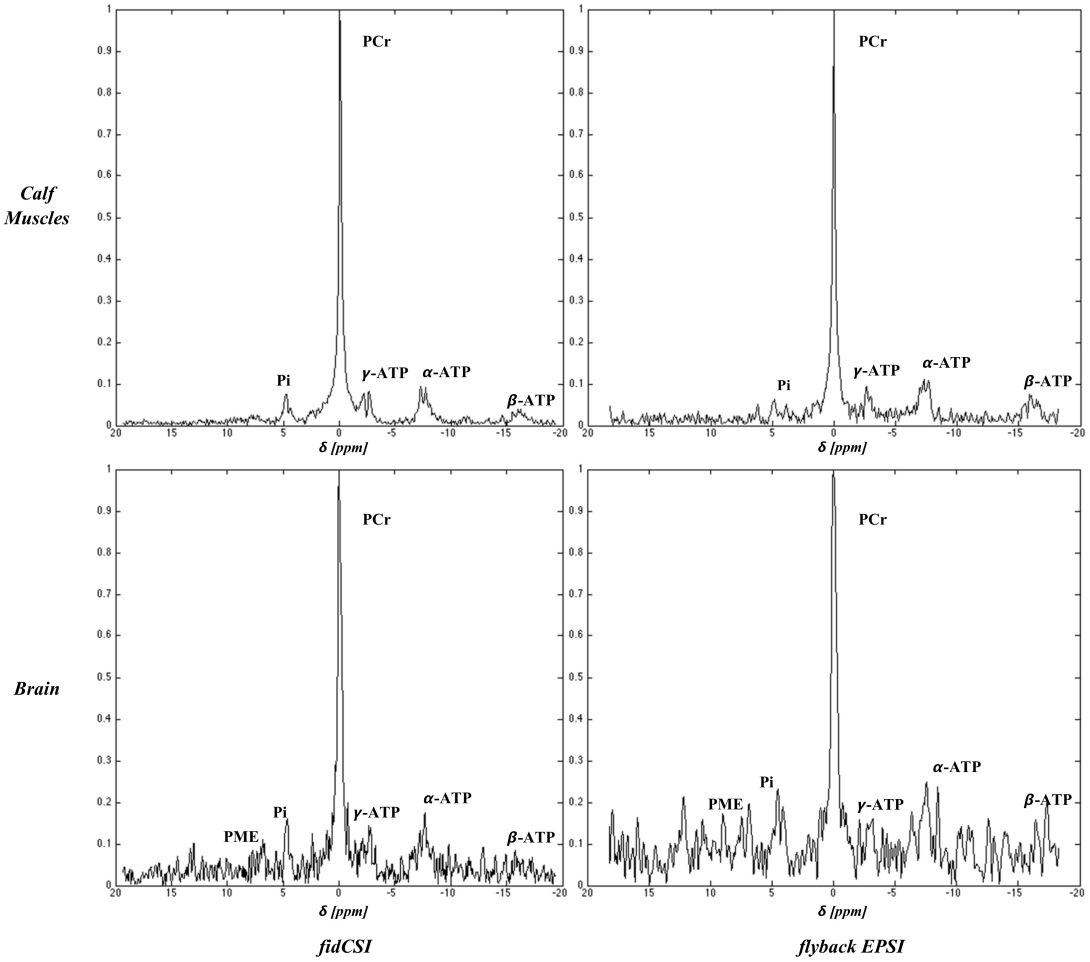

FIGURE 4.4: Examples of spectra obtained from the same spatial position using the fidCSI and flyback EPSI sequences for the in vivo experiments. Calf muscles spectra were acquired using 4 averages whereas brain spectra used 8 averages. For the EPSI examples, sequences used were EPSImH and EPSIbH. The corresponding acquisition times were 10:00 min, 19:36 min, 2:00 min and 5:36 min for fidCSI in muscle, brain, EPSImH and EPSIbH respectively.

4.3.6 Discussion

The feasibility of implementing MRSI using flyback readout trajectories in human brain and leg muscle in vivo was clearly demonstrated as shown (Figs. 4.3 and 4.4). Scan time was considerably shortened, compared to fidCSI, especially for relative low BW_{spec} (i.e. 1322Hz) where a maximum acceleration factor of 10 was achieved for the muscle experiments using the same number of averages. In order to increase the BW_{spec} there is a penalty of doubling scan time due to the interleaving applied, however this is not prohibitive for clinical studies and comes with a gain in SNR. Furthermore, such increase in SNR would allow to reduce the number of averages needed to get good quality data, as this interleaved scheme is an averaging process itself. Each two excitations acquire the same K-space data with a time delay to account for the spectral bandwidth. Thus, the implementation presented herein allows acquisition of reliable ^{31}P-MRSI in vivo in a relatively short scan time.

The SNRt values remained consistent across experimental settings (i.e. phantom, muscle and brain) and showed a reduction of roughly 5-8%, when comparing to the theoretical value E_{SNR}. This reduction is consistent with that observed in an earlier implementation of this sequence (Santos-Díaz et al. 2016a) and in proton experiments using a flyback EPSI readout, where the reduction was attributed to system instabilities due to the rapidly switching gradient (Cunningham et al. 2005; Chen et al. 2007). The current implementation of flyback trajectories created in real time allowed rapid optimization of prescription parameters such as FOV, spatial resolution and BW_{spec}. Thus the trajectories used in this current work

improved, compared to those previously reported (Obruchkov and Noseworthy 2009; Santos-Díaz et al. 2016a; Santos-Díaz et al. 2016b), where the pre-calculated waveforms constrained any flexibility in the prescription. Other main improvements were the wider spectral bandwidth and faster acquisition time for the low BW_{spec} implementation (i.e. EPSImL sequence).

The spectral fitting showed no difference in amplitude and FWHM for most of the metabolites analyzed. As expected, the best fit was PCr due to its higher concentration compared to the others. However, the fitting algorithm was unable to fit muscle Pi for either of the sequences tested, likely the result of acquisition parameters (low TR, 90 deg flip angle and low number or averages) and the substantial difference in concentration of this metabolite compared to PCr for resting muscle. It is also worth mentioning that for these experiments, β-ATP wasn't fitted for the EPSI sequence due to the slightly reduced spectral bandwidth compared to fidCSI (i.e. it was far enough up-field that it wasn't sampled, given the BW). In the brain experiments, PME, PDE and α-ATP were not fitted for either of the sequences in at least 3 of the participants, for this reason they were excluded from the analysis. These results all together suggest that EPSI and fidCSI sequences offer comparable results.

Minimum acquisition time achievable for fidCSI with the resolution and field of view tested was 2:30 and 2:27 minutes for $2 \times 2cm^2$ and $3 \times 3cm^2$ respectively (using one average only). Here we showed that flyback-EPSI was capable of acquiring useful data in less than this minimum achievable limit, clearly depicted in the muscle test shown (Figure 4.4) where the acquisition time for EPSI was 2:00

minutes. This acceleration of x1.25 may seem irrelevant, however improvement in the RF-coil set up and some acquisition parameters such as flip angle and voxel size will allow to reduce the number of averages used to acquire useful data, reaching thus meaningful acceleration factors.

TABLE 4.4: Spectral fitting results for the fidCSI and EPSI (EPSImH, EPSIbH) sequences tested in vivo. Amp: Amplitude, expressed in normalized units [NU]. FWHM: full width half maximum, expressed in Hz. The P value for each metabolite was obtained using a paired t-test for all metabolites, except for Pi where a Wilcoxon test was used instead.

Metabolite	FidCSI		EPSI		p value amp	p value FWHM
	Amp (NU)	FWHM (Hz)	Amp(NU)	FWHM(Hz)		
Muscle						
PCr	68.72 ± 4.91	7.96 ± 3.14	69.83 ± 3.34	7.66 ± 2.55	0.62	0.20
γ-ATP	1.34 ± 0.6	3.82 ± 0.96	4.68 ± 1.73	7.36 ± 3.06	0.02	0.1
α-ATP	7.53 ± 3.46	10.99 ± 2.7	2.71 ± 1.23	12.48 ± 14.4	0.1	0.85
Brain						
PCr	47.57 ± 13.96	7.09 ± 1.06	43.20 ± 11.78	7.25 ± 0.7	0.27	0.78
Pi	4.94 ± 2.16	10.49 ± 0.73	6.38 ± 1.22	10 ± 0.1	0.16	0.42
γ-ATP	4.35 ± 1.42	6.64 ± 1.85	6.66 ± 1.75	7.5 ± 2.92	0.03	0.37
β-ATP	5.09 ± 3.46	10.87 ± 6.31	3.94 ± 2.0	5.39 ± 3.19	0.51	0.1

The utility of Phosphorus magnetic resonance spectroscopy (^{31}P-MRS) is unquestionable. Information contained in brain spectra have proven useful in tumor grading (Novak et al. 2014; Vettukattil et al. 2012) and in better understanding psychiatric disorders (Harper et al. 2016), as examples. When referring to skeletal muscle metabolism, this method aims to study mitochondrial function at rest and during exercise recovery (Kemp et al. 2015; Valkovič et al. 2017). However, overcoming the low intrinsic SNR limitation is challenging, and as a result single voxel data and long acquisition times are common. Thus, obtaining multi-voxel information over a relatively short scan time is still the ultimate goal for this method.

Furthermore, studies involving muscle energy dynamics require a temporal resolution of at least 10 seconds. In order to address the low SNR constraint, efforts have focused on the development of fast techniques using ultra high field magnets (i.e. 7T), where results have shown promise (Valkovic et al. 2016). However the lack of clinical approval and very limited availability of 7T technology are major limitations. The EPSI sequence presented herein shows an option on how to address the challenge, as it is capable of acquiring MRSI data in acceptable scan time and it even shows potential to perform muscle phosphocreatine dynamics experiments (Santos-Díaz et al. 2017), all using a clinical scanner.

TABLE 4.5: Comparison of accelerated ^{31}P-MRSI methods. Acceleration factors and SNRt values are either extracted or calculated from the reference.
[a]The high value of SNR per unit of time (SNRt) for compressed sensing is due to the denoising nature of its reconstruction algorithm.

Ref	Method	Tissue	B_0	FOV(cm)	Matrix size	Acc	SNRt(%)
Raghavan et al. 2009	GRAPPA	Phantom	3T	40	24×24	4	NR
Hatay et al. 2017	Compressed Sensing	Brain	3T	24	8×8	5.33	399[a]
Wilhelm and Bachert 2001	Sinusoidal EPSI	Muscle	1.5T	20	8×8	8	73
Ulrich et al. 2007	Sinusoidal EPSI	Brain	1.5T	32	8×8	8	65
This work	Flyback EPSI	Muscle	3T	20	10×10	10	68
This work	Flyback EPSI	Brain	3T	21	7×7	7	70

The ^{31}P-EPSI was previously explored in calf muscle (Wilhelm and Bachert 2001) and brain (Ulrich et al. 2007) at 1.5T. Both studies reported the use of a sinusoidal gradient waveform with a time varying readout to achieve equally spaced samples in k-space. Additionally, echoes were separated in odd and even data points to compensate for imperfections of the oscillating gradients, making the sequence sensitive to eddy currents and time delays. Features of flyback readout

gradients (Posse et al. 2013; Zierhut et al. 2009) such as insensitivity to timing errors and the simplicity in data processing makes this sequence a worthy candidate for fast ^{31}P-MRSI acquisition.

This work tested the feasibility of acquiring phosphorus spectroscopic imaging data in a fraction of the time required by regular fidCSI with an acceptable penalty in SNR. Spatial localization techniques for phosphorus spectroscopic imaging are very limited due to the short T_2 relaxation times (i.e. $T_2 \approx 60ms$ for γ-ATP at 3T) and wide spectral dispersion. Efforts to accelerate the acquisition of this type of data have focused on the use of parallel imaging (Raghavan et al. 2009) and compressed sensing approaches of MRSI traditional localization methods (Hatay et al. 2017) and PCr imaging (Parasoglou et al. 2012), however these techniques have their own limitations such as low availability of multi-channel receiver coils in the case of parallel imaging or are at early stages of development for ^{31}P studies in the case of compressed sensing. Thus the EPSI approach is a feasible option to acquire fast ^{31}P-MRSI data at a relatively wide spectral bandwidth due to its fair trade of SNR and acquisition time (Table 4.5). The main limitations of this study include the difference found in the fitted amplitude of γ-ATP likely to be result of the small sample size, and the use of surface transmit/receive coils. Further testing with a volume coil will allow an improved analysis of the ^{31}P-EPSI sequence.

4.3.7 Conclusion

This work describes the design and 3T clinical scanner implementation of a ^{31}P-EPSI sequence with a flyback trajectory. The results correspond very well to a fidCSI acquisition using equivalent parameters. The sequence was capable of achieving phosphorus spectroscopic imaging data in a fraction of the time of the traditional phase encoding method. Even though ^{31}P spectroscopic imaging can provide clinically important information concerning tissue metabolism, it has never been clinically feasible due to the excessive acquisition time required. Significant acceleration can result from an echo planar readout. However, this comes with an SNR penalty compared to fidCSI, and the balance between acquisition speed and SNR may not be worth the effort, especially in static studies (i.e. most brain experiments). Adding other speed improvements such as parallel imaging and/or compressed sensing may improve the speed gain, eventually making ^{31}P spectroscopic imaging a clinical possibility.

Acknowledgements

Funding was provided through a CONACYT (Mexico) scholarship granted to ASD (CVU: 304930) and a NSERC Discovery Grant (RGPIN-2017-06318) to MDN.

Compliance with ethical standards

Conflict of interest: Dr. M. Noseworthy has, within the past year, received honoraria for 2 lectures given for GE Healthcare Canada. Dr. Rolf Schulte works for

General Electric Healthcare, Munich. None of the other authors have any potential conflicts of interest to disclose. The other authors declare that the research was conducted in the absence of any commercial or financial relationships that could be construed as a potential conflict of interest.

Ethical standards: All procedures performed in studies involving human participants were in accordance with the ethical standards of the institutional and/or national research committee and with the 1964 Helsinki declaration and its later amendments or comparable ethical standards.

Informed Consent: Informed consent was obtained from all individual participants included in the study. All data used in the study was de-identified and subsequently free of any information that could lead to their identification.

Appendix

The flyback-EPSI waveform is generated "on the fly" with the purpose of having flexibility in the prescription parameters. The waveform is achieved by creating a pair of gradient trapezoids gepsi and gflyb with the same area, constrained to maximizing SNR and minimizing the duration of gflyb without exceeding PNS threshold limitations. The algorithm to create the trapezoid pair is as follow:

INPUT

FOV: Field of view

RES: Spatial resolution

BW_{spec}: Spectral bandwidth

OUTPUT

gepsi: Readout trapezoid of flyback EPSI trajectory

gflyb: Rewind trapezoid of the flyback EPSI trajectory

Constrains

$\delta t : Maximum sampling rate/decimation (min\, decimation = 1)$

$Itlv : interleaves, maxitlv = 4$

$\%Initialization$

$T = 1/BW_{spec} = Tgepsi + Tgflyb$

$Decimation(dec) = max(dec)$

$Itlv = 1; BW spatial = 1/\delta t \times dec$

$\%Iterations$

$while(itlv \leq max[itlv])\{$

$while(dec \geq min[dec])$

$\{$

$T_{cons\_gepsi} = RES \times \delta t$

$G = 4\pi/(\gamma \times \delta t \times FOV)$

$Calculate\, gepsi\, ramp\, (\tau); \delta G_{lim} = SR_{min}(\tau + c)$

$Calculate\, gepsi\, area\, (A_{gepsi}); A_{gepsi} = G(RES \times \delta t \times \tau)$

$Calculate\, gflyb; A_{gflyb} = A_{gepsi}$

$Calculate\, trapezoid\, pair\, duration\, (t); t = tgepsi + tgflyb$

$If(t < T)Break;$

$dec = dec - 1$

$\}$

$itlv = itlv + 1\}$

$if(t < T)recalculategflyb; t = T$

$success;$

References

Bogner, W., Chmelik, M., Schmid, A., Moser, E., Trattnig, S., and Gruber, S. (2009) Assessment of 31P relaxation times in the human calf muscle: a comparison between 3 T and 7 T in vivo *Magnetic Resonance in Medicine: An Official Journal of the International Society for Magnetic Resonance in Medicine* 62.(3), 574–582.

Chen, A. P., Cunningham, C. H., Ozturk-Isik, E., Xu, D., Hurd, R. E., Kelley, D. A., Pauly, J. M., Kurhanewicz, J., Nelson, S. J., and Vigneron, D. B. (2007) High-speed 3T MR spectroscopic imaging of prostate with flyback echo-planar encoding *Journal of Magnetic Resonance Imaging: An Official Journal of the International Society for Magnetic Resonance in Medicine* 25.(6), 1288–1292.

Cunningham, C. H., Vigneron, D. B., Chen, A. P., Xu, D., Nelson, S. J., Hurd, R. E., Kelley, D. A., and Pauly, J. M. (2005) Design of flyback echo-planar readout gradients for magnetic resonance spectroscopic imaging *Magnetic Resonance in Medicine: An Official Journal of the International Society for Magnetic Resonance in Medicine* 54.(5), 1286–1289.

Harper, D. G., Jensen, J. E., and Renshaw, P. F. (2016) Phosphorus spectroscopy (31P MRS) of the brain in psychiatric disorders in: Wiley Online Library, 1257–1270.

Hatay, G. H., Yildirim, M., and Ozturk-Isik, E. (2017) Considerations in applying compressed sensing to in vivo phosphorus MR spectroscopic imaging of human brain at 3T *Medical & biological engineering & computing* 55.(8), 1303–1315.

Kemp, G., Ahmad, R., Nicolay, K., and Prompers, J. (2015) Quantification of skeletal muscle mitochondrial function by 31 P magnetic resonance spectroscopy techniques: a quantitative review *Acta physiologica* 213.(1), 107–144.

Lee, J.-H., Komoroski, R. A., Chu, W.-J., and Dudley, J. A. (2012) Methods and Applications of Phosphorus NMR Spectroscopy In Vivo *Annual Reports on NMR Spectroscopy* 75, 115.

Noeske, R. and Schulte, R. (2016) Flexible flyback EPSI waveform generation under the constraint of peripheral nerve stimulation in: *Proceedings of the 24th Annual Meeting of ISMRM, Singapore*, 3948.

Novak, J., Wilson, M., MacPherson, L., Arvanitis, T. N., Davies, N. P., and Peet, A. C. (2014) Clinical protocols for 31P MRS of the brain and their use in evaluating optic pathway gliomas in children *European journal of radiology* 83.(2), e106–e112.

Obruchkov, S. I. (2011) Echo Planar Spectroscopic Imaging and 31P In Vivo Spectroscopy PhD thesis.

Obruchkov, S. I. and Noseworthy, M. D. (2009) Echo planar spectroscopic imaging of phosphorus and hydrogen using flyback echo planar readout gradients *Magnetic Resonance Materials in Physics, Biology and Medicine* 22.(supp(1)), 56–57.

Parasoglou, P., Feng, L., Xia, D., Otazo, R., and Regatte, R. R. (2012) Rapid 3D-imaging of phosphocreatine recovery kinetics in the human lower leg muscles with compressed sensing *Magnetic resonance in medicine* 68.(6), 1738–1746.

Posse, S., Otazo, R., Dager, S. R., and Alger, J. (2013) MR spectroscopic imaging: principles and recent advances *Journal of Magnetic Resonance Imaging* 37.(6), 1301–1325.

Posse, S., Tedeschi, G., Risinger, R., Ogg, R., and Bihan, D. L. (1995) High speed 1H spectroscopic imaging in human brain by echo planar spatial-spectral encoding *Magnetic resonance in medicine* 33.(1), 34–40.

Purvis, L. A., Clarke, W. T., Biasiolli, L., Valkovič, L., Robson, M. D., and Rodgers, C. T. (2017) OXSA: An open-source magnetic resonance spectroscopy analysis toolbox in MATLAB *PloS one* 12.(9), e0185356.

Raghavan, R. S., Panda, A., Valette, J., James, J., Heberlein, K., Boettcher, U., Henry, P., Bansal, N., and Dydak, U. (2009) 31P spectroscopic imaging with GRAPPA in: *Proceedings of the 17th Annual Meeting of ISMRM, Honolulu, Hawaii, USA*, 4317.

Santos-Díaz, A., Akbari, A., and Noseworthy, M. (2016a) 31P MRSI of human calf muscles using flyback echo planar spectroscopic imaging (EPSI) readout gradients in: *Proceedings of the 24th Annual Meeting of ISMRM, Singapore*, 3936.

Santos-Díaz, A., Akbari, A., and Noseworthy, M. D. (2016b) Phosphorus echo planar spectroscopic imaging (EPSI) of the brain using flyback readout gradients *Magnetic Resonance Materials in Physics, Biology and Medicine* 29.(supp(1)), 474.

Santos-Díaz, A., Harasym, D., and Noseworthy, M. D. (2017) Dynamic phosphorus echo planar spectroscopic imaging (31P-EPSI) of human calf muscles using flyback readout trajectories *Magnetic Resonance Materials in Physics, Biology and Medicine* 30.(supp(1)), 260.

Ulrich, M., Wokrina, T., Ende, G., Lang, M., and Bachert, P. (2007) 31P-{1H} echo-planar spectroscopic imaging of the human brain in vivo *Magnetic Resonance in Medicine: An Official Journal of the International Society for Magnetic Resonance in Medicine* 57.(4), 784–790.

Valkovič, L., Chmelík, M., and Krššák, M. (2017) In-vivo 31P-MRS of skeletal muscle and liver: a way for non-invasive assessment of their metabolism *Analytical biochemistry* 529, 193–215.

Valkovic, L., Chmelík, M., Meyerspeer, M., Gagoski, B., Rodgers, C. T., Krssák, M., Andronesi, O. C., Trattnig, S., and Bogner, W. (2016) Dynamic 31P–MRSI using spiral spectroscopic imaging can map mitochondrial capacity in muscles of the human calf during plantar flexion exercise at 7 T *NMR in Biomedicine* 29.(12), 1825–1834.

Vettukattil, R., Gulati, M., Sjøbakk, T. E., Jakola, A. S., Kvernmo, N. A., Torp, S. H., Bathen, T. F., Gulati, S., and Gribbestad, I. S. (2012) Differentiating diffuse World Health Organization grade II and IV astrocytomas with ex vivo magnetic resonance spectroscopy *Neurosurgery* 72.(2), 186–195.

Wilhelm, T. and Bachert, P. (2001) *In vivo31P echo-planar spectroscopic imaging of human calf muscle.*

Zierhut, M. L., Ozturk-Isik, E., Chen, A. P., Park, I., Vigneron, D. B., and Nelson, S. J. (2009) 1H spectroscopic imaging of human brain at 3 Tesla: Comparison of fast three-dimensional magnetic resonance spectroscopic imaging techniques *Journal of Magnetic Resonance Imaging: An Official Journal of the International Society for Magnetic Resonance in Medicine* 30.(3), 473–480.

Chapter 5

Dynamic ^{31}P Spectroscopic Imaging of Skeletal Muscles combining Flyback EPSI and Compressed Sensing

5.1 Context of the study

Phosphorus magnetic resonance spectroscopy (^{31}P-MRS) and Phosphorus Magnetic Resonance Spectroscopic Imaging (^{31}P-MRSI) are methods capable to assess energy metabolism by tracking important metabolites such as Phosphocreatine (PCr), inorganic phosphate (Pi) and adenosine tri-phosphate (ATP). Further to the analysis of the resting spectra, it is of particular interest to perform dynamic studies of skeletal muscle metabolism through an exercise challenge and subsequent

recovery, as this can assess mitochondrial function. To do so, a high temporal resolution (on the order of seconds) is needed as the recovery of the PCr signal happens within a few minutes.

In this study, we further accelerated the Echo planar spectroscopic imaging (EPSI) sequence using flyback readout gradients (see Chapt. 4) by combining it with compressed sensing (CS) to achieve a temporal resolution of 9 seconds. The sequence was first tested in phantom experiments to assess its performance compared to fully sampled EPSI (fidEPSI) and phase encoded CSI (fidCSI). Then, it was tested in 11 healthy volunteers during an exercise-recovery challenge of the lower leg muscles. Voxels containing tissue from different muscle groups were evaluated by measuring %PCr depletion, time constant of PCr recovery (τPCr) and intracellular pH at rest and following the exercise. Dynamic experiments showed differences in PCr depletion when comparing soleus with gastrocnemius muscles. Calculated pH, τPCr and %PCr drop were consisted with previously reported values.

This study presents a highly accelerated ^{31}P-MRSI sequence combining flyback EPSI and CS capable of assessing energy metabolism of multiple muscle groups of the lower leg simultaneously using a clinical 3T MR system.

5.2 Declaration statement

Alejandro Santos Díaz, as first author, developed the highly accelerated pulse sequence, optimized the protocol, recruited the participants, acquired the data, performed the data processing and reconstruction as well as the statistical analysis. Additionally, drafted the article including tables and figures.

Diana Harasym is a masters student in our group, she helped collecting part of the data and and contributed with the manuscript.

Dr. Michael D Noseworthy, as corresponding author, is the primary investigator of our group. He conceptualized the project as part of his as part of his well established trajectory in the development of technology and applications of multi-nuclear magnetic resonance imaging (MRI). He also performed a critical revision to the manuscript and performed the appropriate corrections in order to be published. Additionally, he provided constant guidance and advice during the development of the whole project.

This paper was submitted for publication to the journal Magnetic Resonance in Medicine (MRM) on June 29^{th}, 2018.

5.3 (Research article) Dynamic ^{31}P Spectroscopic Imaging of Skeletal Muscles combining Fly-back EPSI and Compressed Sensing

Alejandro Santos-Díaz[1,2], Diana Harasym[1,2] and Michael D. Noseworthy[1,2,3]

1. School of Biomedical Engineering, McMaster University, Hamilton Ontario, Canada

2. Imaging Research Center, St. Joseph's Healthcare, Hamilton, Ontario, Canada

3. Electrical and Computing Engineering, McMaster University, Hamilton Ontario, Canada

Corresponding author:
Dr. Michael D. Noseworthy, Ph.D.
Director, McMaster School of Biomedical Engineering,
Professor, Department of Electrical and Computer Engineering,
McMaster University.
Engineering Technology Building, ETB-406
1280 Main St. West, Hamilton,
Ontario. Canada L8S 4K1
Phone: +1 (905) 525-9140 ext.23727
`http://www.ece.mcmaster.ca/~mikenose/web/HOME.html`

Text word Count: 2,900
Number of figures/tables: 4/2
Number of references: 37

Key words: Dynamic ^{31}P-MRSI; Compressed Sensing; MRSI; EPSI; muscle metabolism.

5.3.1 Abstract

Purpose: Dynamic ^{31}P-MRSI experiments require temporal resolution in the order of seconds to assess different muscle groups simultaneously. A highly accelerated pulse sequence that combines flyback EPSI and compressed sensing was developed and tested in a phantom and 11 healthy volunteers during an exercise-recovery challenge of the lower leg muscles, using a clinical 3T MR system.

Methods: A flyback EPSI readout designed to achieve $2.25 \times 2.25 cm^2$ resolution over a $18 \times 18 cm^2$ FOV (i. e. 8×8 matrix) was combined with compressed sensing through the inclusion of pseudorandom gradient blips to sub-sample the $k_y - k_t$ dimensions by a factor of 2.7x, achieving a temporal resolution of 9 seconds. The sequence was first tested in phantom experiments to assess its performance compared to fully sampled EPSI (fidEPSI) and phase encoded CSI (fidCSI). Then, it was tested in 11 healthy volunteers during an exercise-recovery challenge of the lower leg muscles. Voxels containing tissue from different muscle groups were evaluated measuring %PCr depletion, time constant of PCr recovery (τPCr) and intracellular pH at rest and following the exercise.

Results: The sequence achieved an SNR approximately 50% higher when compared to fidCSI. No statistical differences were found in the metabolite ratio, pH or linewidth when compared to fidEPSI and fidCSI in the phantom study. Dynamic experiments showed differences in PCr depletion when comparing soleus with gastrocnemius muscles. Calculated pH, τPCr and %PCr drop are consisted with reported values.

Conclusion: Highly accelerated ^{31}P-MRSI combining flyback EPSI and compressed sensing is capable of assessing energy metabolism of multiple muscle groups of the lower leg simultaneously using a clinical 3T MR system.

5.3.2 Introduction

Phosphorus magnetic resonance spectroscopy (^{31}P-MRS) and spectroscopic imaging (^{31}P-MRSI) are non-invasive methods capable of assessing in vivo energy metabolism. Tracking metabolites such as Phosphocreatine (PCr), Adenosin triphosphate (ATP) and inorganic phosphate (Pi) in skeletal muscle is of particular interest due to its physiological importance and high metabolic activity (Kemp et al. 2015; Valkovič et al. 2017). Further to the analysis of resting spectra, the relatively easy access of lower leg muscles along with the voluntary control to exercise them allow metabolic studies to be performed in a dynamic fashion through an exercise-recovery challenge and thus assess mitochondrial function (Kemp et al. 2015; Kemp and Radda 1994). In order to perform these types of experiments, a high temporal resolution (i.e. <10 seconds) is needed and it represents the main challenge for ^{31}P-MRS acquisitions, which already suffer from low intrinsic signal to noise ratio (SNR). Thus, very coarse signal localization is often performed using small surface coils to retain enough SNR (Edwards et al. 2012). However, this localization cannot distinguish between the different muscle groups recruited during exercise, or is limited to superficial structures. A way to overcome such a limitation is by using single voxel ^{31}P-MRS to localize specific muscles, which has been successfully implemented at 3T (Meyerspeer et al. 2005) and has also taken advantage of the SNR boost at ultra high field (Meyerspeer et al. 2011; Valkovic et al. 2014; Niess et al. 2017), however they cannot assess more than two different muscles simultaneously, leading to the desire for methods able to map multiple muscle groups during the same acquisition. Although frequency selective ^{31}P-MR

imaging is able to track PCr recovery of multiple muscles simultaneously (Parasoglou et al. 2012; Parasoglou et al. 2013) and can even provide a non-localized insight into pH modulation during exercise (Schmid et al. 2016; Khegai et al. 2018), it does not provide the same information as ^{31}P-MRS (e.g. no information on ATP is given).

^{31}P-MRSI can provide spatially resolved spectroscopic information. However, the low temporal resolution of the traditional phase encode method is suitable for dynamic studies only through extensive gated protocols (Slade et al. 2006). Amongst the different acceleration options, a recent study using a non-Cartesian trajectory showed promise at 7T (Valkovic et al. 2016), however the lack of availability of ultra high field systems strongly limits its use. Other recent efforts have explored a non-symmetric echo planar readout (Santos-Díaz et al. 2018; Santos-Díaz et al. 2017) and sparse sampling methods (Hatay et al. 2017; Ma et al. 2017). In regards to the later, compressed sensing (Lustig et al. 2007) has gained popularity over the past years and has successfully been extended to multinuclear spectroscopic applications. In particular hyperpolarized ^{13}C studies have exploited its underlying principles and developed very fast imaging approaches even capable of tracking cellular metabolism (Hu et al. 2008; Hu et al. 2010; Larson et al. 2011; Cao et al. 2016; Chen et al. 2018). Based on this framework and preliminary proof of concept (Santos-Díaz et al. 2017; Santos-Díaz and Noseworthy 2017), the purpose of this study was to develop a highly accelerated ^{31}P-MRSI sequence combining flyback EPSI and compressed sensing capable of tracking calf muscles metabolism in an exercise-recovery challenge using a clinical 3T MR system.

5.3.3 Methods

MR system and Pulse sequence

All experiments were performed using a 60cm bore 3T GE MR750 (GE Healthcare, Milwaukee, WI) scanner (50mT/m amplitude and 200T/m/s slew rate gradient system). The pulse sequence developed for this study was built on a recently presented flyback EPSI sequence "fidepsi" (Santos-Díaz et al. 2018) written in the EPIC programming language version DV 25 (GE Healthcare, Milwaukee, WI), due to its flexibility to design the trajectory. To further accelerate the EPSI readout and achieve a temporal resolution capable of tracking the dynamic PCr response, we implemented a compressed sensing approach similar to the work of Hu et al (Hu et al. 2008). Where the inclusion of pseudo randomly distributed blips in the k_y direction during the flyback readout allowed to sample multiple $k_y - k_t$ lines within the same phase encoding step. Figure 5.1(a) shows the pulse sequence diagram. The pulse duration of the blips was set to be equal to, or slightly less than, the rewind segment of the EPSI trajectory (0.188 ms), whereas the amplitude was determined by the pulse sequence to achieve a blip area equal to, or a multiple of, the phase encode increment. Flyback EPSI trajectory was designed to achieve $2.25 \times 2.25 cm^2$ resolution over an $18 \times 18 cm^2$ field of view (i.e. 8×8 voxels), a spectral bandwidth of 1420 Hz and 512 spectral points. The sub-sampling scheme was designed to acquire an entire 2D-MRSI dataset (one frame) using three excitations as seen in the *k-space* sampling schedule of Figure 5.1(b). The first excitation acquires the top three $k_y - k_t$ lines whereas the second and third acquire the two central and three bottom *k-space* lines respectively. Thus the

compressed sensing acceleration factor was 2.7x, which adds up to an acceleration factor of 8x using the EPSI sequence compared to traditional phase encoded MRSI.

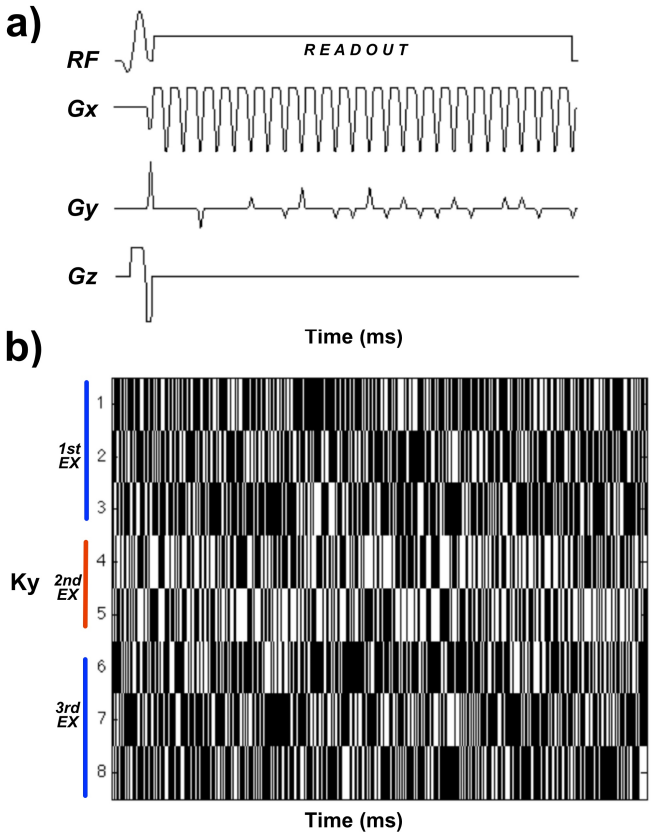

FIGURE 5.1: **a)** Pulse sequence diagram showing the flyback EPSI readout and randomly distributed blips in the Gx and Gy logical gradient axes respectively. **b)** Sub-sampling schedule for the sequence (i.e. white spaces indicate location of samples, black are absence) to achieve a 2D-MRSI dataset (frame). The first excitation acquires the first three $K_y - K_t$ lines whereas the second and third acquire the two central and three bottom *k-space* lines respectively. The K_x dimension is fully sampled by the flyback EPSI readout.

Participants and data acquisition

The proposed sequence was first characterized using a custom-built spherical phantom (volume = 1L, pH=6.7) containing 30 mmol/L and 10 mmol/L concentrations of sodium phosphate (P1) and phosphocreatine disodium salt (P2) respectively in order to mimic in vivo differences in chemical shift and amplitude. Acquisitions for characterization consisted on collecting three 2D-MRSI datasets using (a) phase encoded MRSI (fidCSI), (b) flyback-EPSI (fidEPSI) and (c) flyback EPSI combined with compressed sensing (fidepsiCS). Parameters were matched for all sequences: TR = 1500ms; flip angle = 55°; FOV = $18 \times 18 cm^2$; matrix size = 8×8; slice thickness = 4cm; spectral bandwidth = 1420Hz; spectral points = 512. To compare the performance between sequences, acquisition times were matched by setting the number of averages to 1, 8 and 21 for fidCSI, fidEPSI and fidepsiCS respectively, and SNR, amplitude ratio (AmpRatio) and linewidth (LW) of the metabolites were measured. Afterwards, 32 frames were collected over time using two averages, only applying the compressed sensing approach to achieve the 9 seconds temporal resolution used for the dynamic experiments and to compare different voxel positions. Four "dummy" scans were included in all experiments to allow the system to reach steady state.

To assess the point spread function (PSF) of the proposed MRSI sequence, a two-compartment phantom was used. The outer compartment was a cylindrical container (10cm diameter, 12cm length) filled with an agar solution. The inner compartment was an acrylic rectangular shape of $2.2 \times 2.2 \times 8 cm^3$ inner side length filled with a 1 mol/L solution of sodium phosphate. This was fixed inside the

cylinder at 2.5 cm from the wall. Three 2D-MRSI datasets were acquired in the transverse plane using fidCSI, fidEPSI and fidepsiCS. Acquisition parameters were matched to the experiments described above, using one, one and two averages, to get acquisition times of 1:42 min, 18 sec and 15 sec, respectively. The full width half maximum (FWHM) of the PSF was measured in both X and Y axis to compare the spatial selectivity of each sampling strategy.

A total of 11 healthy volunteers (three female, eight male, 30 ± 6 years of age) gave their consent to participate in this study. Dynamic experiments were performed using a home made wooden ergometer designed for plantar flexion within the magnet bore (Rockel et al. 2017; Davis and Noseworthy 2016) and an in-house designed/built 31P-tuned (51.705 MHz), 7.62cm diameter surface coil ($B_{1max} = 7.48(\mu T)$) matched specifically for calf muscles. Radiofrequency excitation was first calibrated to a 90° flip angle using an automated procedure based on the Bloch-Siegert shift (Schulte et al. 2011), then for the dynamic acquisitions flip angle was set to 40° (close to the Ernst angle excitation), width all other parameters identical to the phantom setup. Excitation pulse used was an asymmetric partially self-refocused SINC pulse with one side-lobe before the main lobe, duration of 1.8ms and bandwidth of 2289Hz. During the experiment, volunteers were lying on the ergometer in a supine position width the coil was placed below the right gastrocnemius. The region of interest was shimmed on a set of T_2 weighted proton images acquired using the system's body coil and used as an anatomical reference. First, a high quality non-localized spectrum (pulse-acquire sequence, same excitation, 16 averages) was acquired to get baseline reference measurements of metabolite amplitudes and global pHi. The dynamic protocol was subsequently

run, consisting of a baseline 16 frames at rest (9sec x 16 = 2.4 minutes), followed by three minutes of plantar flexion with a frequency of 0.5 Hz (90 repetitions), extended knee and acting on a load of 40% - 50% maximum voluntary contraction (MVC) determined the day previously. Subsequently, 32 frames (4.8 minutes) were acquired during recovery with no acquisition during the exercise. All procedures were done in accordance to ethical standards of our institutional research ethics board as defined by the 1964 Helsinki declaration for human ethics.

Data reconstruction and processing

All data processing and reconstruction was performed using MATLAB R2015b (The Mathworks, Natick, MA, USA) as follows. First, data were re-shaped from the raw blipped acquisition to a raw fidepsi format, zero filling the missing sampling points according to the sub-sampling schedule, and then reordered to a 4D matrix of *k-space* data with dimensions $k_t - k_x - k_y - \#frame$. The missing *k-space* samples were filled using a modified 2D implementation of an iterative low-rank Hankel matrix completion reconstruction algorithm (Qu et al. 2015). This method exploits the sparsity of the NMR signal, reconstructing a spectrum with the least number of spectral peaks rather than seeking the fewest non-zero spectral intensities as seen with traditional compressed sensing methods (Shchukina et al. 2017). This property makes it more robust in reconstructing signals regardless of their linewidth. A data consistency parameter (λ) and reconstruction tolerance threshold (tol) values were empirically determined as 800 and 0.00005 respectively. In our approach, as the k_x dimension is fully sampled by the EPSI trajectory, each $k_y - k_t$

plane is reconstructed separately to build one full data frame. After phase correction, to account for the tilt of the EPSI readout, followed by an inverse Fourier transformation in the spatial dimensions, data was zero filled to 1024 points and Fourier transformed in the spectral dimension to achieve a 2D MRSI data set. Finally, this procedure was repeated on a frame-by-frame basis for the whole experiment (48 frames total, i.e. 16 baseline and 32 recovery).

In order to assess metabolism of different muscle groups, four voxels were selected an analyzed during the experiment, containing mostly tissue from the gastrocnemius lateralis (GL), gastrocnemius medialis (GM), soleus (SOL) and a mixture of muscles (MIX). Spectral fitting was performed using the OXSA toolbox (Purvis et al. 2017) with prior knowledge set to focus on the evolution of PCr and Pi only, as these two metabolites are those expected to be affected by an exercise challenge (Valkovič et al. 2017). A mono-exponential curve was then fitted to the evolution of the PCr signal during the recovery period in order to calculate the time constant of PCr recovery rate (τPCr). Additionally PCr drop percentage (dPCr) and intracellular pH at rest (pH_{rest}) and the end of exercise (pH_{end}) were calculated. The later was determined using the modified Henderson-Hasselbalch equation $pH = pK_A + log[(\delta - \delta_{HA})/(\delta_A - \delta)]$ (Moon and Richards 1973), where $pK_A = 6.75$ is the dissociation constant of Pi, whereas $\delta_{HA} = 3.27$ and $\delta_A = 5.63$ are the values for the chemical shifts of the protonated and non-protonated forms of Pi, respectively, and δis the measured chemical shift of the Pi peak. The localized pH values at rest were determined using the average of the 16 acquisitions at rest, for each voxel. Statistical analysis was performed using the R software (`http://www.R-project.org`). A one-way ANOVA and Kruskal-Wallis tests were used to compare dPCr and pH_{end} values, respectively. Finally, multiple comparison

tests were analyzed.

5.3.4 Results

The fidepsiCS sequence showed an SNR substantially increased when compared to fidCSI and fidEPSI, respectively. The one way-ANOVA showed no differences between any of the sequences when comparing amplitude ratios, linewidth of any of the metabolites and calculated pHi. These results are summarized in Table 5.1. Additionally, the repeated phantom acquisitions showed no differences in metabolite ratio when comparing different voxel positions. Figure 5.2 depicts sample spectra of comparable quality, acquired from the phantom experiments using matched scan times. The effective voxel sizes at the FWHM of the compared sequences were $2.40 \times 2.69 cm^2$, $3.94 \times 2.86 cm^2$ and $2.57 \times 2.77 cm^2$ for fidCSI, fidEPSI and fidepsiCS, respectively. Figure 5.3 shows the line profiles across each axis and intensity maps of the PSF's, where it is possible to observe that fidepsiCS improves the voxel bleeding when comparing to fidEPSI, and offers results comparable to fidCSI.

Figure 5.4 depicts an example of different muscle groups analyzed, and the evolution of the fitted amplitudes for PCr and Pi signals. The different metabolic responses for each muscle group are shown, as well as a voxel with a mixture of muscles, to stress the importance of spatial localization in these types of experiments.

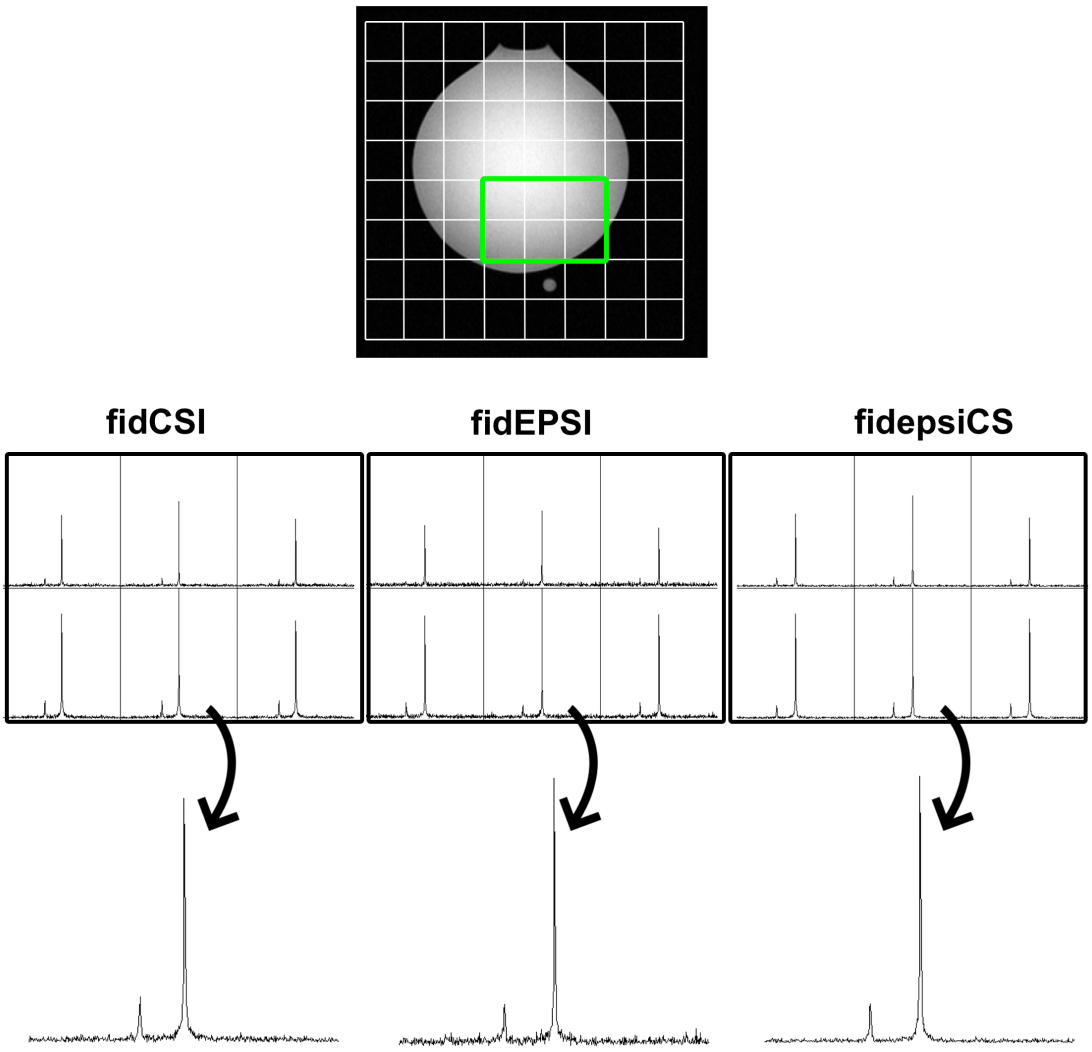

FIGURE 5.2: (Top) Spatial reference of the phantom experiments and corresponding MRSI matrix. (Middle) Sample spectra from a 6×6 region of interest using each of the sequences. (Bottom) Representative spectrum from the same spatial position showing comparable quality of spectra.

With exercise the mean drop in the amplitude of the PCr signal was 61.8 ± 15.7, 63.4 ± 17.6, 58 ± 15.3 and 21.9 ± 6.9 for the GL, GM, MIX and SOL muscles, respectively. A statistically significant difference was found between the percent

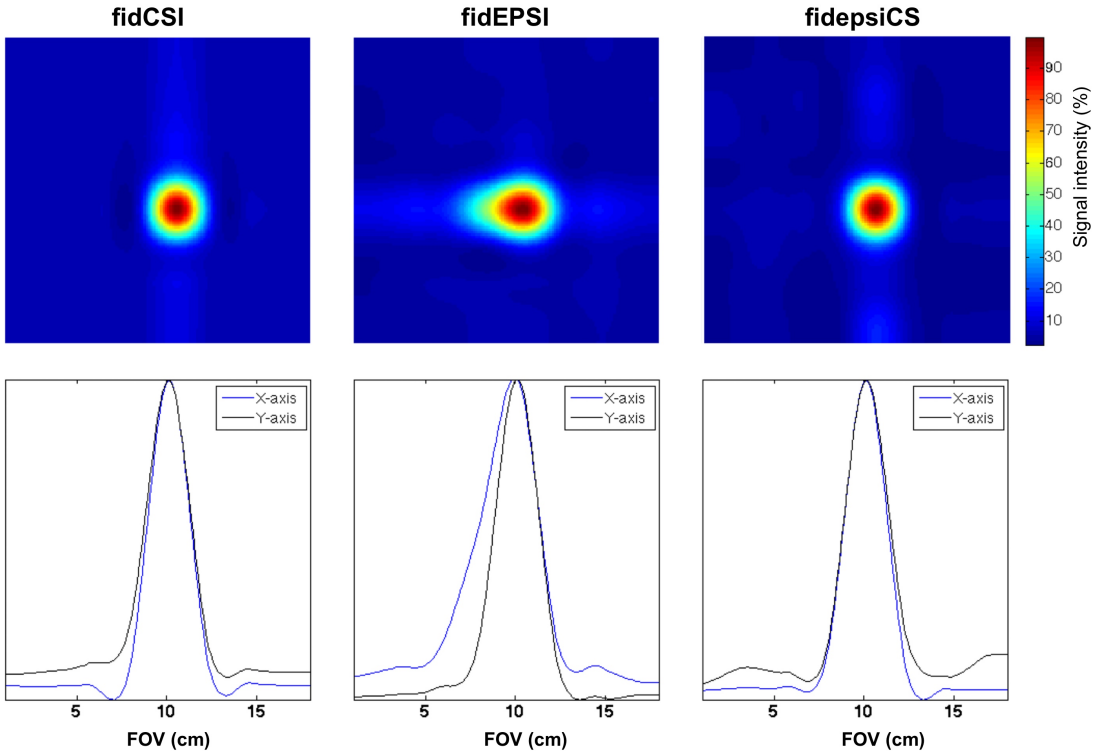

FIGURE 5.3: Point spread function (PSF) and line profiles of the different sampling methods using slice selective 2D-MRSI and a point source phantom. Sequences compared were fidCSI (left column), fidEPSI (central column) and fidepsiCS (right column). The bottom row shows the line profiles in the X (blue) and Y (black) axis. True voxel sizes measured as the FWHM in each axis were $2.40 \times 2.69 cm^2$, $3.94 \times 2.86 cm^2$ and $2.57 \times 2.77 cm^2$ for fidCSI, fidEPSI and fidepsiCS, respectively. The 2D intensity maps were interpolated to 128x128 point images for visualization purposes, however the voxel sizes at FWHM were measured from the original data.

PCr drop of SOL when compared to GM, GL and MIX but not between the later three. Additionally, there was a drop in the pH from neutral values at rest to 6.73 ± 0.08, 6.71 ± 0.09, 6.75 ± 0.08 and 6.94 ± 0.06 at the end of the exercise for GL, GM, MIX and SOL respectively. Sample spectra for each muscle group taken during baseline and end of exercise are depicted in Figure 5.5(a-d). Figure 5.5e

shows an example of the spectra acquired over time during baseline and recovery for the GM, where the PCr depletion is clearly depicted. The signal for Pi is not distinguishable for resting spectra, but it is well defined at the beginning of the recovery period as it reaches comparable amplitude to PCr due to the depletion of the later during exercise. Table 5.2 summarizes the results of the exercise-recovery experiment including the calculated values for pHi (pH_{rest} and pH_{end}) and τPCr. Global pHi at rest calculated from the high quality spectrum acquired before the dynamic experiment was 7.01 ± 0.03.

5.3.5 Discussion

In this study we presented a highly accelerated ^{31}P-MRSI pulse sequence capable of simultaneously track the evolution of PCr and changes in intracellular pH of multiple muscle groups from the human calf induced by an exercise challenge at a clinical field strength (3T). The performance of this sequence was evaluated in phantom experiments and its feasibility for dynamic experiments tested in 11 healthy volunteers.

When comparing to fidCSI and fully sampled EPSI, our compressed sensing approach achieved a considerably higher SNR and comparable results in metabolite amplitudes and FWHM (Table 5.1). The increased SNR is a result of the low-rank reconstruction algorithm, and is in agreement with previously reported denoising effects from compressed sensing reconstructions (Lustig et al. 2007; Hu et al. 2008;

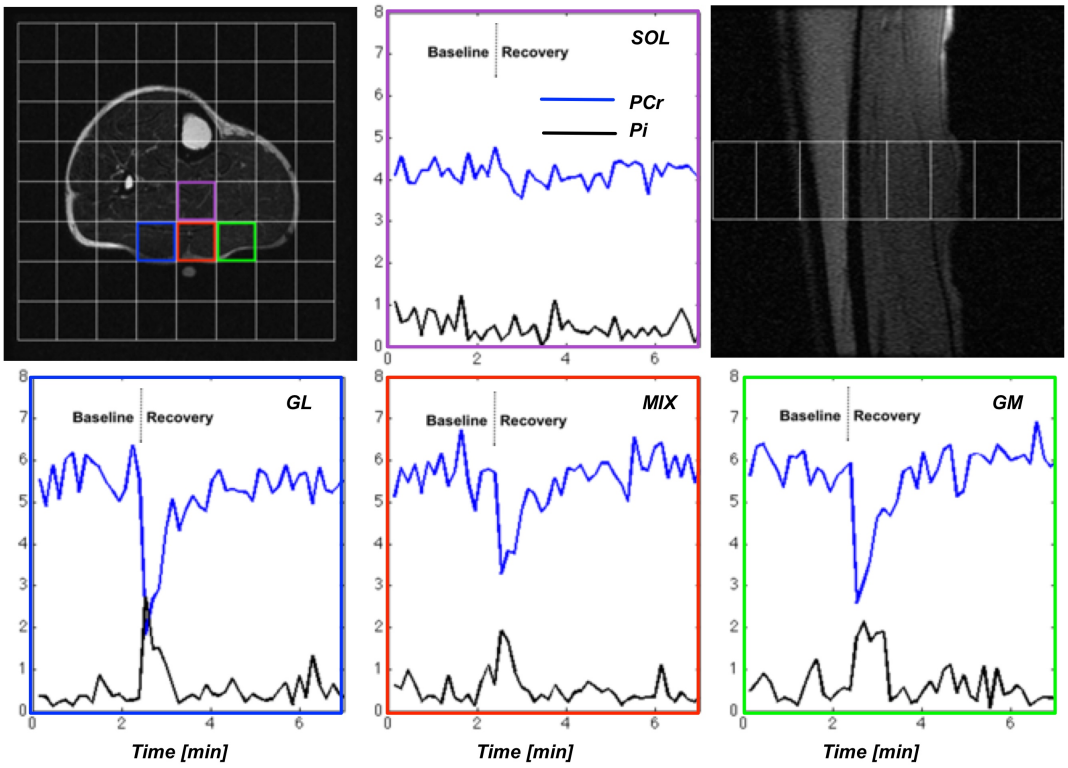

FIGURE 5.4: Data acquisition matrix on the axial plane of an anatomical image (top left). Sagittal image showing the slice profile (top right). Temporal evolution of the PCr and Pi signals for different muscle groups analyzed. Units of amplitude were normalized to the same reference. Voxels were selected to include in the analysis gastrocnemius lateralis (GL), gastrocnemius medialis (GM), soleus (SOL) and a mixture of muscles (MIX).

Hu et al. 2010; Larson et al. 2011).

Compressed sensing in MRI is a technique that has grown substantially over the past decade due to its capability to accelerate acquisition time. One of its main requirements is that the signal of interest must hold sufficient SNR in order to be properly reconstructed (Lustig et al. 2007). For this reason, hyperpolarized ^{13}C experiments have widely exploited this method and have lead the development of

TABLE 5.1: Results for the phantom experiments. Phase encoded MRSI (fidCSI), flyback Echo Planar Spectroscopic Imaging (fidEPSI) and flyback EPSI combined with compressed sensing (fidepsiCS). Bottom row shows p-values for the ANOVA and Kruskal-Wallis tests. Values were calculated as the average of the six different voxel positions with the highest SNR. Acq. Time: Acquisition time; Avgs: Number of averages; P1/P2: Amplitude ratio calculated as amplitude of sodium phosphate the peak (P1) divided by the amplitude of the phosphocreatine disodium salt peak (P2). LW_P1: Linewidth of P1; LW_P2: Linewidth of P2.

Sequence	Acq. Time	N-Avgs	SNR	P1/P2	pH	LW_P1	LW_P2
fidCSI	1:42	1	59.8 ± 26.5	3.8 ± 0.5	6.74 ± 0.02	2.7 ± 1.7	4.5 ± 0.6
fidEPSI	1.42	8	35.2 ± 16.4	3.7 ± 0.8	6.70 ± 0.02	2.77 ± 0.9	4.6 ± 0.6
fidepsiCS	1:41	21	92.1 ± 41.6	4.4 ± 0.7	6.7 ± 0.01	2.24 ± 0.55	4.3 ± 0.7
				$p = 0.24$	$p = 0.23$	$p = 0.95$	$p = 0.46$

very fast imaging and spectroscopic techniques (Hu et al. 2008; Hu et al. 2010; Larson et al. 2011; Cao et al. 2016; Chen et al. 2018). Despite the low intrinsic SNR of phosphorus experiments, our study has shown the feasibility of using similar methods to assess muscle energy metabolism.

TABLE 5.2: Results for dynamic acquisition of human calf muscles (n=11). GL: Gastrocnemius lateralis. GM: gastrocnemius medialis. MIX: mixture of muscles. SOL: soleus muscle. dPCr: drop of PCr signal. pH_{base}: pH at rest.pH_{end}: pH at the end of . (*) Indicates significance, $p < 0.01$.

	GL	GM	MIX	SOL
dPCr(%)	61.8 ± 15.7	63.4 ± 17.6	58 ± 15.3	$21.9 \pm 6.9^*$
τPCr (s)	38.7 ± 13.7	58.8 ± 17.3	52.9 ± 20.2	49 ± 24.1
pH_{base}	7.02 ± 0.06	7.03 ± 0.06	7.04 ± 0.05	7.02 ± 0.05
pH_{end}	6.73 ± 0.08	6.71 ± 0.09	6.75 ± 0.08	$6.94 \pm 0.06^*$

Albeit with relatively coarse spatial resolution, the capability of our sequence to assess different muscle groups simultaneously is evident by the difference found in

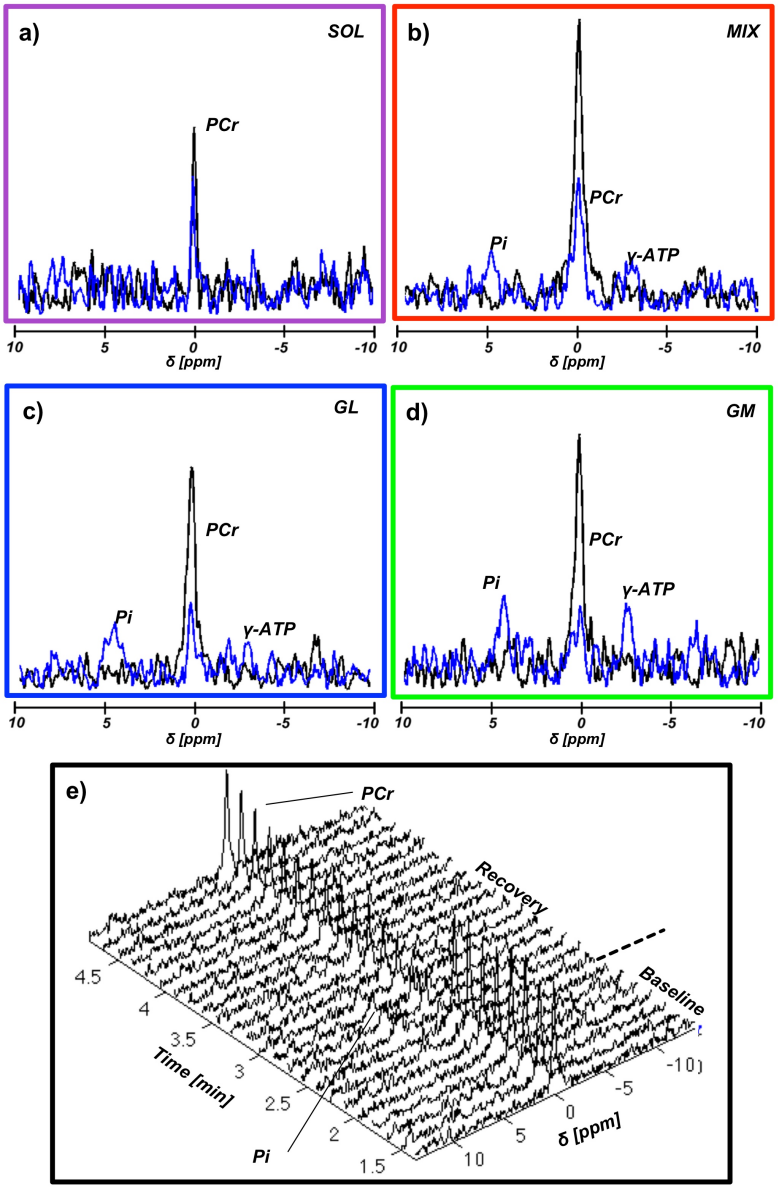

FIGURE 5.5: **(a-d)** Representative spectra for each muscle group acquired at rest (black dotted line) and at the end of the exercise (blue solid line). Reduced PCr and increased Pi signal amplitudes at the end of exercise are clearly depicted. Additionally, Pi signal at rest is not distinguishable. **e)** Example of the time evolution for the spectra from the GM. PCr depletion and recovery is shown as well as the increase in Pi at the end of the exercise. The color-coding has the purpose to clearly differentiate each spectrum.

the PCr depletion between gastrocnemius and soleus groups but not within GM, GL and MIX (Table 5.2). Also the analysis of the PSF indicates that the presented sequence has an effective voxel size roughly 0.4cm larger than the nominal value, indicating a relatively reduced voxel bleeding effect. The common method to perform dynamic ^{31}P-MRS experiments restricts the acquisition to the sensitivity volume of the coil used, thus measurements from specific muscle groups may be biased (Meyerspeer et al. 2012). This limitation has promoted the development of localized ^{31}P-MRS methods (Meyerspeer et al. 2011; Valkovic et al. 2014; Niess et al. 2017), although the simultaneous analysis of multiple muscle groups is still limited, especially at a clinical field strength. Additionally, these sequences often require multiple selective RF pulses for accurate localization, resulting in higher SAR levels and longer echo times, which affects the sensitivity for ^{31}P metabolites such as ATP (Meyerspeer et al. 2011). On the other hand ^{31}P-MRI methods aim to solve these problems by creating metabolic maps from a whole region (Parasoglou et al. 2012; Parasoglou et al. 2013; Schmid et al. 2016; Khegai et al. 2018; Greenman and Smithline 2011), while losing the ability to assess local pH information. In our approach, we target a multi-voxel spectroscopic acquisition using a pulse-acquire scheme that addresses the above-mentioned limitations.

The very limited availability of ultra high field MRI systems (e.g. 7T) narrow the use of recent ^{31}P-MRSI approaches using spiral encoding that addresses most requirements for phosphorus dynamic studies (Valkovic et al. 2016). Unlike this method, our approach was developed under a clinical framework, making it easily transferable.

Calculated values for τPCr and pH_i are in agreement with previous reports in

healthy volunteers (Valkovic et al. 2016; Niess et al. 2018). Exhaustive assessment of mitochondrial function was out of the scope of this paper. However, the method shows feasibility as certain parameters, such as the initial PCr recovery rate (V_{PCr}) and the maximal rate of oxidative phosphorylation (Q_{max}), could be calculated from the information acquired in this study (Valkovič et al. 2017).
Dynamic ^{31}P-MRSI experiments still remain challenging, especially at clinical field strength. Although our approach shows the feasibility to address many of the challenges, some limitations still exist. First, a deeper analysis on the effects caused by the subsampling and reconstruction processes on metabolite quantification using different acceleration factors and multiple values for the data consistency parameter λwill help to better characterize this sequence. Additionally, the current implementation is computationally expensive, as it requires approximately six hours to reconstruct each dataset on a computer cluster with processing speed of 2.3 GHz, 24 cores and 128 GB of RAM from the SHARCNET (www.sharcnet.ca). These obstacles may be overcome by implementing recent variations in the reconstruction algorithm (Guo and Qu 2018; Guo et al. 2017).

5.3.6 Conclusion

We presented a highly accelerated ^{31}P-MRSI sequence that combines a flyback EPSI readout with compressed sensing. In spite of the relatively coarse spatial resolution, it is capable to assess energy metabolism of multiple muscle groups from the lower leg simultaneously during an exercise-recovery challenge, using a clinical 3T MR system. Our results suggest that this approach may be used as

a tool for assessment of individual muscles mitochondrial capacity in a clinical setting.

Acknowledgements

Thank you to Dr. Peder Larson from UCSF and Dr. Rolf Schulte from GE Healthcare for their help and insight in regard the implementation of the subsampling scheme.

Funding was provided through a CONACYT (Mexico) scholarship granted to ASD (CVU: 304930) and a NSERC Discovery Grant (RPGIN-2017-06318) to MDN.

References

Cao, P., Shin, P. J., Park, I., Najac, C., Marco-Rius, I., Vigneron, D. B., Nelson, S. J., Ronen, S. M., and Larson, P. E. (2016) Accelerated high-bandwidth MR spectroscopic imaging using compressed sensing *Magnetic resonance in medicine* 76.(2), 369–379.

Chen, H.-Y., Larson, P. E., Gordon, J. W., Bok, R. A., Ferrone, M., Criekinge, M. van, Carvajal, L., Cao, P., Pauly, J. M., Kerr, A. B., et al. (2018) Technique development of 3D dynamic CS-EPSI for hyperpolarized 13C pyruvate MR molecular imaging of human prostate cancer *Magnetic resonance in medicine*.

Davis, A. D. and Noseworthy, M. D. (2016) Motion and distortion correction of skeletal muscle echo planar images *Magnetic resonance imaging* 34.(6), 832–838.

Edwards, L. M., Tyler, D. J., Kemp, G. J., Dwyer, R. M., Johnson, A., Holloway, C. J., Nevill, A. M., and Clarke, K. (2012) The reproducibility of 31-phosphorus MRS measures of muscle energetics at 3 Tesla in trained men *PloS one* 7.(6), e37237.

Greenman, R. L. and Smithline, H. A. (2011) The feasibility of measuring phosphocreatine recovery kinetics in muscle using a single-shot 31P RARE MRI sequence *Academic radiology* 18.(7), 917–923.

Guo, D., Lu, H., and Qu, X. (2017) A Fast Low Rank Hankel Matrix Factorization Reconstruction Method for Non-Uniformly Sampled Magnetic Resonance Spectroscopy *IEEE Access* 5, 16033–16039.

Guo, D. and Qu, X. (2018) Improved Reconstruction of Low Intensity Magnetic Resonance Spectroscopy With Weighted Low Rank Hankel Matrix Completion *IEEE Access* 6, 4933–4940.

Hatay, G. H., Yildirim, M., and Ozturk-Isik, E. (2017) Considerations in applying compressed sensing to in vivo phosphorus MR spectroscopic imaging of human brain at 3T *Medical & biological engineering & computing* 55.(8), 1303–1315.

Hu, S., Lustig, M., Balakrishnan, A., Larson, P. E., Bok, R., Kurhanewicz, J., Nelson, S. J., Goga, A., Pauly, J. M., and Vigneron, D. B. (2010) 3D compressed sensing for highly accelerated hyperpolarized 13C MRSI with in vivo applications to transgenic mouse models of cancer *Magnetic Resonance in Medicine: An Official Journal of the International Society for Magnetic Resonance in Medicine* 63.(2), 312–321.

Hu, S., Lustig, M., Chen, A. P., Crane, J., Kerr, A., Kelley, D. A., Hurd, R., Kurhanewicz, J., Nelson, S. J., Pauly, J. M., et al. (2008) Compressed sensing

for resolution enhancement of hyperpolarized 13C flyback 3D-MRSI *Journal of magnetic resonance* 192.(2), 258–264.

Kemp, G., Ahmad, R., Nicolay, K., and Prompers, J. (2015) Quantification of skeletal muscle mitochondrial function by 31 P magnetic resonance spectroscopy techniques: a quantitative review *Acta physiologica* 213.(1), 107–144.

Kemp, G. and Radda, G. (1994) Quantitative interpretation of bioenergetic data from 31P and 1H magnetic resonance spectroscopic studies of skeletal muscle: an analytical review. *Magnetic resonance quarterly* 10.(1), 43–63.

Khegai, O., Madelin, G., Brown, R., and Parasoglou, P. (2018) Dynamic phosphocreatine imaging with unlocalized pH assessment of the human lower leg muscle following exercise at 3T *Magnetic resonance in medicine* 79.(2), 974–980.

Larson, P. E., Hu, S., Lustig, M., Kerr, A. B., Nelson, S. J., Kurhanewicz, J., Pauly, J. M., and Vigneron, D. B. (2011) Fast dynamic 3D MR spectroscopic imaging with compressed sensing and multiband excitation pulses for hyperpolarized 13C studies *Magnetic resonance in medicine* 65.(3), 610–619.

Lustig, M., Donoho, D., and Pauly, J. M. (2007) Sparse MRI: The application of compressed sensing for rapid MR imaging *Magnetic Resonance in Medicine: An Official Journal of the International Society for Magnetic Resonance in Medicine* 58.(6), 1182–1195.

Ma, C., Clifford, B., Liu, Y., Gu, Y., Lam, F., Yu, X., and Liang, Z.-P. (2017) High-resolution dynamic 31P-MRSI using a low-rank tensor model *Magnetic resonance in medicine* 78.(2), 419–428.

Meyerspeer, M., Krššák, M., Kemp, G., Roden, M., and Moser, E. (2005) Dynamic interleaved 1 H/31 P STEAM MRS at 3 Tesla using a pneumatic force-controlled plantar flexion exercise rig *Magnetic Resonance Materials in Physics, Biology and Medicine* 18.(5), 257–262.

Meyerspeer, M., Robinson, S., Nabuurs, C. I., Scheenen, T., Schoisengeier, A., Unger, E., Kemp, G. J., and Moser, E. (2012) Comparing localized and nonlocalized dynamic 31P magnetic resonance spectroscopy in exercising muscle at 7T *Magnetic resonance in medicine* 68.(6), 1713–1723.

Meyerspeer, M., Scheenen, T., Schmid, A. I., Mandl, T., Unger, E., and Moser, E. (2011) Semi-LASER localized dynamic 31P magnetic resonance spectroscopy in exercising muscle at ultra-high magnetic field *Magnetic resonance in medicine* 65.(5), 1207–1215.

Moon, R. B. and Richards, J. H. (1973) Determination of intracellular pH by 31P magnetic resonance *Journal of Biological Chemistry* 248.(20), 7276–7278.

Niess, F., Fiedler, G. B., Schmid, A. I., Goluch, S., Kriegl, R., Wolzt, M., Moser, E., and Meyerspeer, M. (2017) Interleaved multivoxel 31P MR spectroscopy *Magnetic resonance in medicine* 77.(3), 921–927.

Niess, F., Fiedler, G. B., Schmid, A. I., Laistler, E., Frass-Kriegl, R., Wolzt, M., Moser, E., and Meyerspeer, M. (2018) Dynamic multivoxel-localized 31P MRS during plantar flexion exercise with variable knee angle *NMR in Biomedicine* 31.(6), e3905.

Parasoglou, P., Feng, L., Xia, D., Otazo, R., and Regatte, R. R. (2012) Rapid 3D-imaging of phosphocreatine recovery kinetics in the human lower leg muscles with compressed sensing *Magnetic resonance in medicine* 68.(6), 1738–1746.

Parasoglou, P., Xia, D., Chang, G., and Regatte, R. R. (2013) Dynamic three-dimensional imaging of phosphocreatine recovery kinetics in the human lower leg muscles at 3T and 7T: a preliminary study *NMR in Biomedicine* 26.(3), 348–356.

Purvis, L. A., Clarke, W. T., Biasiolli, L., Valkovič, L., Robson, M. D., and Rodgers, C. T. (2017) OXSA: An open-source magnetic resonance spectroscopy analysis toolbox in MATLAB *PloS one* 12.(9), e0185356.

Qu, X., Mayzel, M., Cai, J.-F., Chen, Z., and Orekhov, V. (2015) Accelerated NMR Spectroscopy with Low-Rank Reconstruction *Angewandte Chemie* 127.(3), 866–868.

Rockel, C., Akbari, A., Kumbhare, D. A., and Noseworthy, M. D. (2017) Dynamic DTI (dDTI) shows differing temporal activation patterns in post-exercise skeletal muscles *Magnetic Resonance Materials in Physics, Biology and Medicine* 30.(2), 127–138.

Santos-Díaz, A., Harasym, D., and Noseworthy, M. D. (2017) Dynamic phosphorus echo planar spectroscopic imaging (31P-EPSI) of human calf muscles using flyback readout trajectories *Magnetic Resonance Materials in Physics, Biology and Medicine* 30.(supp(1)), 260.

Santos-Díaz, A. and Noseworthy, M. (2017) Highly Accelerated 31P-MRSI of Human Calf Muscles combining flyback Echo Planar Spectroscopic Imaging (EPSI) and Compressed Sensing in: *Proceedings of the 25th Annual Meeting of ISMRM, Honolulu, Hawaii*, 2931.

Santos-Díaz, A., Obruchkov, S. I., Schulte, R. F., and Noseworthy, M. D. (2018) Phosphorus magnetic resonance spectroscopic imaging using flyback echo planar readout trajectories *Magnetic Resonance Materials in Physics, Biology and Medicine*, 1–12.

Schmid, A. I., Meyerspeer, M., Robinson, S. D., Goluch, S., Wolzt, M., Fiedler, G. B., Bogner, W., Laistler, E., Krššák, M., Moser, E., et al. (2016) Dynamic PCr and pH imaging of human calf muscles during exercise and recovery using 31P gradient-Echo MRI at 7 Tesla *Magnetic resonance in medicine* 75.(6), 2324–2331.

Schulte, R. F., Sacolick, L., Deppe, M. H., Janich, M. A., Schwaiger, M., Wild, J. M., and Wiesinger, F. (2011) Transmit gain calibration for nonproton MR using the Bloch–Siegert shift *NMR in Biomedicine* 24.(9), 1068–1072.

Shchukina, A., Kasprzak, P., Dass, R., Nowakowski, M., and Kazimierczuk, K. (2017) Pitfalls in compressed sensing reconstruction and how to avoid them *Journal of biomolecular NMR* 68.(2), 79–98.

Slade, J. M., Towse, T. F., DeLano, M. C., Wiseman, R. W., and Meyer, R. A. (2006) A gated 31P NMR method for the estimation of phosphocreatine recovery time and contractile ATP cost in human muscle *NMR in Biomedicine: An International Journal Devoted to the Development and Application of Magnetic Resonance In vivo* 19.(5), 573–580.

Valkovič, L., Chmelík, M., and Krššák, M. (2017) In-vivo 31P-MRS of skeletal muscle and liver: a way for non-invasive assessment of their metabolism *Analytical biochemistry* 529, 193–215.

Valkovic, L., Chmelík, M., Meyerspeer, M., Gagoski, B., Rodgers, C. T., Krssák, M., Andronesi, O. C., Trattnig, S., and Bogner, W. (2016) Dynamic 31P–MRSI

using spiral spectroscopic imaging can map mitochondrial capacity in muscles of the human calf during plantar flexion exercise at 7 T *NMR in Biomedicine* 29.(12), 1825–1834.

Valkovic, L., Chmelik, M., Just Kukurova, I., Jakubova, M., Kipfelsberger, M. C., Krumpolec, P., Tussek Jelenc, M., Bogner, W., Meyerspeer, M., Ukropec, J., et al. (2014) Depth-resolved surface coil MRS (DRESS)-localized dynamic 31P-MRS of the exercising human gastrocnemius muscle at 7 T *NMR in Biomedicine* 27.(11), 1346–1352.

Chapter 6

Comparison of Compressed Sensing reconstruction algorithms for ^{31}P Magnetic Resonance Spectroscopic Imaging

6.1 Context of the study

Phosphorus MR spectroscopy and spectroscopic imaging (^{31}P-MRS/MRSI) provide information about energy metabolism, membrane degradation and pH in vivo. These methods have been applied in the study of both healthy and diseased conditions in different types of tissue such as skeletal muscle and brain. In spite of their proven utility, ^{31}P-MRS/MRSI are not often used primarily because of excessive scan time. Furthermore, low intrinsic signal to noise ratio (SNR) also represents a major limitation as it leads to coarse spatial resolution and prolonged acquisition

times. In addition, relatively short T_2 relaxation times of phosphorus metabolites (i.e. $T_{2-ATP} \approx 50ms$) make pulse-acquire sequences preferable.

In the last decade, compressed sensing (CS) has grown substantially as an acceleration method to acquire MR signals as it takes advantage of their intrinsic sparsity. As a result, multiple data processing methods have been proposed to accurately reconstruct the desired signals.

Taking this background and the previous work developed in chapters 4 and 5, in this study we compared two different reconstruction methods for highly accelerated Phosphorus Magnetic Resonance Spectroscopic Imaging (^{31}P-MRSI) combining flyback Echo planar spectroscopic imaging (EPSI) and CS. We tested both algorithms in data acquired from phantom experiments and further tested one of them using in vivo data from the brain of five healthy volunteers. Our results prove the superiority of one of the methods and discusses relevant factors one needs to consider when using such algorithms.

6.2 Declaration statement

Alejandro Santos Díaz, as first author, developed the highly accelerated pulse sequence, optimized the protocols, recruited the participants, acquired the data, performed the data processing and reconstruction as well as the statistical analysis. Additionally, drafted the article including tables and figures.

Dr. Michael D Noseworthy, as corresponding author, is the primary investigator of our group. He conceptualized the project as part of his as part of his well

established trajectory in the development of technology and applications of multinuclear magnetic resonance imaging (MRI). He also performed a critical revision to the manuscript and performed the appropriate corrections in order to be published. Additionally, he provided constant guidance and advice during the development of the whole project.

This paper was submitted for publication to the journal Magnetic Resonance Imaging on October 11^{th}, 2018.

6.3 (Research Article) Comparison of Compressed Sensing reconstruction algorithms for ^{31}P Magnetic Resonance Spectroscopic Imaging

Alejandro Santos-Díaz[1,2] and Michael D. Noseworthy[1,2,3]

1. School of Biomedical Engineering, McMaster University, Hamilton Ontario, Canada
2. Imaging Research Center, St. Joseph's Healthcare, Hamilton, Ontario, Canada
3. Electrical and Computing Engineering, McMaster University, Hamilton Ontario, Canada

Corresponding author:
Dr. Michael D. Noseworthy, Ph.D.
Director, McMaster School of Biomedical Engineering,
Professor, Department of Electrical and Computer Engineering,
McMaster University.
Engineering Technology Building, ETB-406
1280 Main St. West, Hamilton,
Ontario. Canada L8S 4K1
Phone: +1 (905) 525-9140 ext.23727
`http://www.ece.mcmaster.ca/~mikenose/web/HOME.html`

Text word Count: 2,730
Number of figures/tables: 4/2
Number of references: 21

Key words: ^{31}P-MRSI; Compressed Sensing; Low Rank; EPSI; .

6.3.1 Abstract

Phosphorus MR spectroscopy and spectroscopic imaging (^{31}P-MRS/MRSI) provide information about energy metabolism, membrane degradation and pH in vivo. In spite of their proven utility, ^{31}P-MRS/MRSI are not often used primarily because of excessive scan time. Furthermore, low signal to noise ratio (SNR) also represents a major limitation as it leads to coarse spatial resolution and prolonged acquisition times. More recently there has been considerable interest in compressed sensing (CS) as an acceleration method for MR signal acquisition. This approach takes advantage of the intrinsic sparsity of the spectral data. In this work, we present a ^{31}P-MRSI sequence that combines a flyback EPSI trajectory and compressed sensing, and we compared two different reconstruction methods, L_1 norm minimization and low rank Henkel matrix completion. Our phantom results showed good preservation of spectral quality for both $\times 2.0$ and $\times 3.0$ acceleration factors, using both CS reconstruction methods. However, in vivo Phosphorus magnetic resonance spectroscopy (^{31}P-MRS) brain data showed the low rank reconstruction approach was most suitable. Overall, this study shows the feasibility of combining a flyback EPSI trajectory and compressed sensing in the acquisition of ^{31}P-MRSI as well as the better suitability of a low rank reconstruction approach.

6.3.2 Introduction

Phosphorus MR spectroscopy and spectroscopic imaging (^{31}P-MRS/MRSI) provide information about energy metabolism, membrane degradation and pH in vivo. These methods have been applied in the study of both healthy and disease conditions in different types of tissue such as skeletal muscle and brain (Valkovič et al. 2017; Kemp et al. 2015; Schmitz et al. 2018; Novak et al. 2014; Harper et al. 2016). In spite of their proven utility, ^{31}P-MRS/MRSI are not often used due to a number of challenges. Specifically, low intrinsic signal to noise ratio (SNR) represents a major limitation as it leads to coarse spatial resolution and very long acquisition times. In addition, relatively short T_2 relaxation times of some phosphorus metabolites (i.e. $T_{2ATP} \approx 50ms$) make pulse-acquire sequences preferable.

In order to reduce acquisition time while preserving sufficient SNR for spectral analysis, different acceleration methods common in MRI have been translated to ^{31}P-MRSI. Methods such as echo planar spectroscopic imaging (Santos-Díaz et al. 2018b; Korzowski and Bachert 2018), spiral trajectories (Valkovic et al. 2016) and variations of compressed sensing CS (Hatay et al. 2017; Ma et al. 2017) have shown promising results in order to acquire spectra of sufficient quality. More recently, compressed sensing has grown in popularity as an acceleration method for acquisition of MR signals. The basic framework behind it states that it is possible to accurately recover signals from a subset of samples as long as three main criteria are met (Lustig et al. 2007): (1) The data have a sparse representation in a transformed domain; (2) the aliasing generated due to the sub-sampling scheme is incoherent and (3) a non-linear reconstruction method is to be used in order to enforce consistency with the measurements and sparsity of the data.

The main task in MR spectroscopy is to find a spectrum Y from a measured free induction decay (FID) signal x by solving $\mathscr{F}x = Y$, where $\mathscr{F}$ is the Fourier transform operator. When non-uniform subsampling is employed, the problem becomes undetermined and can be expressed as $\mathscr{F}_u x = y$, with $\mathscr{F}_u$ as the undersampled Fourier operator. From the different solutions to this problem, the compressed sensing framework seeks to find the sparsest, which is found through L_1 norm minimization as

$$argmin \left\|x\right\|_1 subjectto \left\|\mathscr{F}_u x - y\right\|_2 < \epsilon$$

Where εcontrols the fidelity of the reconstruction to the measured data.

In the original work of compressed sensing applied to MR images, Lustig et al. proposed a non-linear conjugate gradient algorithm to solve the task (Lustig et al. 2007). Soon after, the method was extended to applications of hyperpolarized ^{13}C-MRSI experiments as its intrinsic sparsity makes it a natural candidate for CS (Hu et al. 2008). Furthermore, this work by Hu et al. established the basis for the development of very fast imaging methods capable of tracking cellular metabolism (Hu et al. 2010; Larson et al. 2011; Cao et al. 2016; Chen et al. 2018).
Development of reconstruction methods for non-uniform sampled signals has also been a focus of research in NMR. A recent comparison (Shchukina et al. 2017) points to the strengths and weaknesses of the most common methods used in the field. From this work, the low-rank Hankel matrix completion (LR) algorithm (Qu et al. 2015) is postulated as one of the most robust options to accurately recover the subsampled signals. Briefly, this method exploits the sparsity of a NMR signal from the perspective of finding the solution with the fewest number of spectral peaks rather than finding the spectrum with fewest non-zero values. Thus, the

method is less sensitive to failure when reconstructing broad spectral peak signals. It converges on a solution by minimizing the nuclear norm of a Hankel matrix made up of the FID signal.

Under the compressed sensing framework, the purpose of this study was to analyze and compare the performance of two different reconstruction methods, applied to ^{31}P-MRSI data. The first method was the "traditional" compressed sensing (CS) reconstruction first proposed by Lustig et al. (Lustig et al. 2007) and the second, the low rank Hankel matrix completion (LR) recently presented by Qu et al. (Qu et al. 2015).

6.3.3 Materials and Methods

MR system and pulse sequence

All experiments were performed using a 60cm bore 3T GE MR750 (GE Healthcare, Milwaukee, WI) scanner (50mT/m amplitude and 200T/m/s slew rate gradient system). The pulse sequence developed for this study was built on a recently presented flyback EPSI sequence "fidepsi" written in the EPIC programming language (version DV25.R1, GE Healthcare, Milwaukee, WI), due to its flexibility to design the echo planar trajectory (Santos-Díaz et al. 2018b). Non-uniform undersampling was achieved by the inclusion of pseudo randomly distributed blips in the k_y dimension during the flyback readout to allow sampling multiple $k_t - k_y$ lines during the same phase encoding step. The pulse duration of the blips was set to be equal to, or slightly less than, the rewinder segment of the EPSI trajectory (0.284ms), whereas the amplitude was determined by the pulse sequence

TABLE 6.1: Features of each pulse sequence variation. Acq. Time: Acquisition time. Ex/Avg: Number of excitations per average.

Sequence	Averages	Acq. Time(min)	Ex/Avg
fidCSI	1	3.2	64
fidEPSI	8	3.2	8
fidepsiCS x2.0	8	1.6	4
fidepsiCS x2.0w	8	1.6	4
fidepsiCS x2.7	8	1.2	3
fidepsiCS x4.0	8	0.8	2

to achieve a blip area equal to, or a multiple of, the phase encoding increment. Four different subsampling schemes were implemented for this in order to achieve acceleration factors ranging from 2x to 4x, using different densities for *k-space* coverage. The flyback EPSI trajectory was designed to achieve $2.75 \times 2.75 cm^2$ resolution over a $22 \times 22 cm^2$ field of view (i.e. 8×8 voxels), a spectral bandwidth of 1428 Hz and 512 spectral points. Thus, the compressed sensing implementation herein presented further accelerates the already fast EPSI trajectory. The pulse sequence diagram and sub-sampling schemes are shown in Figure 6.1 whereas Table 6.1 shows the acquisition features for each pulse sequence variant. Of note, when compared to a fully sampled standard fidCSI, the overall acceleration factors for our "fidepsiCS" approach are x16, x24 and x32. However, as the fully sampled case is the EPSI trajectory, we refer to the CS acceleration factors as x2.0, x2.0w, x2.7 and x4.0.

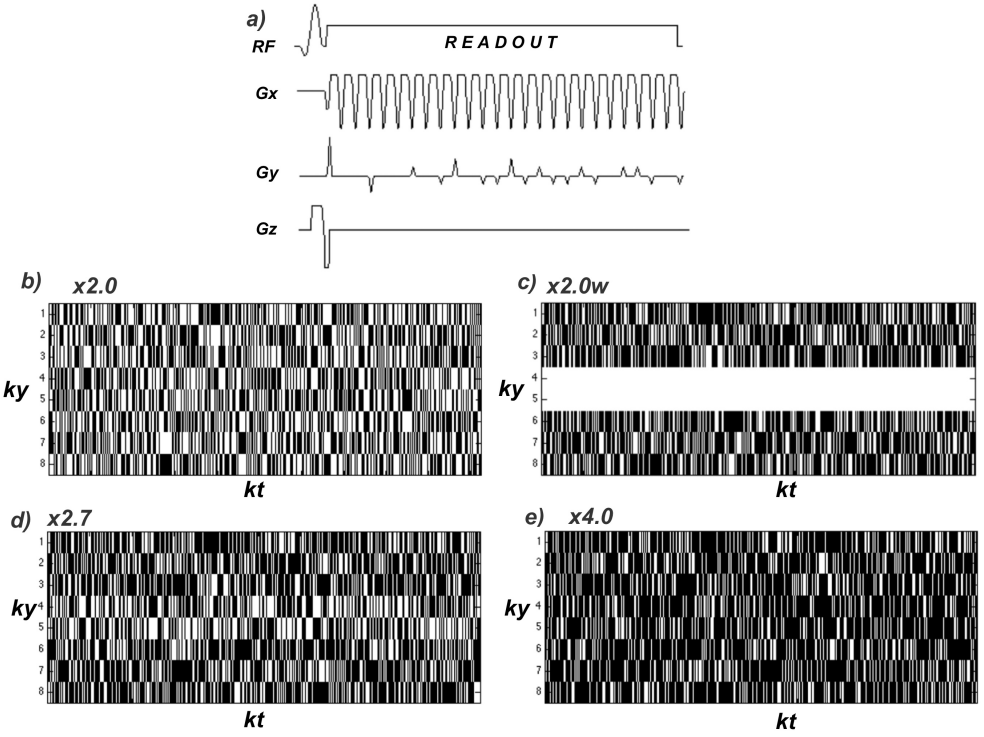

FIGURE 6.1: Pulse sequence diagram **a)** and undersampling schedules **(b-e)**. **b)** Two fold acceleration with uniform sampling density (**x2.0**), one excitation acquires two phase encoding steps. **c)** Two fold acceleration with sampling density weighted at the center of *k-space*(**x2.0w**), first excitation samples first three phase encode steps, second and third fully sample the two central lines and the fourth acquires the later three lines. **d)** Three fold acceleration with sampling density weighted at the center of *k-space* (**x2.7**), first excitation acquires the first three lines whereas the second and third sample the two central and three remaining lines respectively. **e)** Four fold acceleration with uniform sampling (**x4.0**), first excitation acquires first four lines and the second samples the remaining four.

Phantom data acquisition

Data collection was performed using an in house designed/built 24cm diameter quadrature birdcage coil tuned to 51.720 MHz. The pulse sequence was characterized using a custom-built spherical phantom (volume = 1L, pH=6.7) containing

25 mmol/L and 10 mmol/L concentrations of sodium phosphate (P1) and phosphocreatine disodium salt (P2) respectively in order to mimic in vivo differences in chemical shift and amplitude. Acquisitions for characterization consisted on collecting six 2D-MRSI datasets using (a) phase encoded MRSI (fidCSI), (b) flyback-EPSI (fidEPSI) and (c) each of the four variation of flyback EPSI combined with compressed sensing (fidepsiCS) x2.0, x2.0w, x2.7 and x4.0).

Radiofrequency excitation was applied using a 1.8 ms asymmetric partially self-refocused sinc pulse, with one side lobe before the main lobe (bandwidth = 2289 Hz). Parameters were matched for all sequences: TR = 3000ms; flip angle = 50^o; FOV = $22 \times 22cm^2$; matrix size = 8×8; slice thickness = 4cm; spectral bandwidth = 1420Hz; spectral points = 512. Four "dummy" scans were used in all acquisitions to allow the system to reach steady state.

Brain data acquisition

To test the performance of the LR algorithm using ^{31}P in vivo data, a single spectrum was acquired from the parietal lobe of 5 healthy volunteers (24±6 years of age) using a 12.7 cm diameter surface coil (51.705 MHz) matched for brain, a pulse-acquire sequence, squared excitation pulse (0.5ms, 60^o flip angle), 2000 Hz spectral bandwidth, 512 points, 128 averages. The collected FIDs were retrospectively under-sampled (pseudo-randomly selected samples) using 256 (x2.0), 170 (x3.0) and 128 (x4.0) data points to match the acceleration factors of the fidepsiCS sequence, then spectra were reconstructed using 1D implementations of the CS and LR algorithms (Shchukina et al. 2017). The 1D implementation of the CS

algorithm corresponds to solving the problem of L_1 norm minimization by a soft thresholding conjugate gradient search.

Data processing and compressed sensing algorithms

All data processing and reconstruction was performed using MATLAB R2015b (The Mathworks, Natick, MA, USA). First, data was re-shaped from the raw blipped acquisition to a raw fidepsi format, zero filling the missing sampling points according to the sub-sampling schedule, and then reordered to a 3D matrix of *k-space* data with dimensions $k_t - k_x - k_y$, used as the input for both reconstruction methods.

The CS reconstruction was performed as follows: (1) data was inverse Fourier transformed in the fully sampled dimension (k_x) to convert the problem in multiple 2D reconstructions, then (2) missing $k_y - k_t$ points were filled using the non-linear conjugate gradient algorithm adapted from the sparseMRI toolbox (Lustig et al. 2007); (3) Forward Fourier transform was applied in the k_x dimension; and finally (4) data was 3D Fourier transformed. The sparsifying transformation was a 1D length 4 Daubechies Wavelet transform and the total variation and transform weights, as commonly done (Lustig et al. 2007; Hu et al. 2008; Hu et al. 2010; Larson et al. 2011) were empirically chosen as 0.015 and 0.005 respectively.

For the LR reconstruction, data were (1) reordered as a column vectors containing the FID information for each undersampled $k_y - k_t$ plane; (2) each vector was used to build a Hankel matrix, feeding into an alternating direction minimization method; (3) reconstructed FIDs were reshaped back into a $k_x - k_y - k_t$ array of data

that was (4) inverse Fourier transformed in the spatial domain and Fourier transformed in the spectral dimension respectively to achieve the 3D MRSI dataset. The data agreement parameter (λ) and reconstruction tolerance threshold (tol) values were empirically determined as 800 and 0.00005 respectively.

To compare performance of the methods in the phantom experiments, we selected a region of interest at the center containing 3×3 voxels and measured amplitudes and linewidths from the metabolites. For the in vivo data, we measured metabolite ratios and root mean squared error (RMSE) of the original and reconstructed FID signals. All of the data fitting was performed using the AMARES implementation in the OXSA toolbox(Purvis et al. 2017).

6.3.4 Results

Spatial coverage of the data corresponded well between all acquisitions. Figure 6.2 shows an example of the 3×3 voxel region, near the center of our phantom, and a comparison of spectra acquired using fidCSI, fidEPSI and fidepsiCS with all of the acceleration factors for both CS and LR reconstructions. It is clear the best reconstructions happened for the x2.0w variants, as expected due to the fully sampled central *k-space* lines. It is also possible to observe the degradation in spectral quality with higher acceleration factors. To note, the spectra reconstructed with the CS algorithm presents more artifacts when compared to LR.

Results for fitted phantom spectral peak amplitudes and linewidths are shown in Figure 6.3. Overall, there was an increase in the P1/P2 ratio for higher acceleration factors for both methods, however this overestimation is more accentuated for

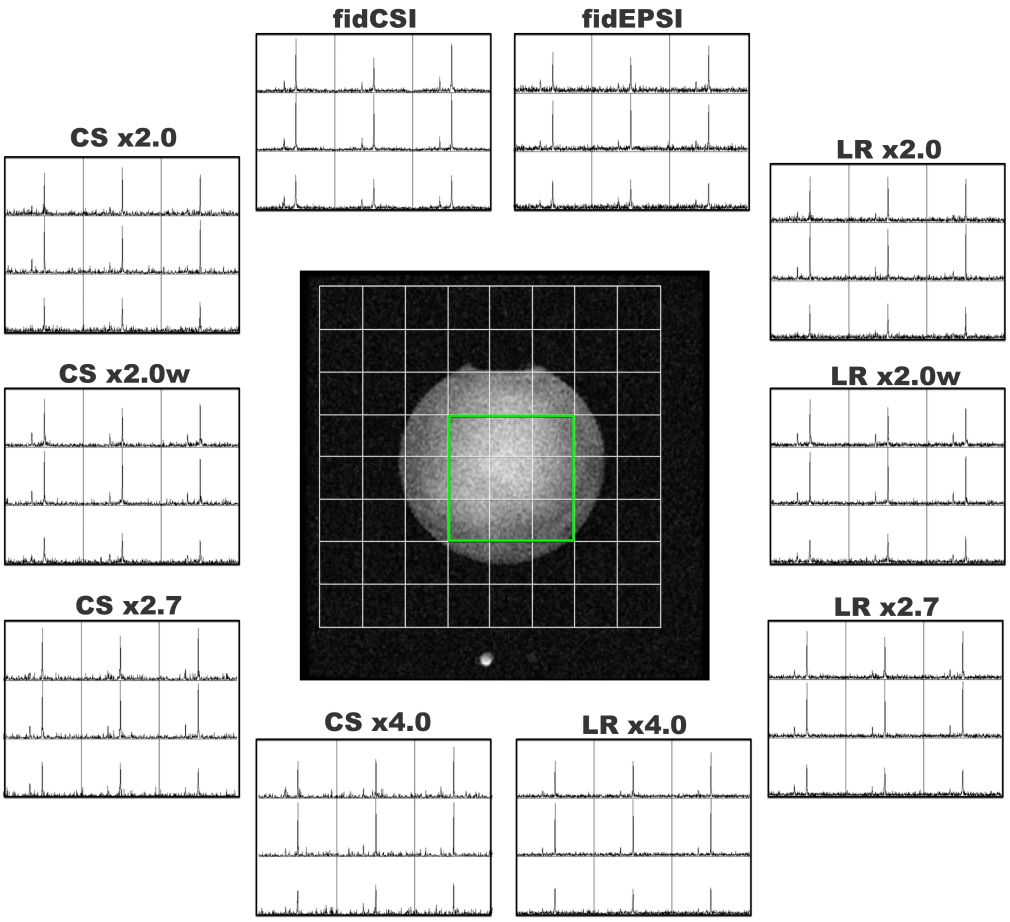

FIGURE 6.2: Example of the acquisition matrix on the reference image and 3×3 voxels region of interest with their corresponding spectra using fidCSI, fully sampled flyback EPSI (fidEPSI) and flyback EPSI combined with compressed sensing (fidepsiCS), using each of the acceleration factors reconstructed with both CS and LR algorithms.

the CS reconstruction. As expected, best reconstructions occurred for the variants with a higher sampling weight in the center of *k-space* (i.e. x2.0w and x2.7). When analyzing metabolite amplitudes independently, CS reconstructions show a higher overestimation of P1 values compared to LR. On the other hand, for the smaller

metabolite (P2), CS reconstructions show a higher attenuation of the signal, specially depicted in the CSx2.0 and CSx4.0. Linewidth values were comparable for all implementations; however, there is a stronger presence of "outliers" for the CS reconstructions.

From in vivo brain acquisition, it is clear that the CS algorithm failed to reconstruct the data. On the other hand, the LR algorithm was capable to achieve reasonable reconstructions, however we observed increasing degradation of spectral quality with higher acceleration factor. Table 6.2 displays metabolite ratios and RMSE for reconstructed spectra. Figure 6.4 shows an example of a fully sampled spectrum and the reconstructions for both algorithms with all acceleration factors, as well as the corresponding magnitude error. Based on such residual error, this figure clearly demonstrates two things; first, the CS algorithm is not suitable for reconstruction of ^{31}P-MRS brain data. And second, signal degradation with the higher acceleration for the LR method, especially in the smaller metabolites such as Pi, PDE and β-ATP.

6.3.5 Discussion

Compressed sensing is becoming a fundamental tool to accelerate acquisition of MR signals. In this work we have compared the performance of two reconstruction algorithms that consider different approaches to the sparse solution, applied to the acquisition of ^{31}P-MRSI data. The first one was the "traditional" compressed sensing reconstruction first proposed by Lustig et al. (Lustig et al. 2007) which seeks for the sparse solution as the signal in the frequency domain with

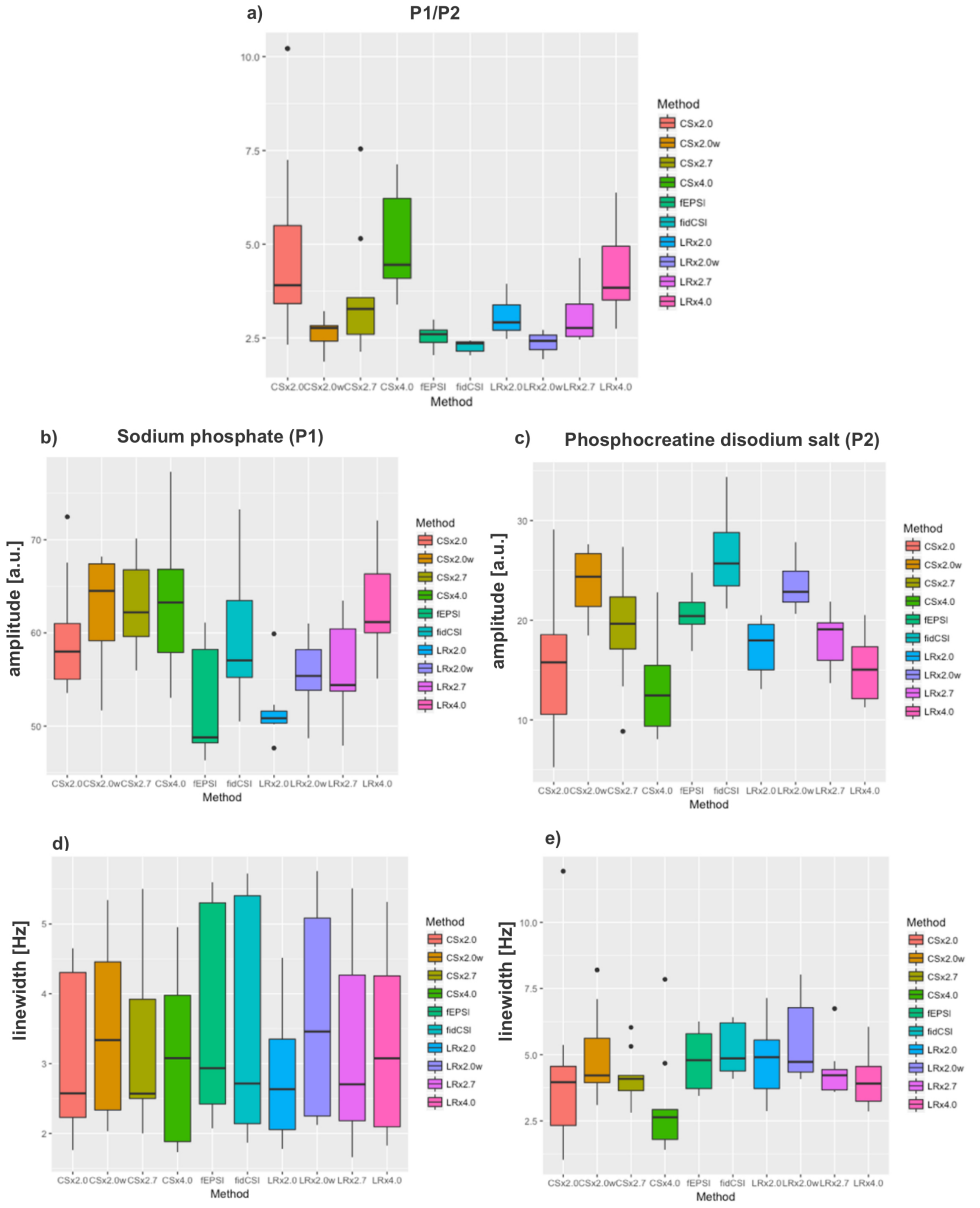

FIGURE 6.3: Box plots for metabolite ratio (a), amplitudes (b,c) and linewidths (d,e) comparing fidCSI, fidEPSI and each of the acceleration factors reconstructed using compressed sensing (CS) and low rank (LR) algorithms. P1: Signal peak from sodium phosphate. P2: Signal peak from phosphocreatine disodium salt. Signal amplitudes are measured in arbitrary units [a.u.]. The truth metabolite ratio in the phantom was 2.31.

the least amount of non-zero values. On the other hand, the low rank Hankel matrix completion approach presented by Qu et al. (Qu et al. 2015) exploits the sparsity of the NMR signal seeking a solution with the least amount of spectral peaks. From our comparison in the phantom data, the LR algorithm performed better than CS as depicted by the reduced amount of visible artifacts shown in the spectra of Figure 6.2. Additionally, the plots shown in Figure 6.3 suggest that although there is a signal degradation affecting metabolite ratios for both methods, the CS reconstruction shows the highest deterioration and the fitted values for LR remain comparable to fully sampled fidEPSI up to the x2.7 acceleration. Of note, the pulse sequence herein presented further accelerates the acquisition compared to the EPSI readout, thus when comparing to fidCSI, the acceleration factors become x16, x24 and x32 as shown by the number of excitations needed per slice of data (i.e. fidCSI requires 64 excitations for one slice of data whereas the fastest fidepsiCS requires only two).

TABLE 6.2: Metabolite ratios and mean root squared error for the reconstruction of the retrospectively undersampled in vivo brain data ($mean \pm SD$ for 5 volunteers, 24 ± 6 years of age). SNR for the acquisitions was 25 ± 8. **FS**: Fully sampled. **LR**: Low rank reconstruction. **CS**: Compressed sensing reconstruction. **x2.0**;Two fold acceleration. **x3.0**; three fold acceleration. **x4.0**; four fold acceleration.

	PCr/PME	PCr/Pi	PCr/PDE	PCr/γ-ATP	PCr/α-ATP	PCr/β-ATP	RMSE
FS	1.68 ± 0.31	4.94 ± 1.66	0.56 ± 0.10	0.98 ± 0.21	1.29 ± 0.25	1.41 ± 0.28	0 ± 0
LRx2.0	1.75 ± 0.41	4.37 ± 1.38	0.60 ± 0.13	0.86 ± 0.20	1.32 ± 0.29	1.56 ± 0.39	0.29 ± 0.07
LRx3.0	1.50 ± 0.21	4.44 ± 2.14	0.52 ± 0.10	0.94 ± 0.23	1.48 ± 0.36	1.49 ± 0.34	0.50 ± 0.10
LRx4.0	2.31 ± 0.82	2.92 ± 1.90	0.47 ± 0.09	0.67 ± 0.38	1.83 ± 0.40	1.79 ± 0.39	0.87 ± 0.09
CSx2.0	0.31 ± 0.30	0.41 ± 0.33	0.81 ± 0.82	0.75 ± 0.16	0.70 ± 0.73	0.23 ± 0.18	3.57 ± 0.26
CSx3.0	0.13 ± 0.1	0.12 ± 0.1	0.33 ± 0.31	0.25 ± 0.18	0.62 ± 0.46	0.06 ± 0.03	3.58 ± 0.25
CSx4.0	0.94 ± 0.92	1.34 ± 0.46	1.59 ± 1.33	6.14 ± 5.1	0.53 ± 0.37	0.21 ± 0.19	3.50 ± 0.27

CS reconstruction was very successful when expanded to hyperpolarized ^{13}C

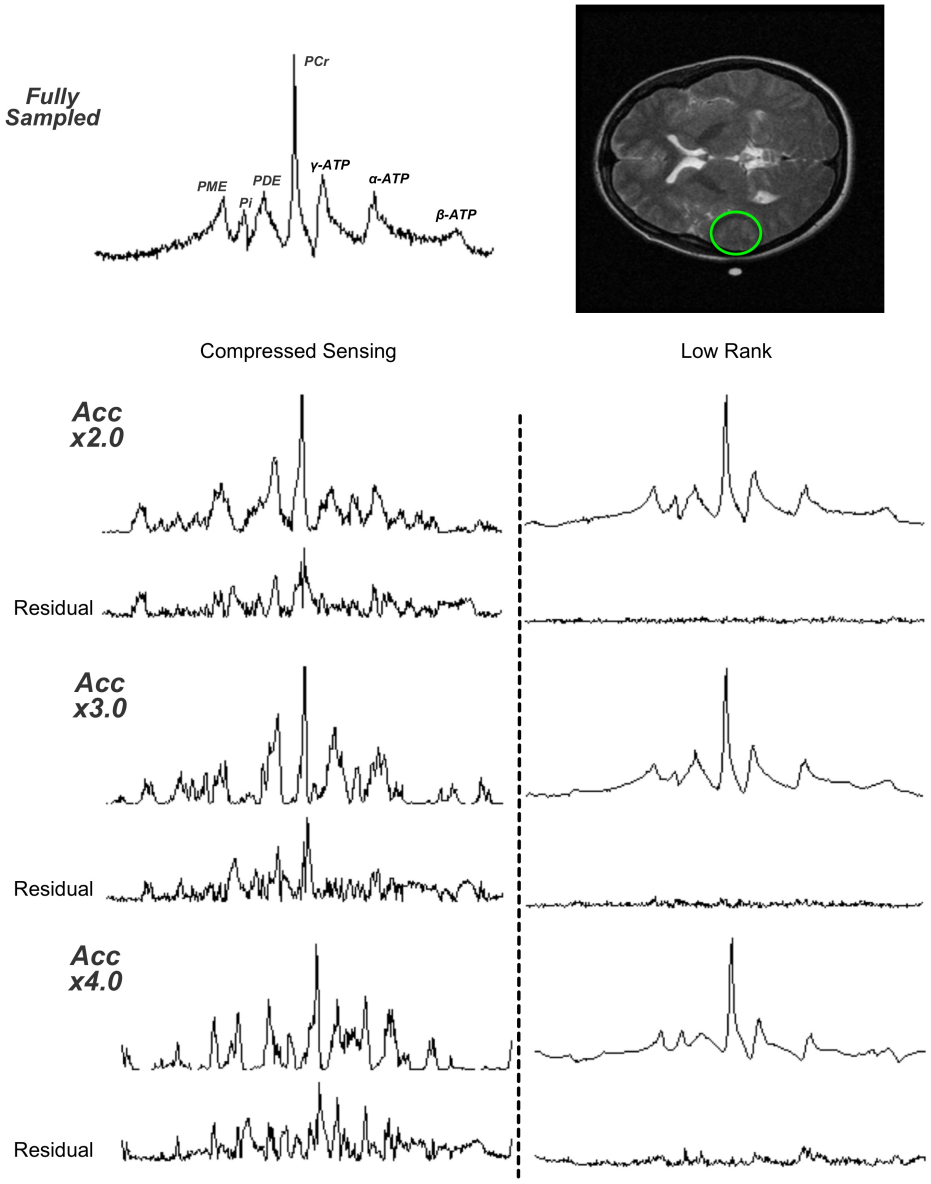

FIGURE 6.4: Example of fully sampled brain spectrum with anatomic reference (Top row). CS (left) and LR (right) reconstructions and corresponding residual error for three undersampling schemes. **Acc x2.0**: Using 256 out of 512 points. **Acc x3.0**: Using 170 out of 512 points. **Acc x4.0**: Using 128 out of 512 points. Note that plotted spectra and magnitude error have the same y-axis scale.

experiments as shown in (Hu et al. 2008; Hu et al. 2010; Larson et al. 2011; Cao et al. 2016). The main reason for this was the very high SNR of the signal, relatively narrow peak linewidths and reduced number of metabolites. In this work, we extrapolated these methods to the acquisition of ^{31}P-MRSI signals where there is an intrinsic low SNR as well as presence of five or more metabolites, all with different amplitudes and linewidths. Thus, based on such differences, especially the broad peaks of some ^{31}P metabolites such as ATP, it was reasonable to suggest that the LR method would perform better, as it approaches the sparsity of the NMR signal seeking for the solution with the least number of spectral peaks rather than the spectrum with fewer non-zero values. Furthermore, from the same group, Cao et al. presented an improved approach where low rank reconstruction was used (Cao et al. 2016).

Our results from the phantom experiments suggest a low to moderate superiority of the LR algorithm. To further demonstrate it, results from the *in vivo* brain data show clear dominance of the low rank approach. Such difference in performance between experiments is due to the fact that the spectrum from the phantom can be considered very sparse as it only contains two metabolites with relatively narrow linewidth, hence the small difference in results. On the other hand, the *in vivo* spectrum is clearly not sparse in the frequency domain, however it has relatively low number of signal components in the time domain, hence it is better suitable for the LR approach. Nonetheless, results showed in Table 6.2 and Figure 6.4 suggest the reconstruction performs well up to a three fold acceleration, consistent with the phantom data as the metabolite ratios were preserved up to the x2.7 acceleration factor.

When designing the undersampling pattern, from the CS literature we know that

the reconstruction will perform better when more samples are acquired at the center of $k - space$ (Lustig et al. 2007; Larson et al. 2011). Our phantom results are consistent with this, however for the 1D case when retrospective undersampling was used, we found that there is a considerable variation in the reconstruction error and thus quality of spectra was highly dependent on the selected samples (data not shown). NMR literature has suggested that a noticeable sensitivity enhancement is observed when matching the sampling density with the envelope of the signal(Kazimierczuk and Orekhov 2015), however that might compromise the overall quality of the results as there is a tradeoff between the sampling density and incoherence of the aliasing generated. This issue is not within the scope of this study and needs further investigation.

In the present work we targeted the feasibility of this pulse sequence in the acquisition of ^{31}P spectra from the brain and although our results show promise, extremely fast acquisitions are rarely needed. On the other hand, ^{31}P-MRS/MRSI has been widely used in the study of muscle dynamics where the high temporal resolution is key (Valkovič et al. 2017; Kemp et al. 2015). Our pulse sequence has been successfully applied in dynamic muscle experiments elsewhere (Santos-Díaz et al. 2018a). A further application of accelerated ^{31}P-MRSI would be in the assessment of myocardial metabolites where speed could be an important benefit.

Conclusions

We presented a ^{31}P-MRSI pulse sequence that combines a flyback EPSI readout with compressed sensing and compared two different reconstruction algorithms. Our phantom experiments suggested that the LR reconstruction performs better

than the CS method. Additionally in vivo brain data acquisition showed the LR reconstruction performed well, when accelerating up to three-fold. Overall, our results suggest that compressed sensing using low rank reconstruction is feasible to accelerate the acquisition of ^{31}P spectroscopic data when relatively low acceleration factors are required.

Acknowledgements

Funding was provided through a CONACYT (Mexico) scholarship granted to ASD (CVU: 304930) and a NSERC Discovery Grant (RGPIN-2017-06318) to MDN.

References

Cao, P., Shin, P. J., Park, I., Najac, C., Marco-Rius, I., Vigneron, D. B., Nelson, S. J., Ronen, S. M., and Larson, P. E. (2016) Accelerated high-bandwidth MR spectroscopic imaging using compressed sensing *Magnetic resonance in medicine* 76.(2), 369–379.

Chen, H.-Y., Larson, P. E., Gordon, J. W., Bok, R. A., Ferrone, M., Criekinge, M. van, Carvajal, L., Cao, P., Pauly, J. M., Kerr, A. B., et al. (2018) Technique development of 3D dynamic CS-EPSI for hyperpolarized 13C pyruvate MR molecular imaging of human prostate cancer *Magnetic resonance in medicine*.

Harper, D. G., Jensen, J. E., and Renshaw, P. F. (2016) Phosphorus spectroscopy (31P MRS) of the brain in psychiatric disorders in: Wiley Online Library, 1257–1270.

Hatay, G. H., Yildirim, M., and Ozturk-Isik, E. (2017) Considerations in applying compressed sensing to in vivo phosphorus MR spectroscopic imaging of human brain at 3T *Medical & biological engineering & computing* 55.(8), 1303–1315.

Hu, S., Lustig, M., Balakrishnan, A., Larson, P. E., Bok, R., Kurhanewicz, J., Nelson, S. J., Goga, A., Pauly, J. M., and Vigneron, D. B. (2010) 3D compressed sensing for highly accelerated hyperpolarized 13C MRSI with in vivo applications to transgenic mouse models of cancer *Magnetic Resonance in Medicine: An Official Journal of the International Society for Magnetic Resonance in Medicine* 63.(2), 312–321.

Hu, S., Lustig, M., Chen, A. P., Crane, J., Kerr, A., Kelley, D. A., Hurd, R., Kurhanewicz, J., Nelson, S. J., Pauly, J. M., et al. (2008) Compressed sensing for resolution enhancement of hyperpolarized 13C flyback 3D-MRSI *Journal of magnetic resonance* 192.(2), 258–264.

Kazimierczuk, K. and Orekhov, V. (2015) Non-uniform sampling: post-Fourier era of NMR data collection and processing *Magnetic Resonance in Chemistry* 53.(11), 921–926.

Kemp, G., Ahmad, R., Nicolay, K., and Prompers, J. (2015) Quantification of skeletal muscle mitochondrial function by 31 P magnetic resonance spectroscopy techniques: a quantitative review *Acta physiologica* 213.(1), 107–144.

Korzowski, A. and Bachert, P. (2018) High-resolution 31 P echo-planar spectroscopic imaging in vivo at 7 T *Magnetic resonance in medicine* 79.(3), 1251–1259.

Larson, P. E., Hu, S., Lustig, M., Kerr, A. B., Nelson, S. J., Kurhanewicz, J., Pauly, J. M., and Vigneron, D. B. (2011) Fast dynamic 3D MR spectroscopic imaging

with compressed sensing and multiband excitation pulses for hyperpolarized 13C studies *Magnetic resonance in medicine* 65.(3), 610–619.

Lustig, M., Donoho, D., and Pauly, J. M. (2007) Sparse MRI: The application of compressed sensing for rapid MR imaging *Magnetic Resonance in Medicine: An Official Journal of the International Society for Magnetic Resonance in Medicine* 58.(6), 1182–1195.

Ma, C., Clifford, B., Liu, Y., Gu, Y., Lam, F., Yu, X., and Liang, Z.-P. (2017) High-resolution dynamic 31P-MRSI using a low-rank tensor model *Magnetic resonance in medicine* 78.(2), 419–428.

Novak, J., Wilson, M., MacPherson, L., Arvanitis, T. N., Davies, N. P., and Peet, A. C. (2014) Clinical protocols for 31P MRS of the brain and their use in evaluating optic pathway gliomas in children *European journal of radiology* 83.(2), e106–e112.

Purvis, L. A., Clarke, W. T., Biasiolli, L., Valkovič, L., Robson, M. D., and Rodgers, C. T. (2017) OXSA: An open-source magnetic resonance spectroscopy analysis toolbox in MATLAB *PloS one* 12.(9), e0185356.

Qu, X., Mayzel, M., Cai, J.-F., Chen, Z., and Orekhov, V. (2015) Accelerated NMR Spectroscopy with Low-Rank Reconstruction *Angewandte Chemie* 127.(3), 866–868.

Santos-Díaz, A., Harasym, D., and Noseworthy, M. D. (2018a) Dynamic 31P Spectroscopic Imaging of Skeletal Muscles combining Flyback EPSI and Compressed Sensing *Magnetic resonance in medicine*.

Santos-Díaz, A., Obruchkov, S. I., Schulte, R. F., and Noseworthy, M. D. (2018b) Phosphorus magnetic resonance spectroscopic imaging using flyback echo planar readout trajectories *Magnetic Resonance Materials in Physics, Biology and Medicine*, 1–12.

Schmitz, B., Wang, X., Barker, P. B., Pilatus, U., Bronzlik, P., Dadak, M., Kahl, K. G., Lanfermann, H., and Ding, X.-Q. (2018) Effects of Aging on the Human Brain: A Proton and Phosphorus MR Spectroscopy Study at 3T *Journal of Neuroimaging*.

Shchukina, A., Kasprzak, P., Dass, R., Nowakowski, M., and Kazimierczuk, K. (2017) Pitfalls in compressed sensing reconstruction and how to avoid them *Journal of biomolecular NMR* 68.(2), 79–98.

Valkovič, L., Chmelík, M., and Krššák, M. (2017) In-vivo 31P-MRS of skeletal muscle and liver: a way for non-invasive assessment of their metabolism *Analytical biochemistry* 529, 193–215.

Valkovic, L., Chmelík, M., Meyerspeer, M., Gagoski, B., Rodgers, C. T., Krssák, M., Andronesi, O. C., Trattnig, S., and Bogner, W. (2016) Dynamic 31P–MRSI using spiral spectroscopic imaging can map mitochondrial capacity in muscles of the human calf during plantar flexion exercise at 7 T *NMR in Biomedicine* 29.(12), 1825–1834.

Chapter 7

Conclusions and future directions

Phosphorus magnetic resonance spectroscopy (^{31}P-MRS) has evolved as a tool that offers invaluable information about energy metabolism and membrane degradation in vivo. Although it has not been exploited as a clinical tool to be used on a daily basis due to the many technical challenges, the technological advancements such as ultra high field MR systems, complex RF-coil arrays, automated spectral analysis tools and new pulse sequences with non-conventional sampling schemes, contribute to the reaching of wider applications. Furthermore, its non invasive nature makes it a remarkable tool to uniquely study cellular energy metabolism under different healthy and pathological conditions.

This work focused on the technical development of tools for the study of skeletal muscle and brain metabolism. Specifically, the contributions are in the field of pulse sequence design, in order to accelerate the acquisition of Phosphorus Magnetic Resonance Spectroscopic Imaging (^{31}P-MRSI) data. In the work presented herein RF coils also had to be designed and built. The coil designs were not novel. However, they were critical in the acquision of data. Nonetheless, all coils that

were manufacutred were optimzied to the tissue of interest (i.e. matched to the specific piece of anatomy, while being tuned to 51.7MHz).

7.1 Main contributions

In Chapter 4 we presented an Echo planar spectroscopic imaging (EPSI) pulse sequence that uses a flyback readout trajectory. This pulse sequence accelerates the acquisition of ^{31}P-MRSI up to a factor equal to the number of phase encoding steps in one of the gradient directions. For the applications presented, the acceleration was up to 10x. Additionally, it offers the flexibility to modify the acquisition parameters as it calculates the flyback trajectories "on the fly" optimizing the signal to noise ratio (SNR).

The evaluation of mitochondrial function in skeletal muscle using ^{31}P-MRS demands a temporal resolution in the order of seconds, in Chapter 5 we pushed further the acceleration achieved by the flyback EPSI sequence by combining it with compressed sensing (CS) and obtained a new scheme that reaches a 9 seconds temporal resolution. This new scheme was then used in a dynamic experiment of PCr recovery.

Compressed sensing is a relatively new method that has grown substantially in the world of magnetic resonance imaging (MRI). Since it was first presented, multiple branches have spread looking for better and faster ways to reconstruct and process the data. In Chapter 6 we showed that a low rank reconstruction

algorithm performs better when compared to a "traditional" CS method, and also proved its feasibility of application in data acquired from the brain.

7.2 Limitations

The main limitations of the work presented in this thesis include the use of surface coils for experimentation, as they provide an inhomogeneous B_1+ excitation field. This inhomogeneity may influence some values obtained for metabolite quantification, specially in the brain experiments.

Specific limitations in regards to the developed pulse sequences include first, the relatively low spectral bandwidth of the fidepsiCS sequence. Although it covered the 'metabolites of interest' for dynamic experiments, it was still insufficient to visualize the triplet β-ATP peak. Additionally, the low-rank reconstruction algorithm used was computationally expensive as explained in the corresponding chapter.

7.3 Future directions

The work developed in this thesis lies under a bigger ongoing project in our research group. That project is focused on the development of new MR based techniques for the study of mild traumatic brain injury (mild Traumatic Brain Injury (mTBI)). The impetus of applying ^{31}P-MRSI to this disorder lies in the possibility of altered brain bioenergetics in this condition. So far, only one study has been reported in

the field describing altered phosphate metabolites following mTBI (Sikoglu et al. 2015). In this study, the authors found a reduced concentration of γ-ATP in the prefrontal cortex of participants whom had a concussion when compared to those without mTBI. Although this works shows strong evidence to support pursuit of phosphate metabolism, it only targeted one brain region and the time range between the day of the concussion and the MRI exam is very broad (i.e. 6 to 185 days). Furthermore, the ^{31}P-MRS pulse sequence used is was a 2D image selected in vivo spectroscopy (ISIS), which usually takes a very long time for the acquisition and is susceptible to motion artifacts. Unquestionably more research needs to be performed. To get to the point of scanning patients required a great deal of technical development. Our accelerated approach is now ready to be applied in a cohort of patients. Ideally, however, a high quality volumetric head ^{31}P-tuned RF-coil is required.

On the technical side, the reconstruction methods implemented for the sequence used in chapters 5 and 6 have room for improvement. In particular, better quality in the spectra and reduced data processing time can be achieved if newer versions of the Low-Rank reconstruction are implemented (Guo et al. 2017; Guo and Qu 2018).

7.4 Conclusion

This work featured the development of new pulse sequences for the fast acquisition of phoshphorus magnetic resonance spectroscopic imaging data, as well as their application in the non-invasive study of skeletal muscle and brain tissue energy

metabolism, using a clinical 3T MR system. These sequences were built under the framework of methods more commonly used in ^{1}H and hyperpolarized ^{13}C MR fields such as echo planar imaging and compressed sensing, and were translated to ^{31}P-MRS applications, pushing the boundaries established by the technical limitations.

With this work we contributed to the stack of available tools for the non invasive assessment of energy metabolism, hoping that it will help to make ^{31}P-MRSI a clinically available technique.

Appendix A

Summary of publications

A1 Journal Articles

1. Santos-Diaz A, Harasym D and Noseworthy M D. (2018) Dynamic ^{31}P Spectroscopic Imaging of Skeletal Muscles combining Flyback EPSI and Compressed Sensing. *Magnetic Resonance in Medicine* [under revision].

2. Santos-Diaz A and Noseworthy M D. (2018) Comparison of Compressed Sensing reconstruction algorithms for ^{31}P Magnetic Resonance Spectroscopic Imaging. *Magnetic Resonance Imaging* [submitted].

3. Santos-Diaz A, Obruchkov S I. Schulte R and Noseworthy M D. (2018) Phosphorus magnetic resonance spectroscopic imaging using flyback readout trajectories. *Magnetic Resonance Materials in Physics, Medicine and Biology*, 1-12.

A2 Peer-review international conference proceedings

1. A. Santos-Díaz and M. Noseworthy (2018) Accelerated in vivo Phosphorus Magnetic Resonance Spectroscopic Imaging combining flyback-EPSI and Compressed Sensing in: *Proceedings of the joint Annual Meeting of ISMRM-ESMRMB, Paris, France*, 1309

2. A. Santos-Díaz et al. (2017) Dynamic phosphorus echo planar spectroscopic imaging (31P-EPSI) of human calf muscles using flyback readout trajectories *Magnetic Resonance Materials in Physics, Biology and Medicine* 30.(supp(1)), 260

3. A. Santos-Díaz and M. Noseworthy (2017) Highly Accelerated 31P-MRSI of Human Calf Muscles combining flyback Echo Planar Spectroscopic Imaging (EPSI) and Compressed Sensing in: *Proceedings of the 25th Annual Meeting of ISMRM, Honolulu, Hawaii*, 2931

4. A. Santos-Díaz et al. (2016b) Phosphorus echo planar spectroscopic imaging (EPSI) of the brain using flyback readout gradients *Magnetic Resonance Materials in Physics, Biology and Medicine* 29.(supp(1)), 474

5. A. Santos-Díaz et al. (2016a) 31P MRSI of human calf muscles using flyback echo planar spectroscopic imaging (EPSI) readout gradients in: *Proceedings of the 24th Annual Meeting of ISMRM, Singapore*, 3936